UNIVERSITY OF CALIFORNIA
SANTA CRUZ

A METAMODELING APPROACH FOR BIAS ESTIMATION OF BIOLOGICAL REFERENCE POINTS

A dissertation submitted in partial satisfaction of the
requirements for the degree of

DOCTOR OF PHILOSOPHY

in

STATISTICAL SCIENCE

by

Nicholas Grunloh

September 2024

The Dissertation of Nicholas Grunloh
is approved:

Professor Herbert Lee, Chair

Edward J. Dick, Ph.D.

Professor Paul Parker

Professor Bruno Sanso

Peter F. Biehl
Vice Provost and Dean of Graduate Studies

Table of Contents

List of Figures

Abstract

A Metamodeling Approach for Bias Estimation of Biological Reference Points

by

Nicholas Grunloh

Stock assessments often assume a two-parameter functional form (e.g. Beverton-Holt, Ricker, or Logistic) for the expected recruitment produced by a given level of spawning output. Mangel et. al. [44] and others have shown that biological reference points (RP) such as $\frac{F^*}{M}$ and $\frac{B^*}{\bar{B}(0)}$ are largely determined by a single parameter (steepness) when using two-parameter relationships. These functions introduce strong correlations between RPs that are pre-determined by the functional form, rather than a biological characteristic of the stock. Mangel et. al. note that use of a three-parameter stock-recruitment relationship allows for independent estimation of these RPs. Built around these ideas, a novel simulation framework is developed to investigate the nature of biases in RP estimates that results from fitting a two-parameter functional form when the true relationship is more complicated. First methods for generating space-filling simulation designs in the RP space of three-parameter models are developed. By simulating misspecified RP inference under common two-parameter models over these simulation designs a Gaussian Process metamodel of two-parameter RP inference is developed to control for a spectrum of common ways that two-parameter models are misspecified. This analysis demonstrates the useful limits of commonly used population dynamics

models, informs the utility of reducing RP bias, and suggests mechanisms for understanding how, and when, the most common two-parameter models fail to estimate RPs. The studied models vary in complexity from the Schaefer model to delay differential models including dynamics of individual growth and lagged maturity. Additionally, the methods presented can easily be extended to further include age-based frameworks.

To my family, friends, and mentors.

Acknowledgments

I am grateful to all of the excellent advisors and teachers I have had throughout my many years at UCSC. Thanks to my advisor Professor Herbie Lee, who's guidance and support has proven to be absolutely invaluable to this research. Thanks to Professor Marc Mangel who's research is the foundation of the science of this work and who's long time role as an advisor in my life has been truly enriching. To the UCSC Statistical Science faculty who have distinctly shaped the philosophy by which I make sense of information in the world. Of course, thanks to my committee members for their time and effort reviewing this work.

I would like to thank the Groundfish Ecology and Stock Assessment teams at the National Marine Fisheries Service in Santa Cruz. Thanks to E.J. Dick who's generous and kind guidance has been pivotal to this work. I would also like to thank John Field for his feedback and continued support of my work. Additional thanks to the NOAA Sea Grant program for its support of this work and more generally for the interdisciplinary partnerships they foster within fisheries research.

I am incredibly lucky to have Brian and Joanne Grunloh as parents. They have always supported me in following my passions, and their encouragement throughout this work has been a immeasurable source of strength. Last but certainly not least, thank you to my partner Anna for her love and patience over the last few years. I stand in awe of her willingness to indulge my various descriptions of minutia about the sea.

Chapter 1

Introduction

Modern fisheries management is a multi-armed system based upon stock assessment. Stock assessments characterize stock dynamics by collecting the available data for a particular stock and analyzing those data with population dynamics models. Population dynamics models are then used to quantify the effect of fishing on the stock and estimate long term sustainable catch levels which are then used by fisheries managers.

In the United States the Magnuson-Stevens Act[1] (MSA) dictates that stock assessment be a primarily scientific endeavor, and requires stock assessment to report *the best available science* to fisheries managers. Furthermore, the MSA requires fisheries managers to base management decisions upon the best available science. There are a number of checks and balances between the scientific and management arms, but ultimately it is fisheries managers that set the actual catch limits (based on science developed by stock assessments) that govern the amount of fish that can be harvested. This system has proven to be effective, but it can create an information bottleneck at the interface of stock assessment and management.

While stock assessment scientists do their best to bracket models with uncertainty, and contextualize results, inevitably not all of the modeling subtlety understood by scientists makes it into the management arm. Fisheries are very often managed based upon reference points (RPs) which serve as simplified heuristic measures of population behavior, and subtlety in how these measures are calculated can get lost in the transfer. Mangel et. al. [44] and others have shown that RPs can be structurally limited by

[1] Magnuson-Stevens Fishery Conservation and Management Act, 2007. Pub. L. No. 94-265.

the most commonly used assessment models. When these limitations are propagated to management these limitations can directly bias how catch limits for fisheries are set. The nature of these limitations manifests from the assumed mathematical form of production which is among the most foundational components of most population dynamics models.

This thesis develops a metamodeling simulation framework for evaluating RP estimates under misspecified two-parameter models of productivity. Analytical and numerical methods are developed for simulating data broadly in RP space under the Schnute and Pella-Tomlinson (PT) three-parameter models. By simulating from three-parameter models and observing RP estimation under misspecified two-parameter models, a metamodel of the RP estimation process makes the consequences of RP estimation with the most common models explicit. The metamodel demonstrates the types of stocks where RP estimation may fail, indicates how RP estimation fails, and quantifies the scale of biases with current models.

The most fundamental model in stock assessment is the *surplus-production model* (SPM). These models focus on modeling population growth via nonlinear parametric ordinary differential equations (ODE). Data for a typical surplus-production model comes in the form of an index of abundance through time which is assumed to be proportional to the reproducing biomass for the modeled population that is vulnerable to fishing. The index is often observed alongside a variety of other known quantities, but

at a minimum, each index will be observed in the presence of some known catch for the period. Figure (1.1) shows the classic Namibian Hake data set [59, 34, 43] exemplifying the form.

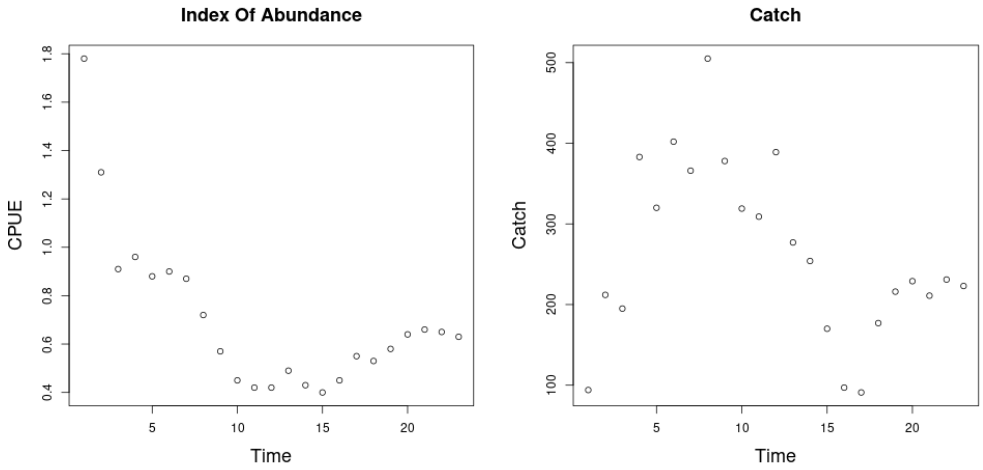

Figure 1.1: *(left)* Index of abundance data, catch per unit effort (CPUE), for Namibian Hake from 1965 to 1987. *(right)* The associated catch data for Namibian Hake over the same time period.

Indices are assumed to have multiplicative log-normal errors, and thus the following observation model arises naturally,

$$I_t = qB_t e^{\varepsilon} \quad \varepsilon \sim N(0, \sigma^2). \tag{1.1}$$

Above q is often referred to as the "catchability parameter"; it serves as the proportionality constant mapping between the observed index of abundance and biomass. σ^2 models residual variation. Biologically speaking q and σ^2 are often treated as nuisance parameters with biological productivity parameters entering the model through a pro-

cess model on biomass.

Biomass is assumed to evolve as an ODE through time. The class of models is largely based on the following form,

$$\frac{dB}{dt} = P(B(t);\boldsymbol{\theta}) - Z(t)B(t). \tag{1.2}$$

Here biomass is assumed to change in time by two processes, net production of biomass into the population, $P(B)$, and various sources of biomass removal, Z, from the population.

Firstly, the population grows through a production function, $P(B)$. Production in this setting is defined as the net biomass increase due to all reproduction and growth processes. The production function is assumed to be a parametric (generally non-linear) function relating the current biomass of the population to an aggregate production of biomass.

Secondly, the population decreases as biomass is removed by various sources that are assumed to remove biomass linearly with biomass. Above, $Z(t)$, is an aggregate rate of removal. Often the fishing rate, $F(t)$, is the only explicitly modeled source of removal $Z(t) = F(t)$, however some models will also included other linear terms in $Z(t)$. Commonly the rate of *natural mortality* (M) is also included as an additional term so that $Z(t) = M + F(t)$.

The general structure in Eq. (1.2) is the conceptual basis for most modern fisheries models used in management [32, 49, 84]. As data permit this general structure is often

expanded to model age, weight, and/or length classes [70, 22] in the population via models called *age structured models* (ASM). ASMs are currently considered best practice when there is considered enough quality data to establish length/age relationships and the vulnerability of each class to fishing mortality (i.e. selectivity) [46, 12]. Modeling age and length/weight structure in the population allows for individual growth and lagged maturity to be modeled as cohorts that age through time. Despite this added complexity, at their core ASMs rely on similar dynamics as seen in Eq. (1.2), however in ASMs the above ODE is expanded to a system of interrelated equations describing how cohorts age through time.

Delay-differential models (DDM), as described in more detail in Chapter (4), can provide an intermediate modeling infrastructure between SPMs and ASMs. By simplifying the model assumptions around growth and maturity, simple ASMs may be represented exactly by DDMs [17, 32]. Furthermore, SPMs can be represented as a limiting case of DDM growth and maturity parameters [82]. This makes DDMs ideal for "data-limited" assessment settings and as a simplified model for understanding the role of growth in stock assessment models. Despite the useful bridge that DDMs provide, their use in stock assessments has been sparing due to the complexity of deriving key management quantities under these models [19, 51].

From a management perspective a major goal of modeling is to accurately infer a quantity known as *maximum sustainable yield* (MSY). One could maximize simple

yield at a particular moment in time (and only for that moment) by fishing all available biomass in that moment. This strategy is penny-wise but pound-foolish (not to mention ecologically devastating) since it doesn't leave biomass in the population to reproduce in the future. We seek to fish in a way that allows (or even encourages) future productivity in the population. This is accomplished by maximizing the equilibrium level of catch over time. Equilibrium yield is modeled by $\bar{Y} = F\bar{B}(F)$, where $\bar{B}$ is the steady state biomass implied by Eq. (1.2), and $\bar{}$ indicates quantities at steady state. MSY is then found by maximizing $\bar{Y}(F)$ with respect to F, and F^* is the fishing rate at MSY. Going forward let * decorate any value derived under the condition of MSY.

Most RPs revolve around the concept of MSY (or robust ways of measuring MSY [33, 60]). Here the focus is primarily on the RPs $\frac{B^*}{\bar{B}(0)}$ and $\frac{F^*}{M}$ (or F^* when appropriate) for their pervasive use in modern fisheries [61]. Here F^* is the afore mentioned fishing rate which results in MSY, M is natural mortality, $\bar{B}(0)$ is the equilibrium biomass in the absence of fishing, and B^* is the equilibrium biomass when fishing at F^* (i.e. $\bar{B}(F^*)$). Thus, $\frac{F^*}{M}$ describes the fraction of mortality due to fishing when the population is expected to yield MSY and $\frac{B^*}{\bar{B}(0)}$ describes the fraction of the unfished population that will remain at MSY. In general $\frac{F^*}{M} \in \mathbb{R}^+$ and $\frac{B^*}{\bar{B}(0)} \in (0,1)$, however under the assumption of two-parameter production, models will be structurally unable to capture the full theoretical range of RPs.

Many of the most commonly used production functions depend only on two-parameters.

For example, the Schaefer model depends only on the biological parameters r and K, and limits RP inference so that under the Schaefer model $\left(F^*, \frac{B^*}{B(0)}\right) \in \left(\mathbb{R}^+, \frac{1}{2}\right)$. The two-parameter Fox model [23] limits $\left(F^*, \frac{B^*}{B(0)}\right) \in \left(\mathbb{R}^+, \frac{1}{e}\right)$. Similarly the two-parameter Cushing [15, 16], Beverton-Holt [4, BH] and Ricker [65] production functions do not model the full theoretical space of RPs. Mangel et. al. [44] show that this is a consequence of two-parameter production functions and suggests the use of three-parameter functions instead.

By fitting the Namibian Hake data from Figure (1.1) with a two-parameter Schaefer model, as compared with a three-parameter PT model, the restrictive RP estimation under two-parameter models can be seen. As will be developed further in Section (2.2.2), both models can be reparameterized directly in terms of their RPs, allowing for straightforward RP inference. Figure (1.2) shows RP estimates in relation to the respective two/three-parameter RP spaces under each model. A number of quirks in these

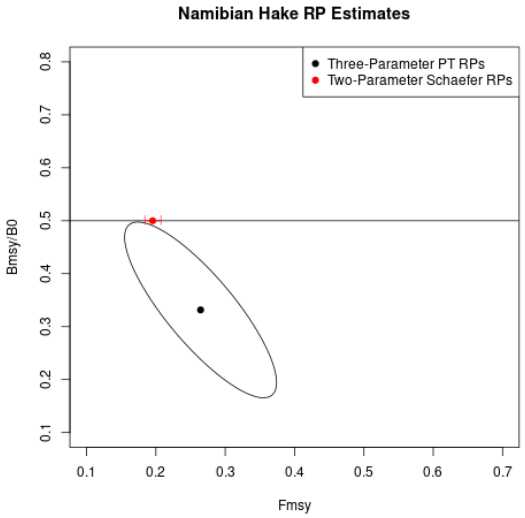

Figure 1.2: Schaefer and PT RP MLEs and associated interquartile confidence regions. The PT curve models the entire two-dimensional RP space shown and the Schaefer model limits RP estimates to the horizontal line at $\frac{B^*}{B(0)} = \frac{1}{2}$.

data have been noted including small sample size, the possible presence of outliers, and changes in the fishing fleet over the modeled period [59, 34, 64]. That said, the use of the Schaefer model here is a classic SPM example and it commonly outperforms more complex models on these data. While the use of the PT model here may well be disputed when compared with the Schaefer model, in many ways the PT model is far more honest about the short-comings of the data in its RP inference. The Schaefer model does not admit many shortcomings in its RP estimates, with unrealistically tight uncertainty bounds in F^*, absolute certainty that $\frac{B^*}{B(0)} = \frac{1}{2}$, and estimating MSY to be about 259 with 95% confidence bounds ranging from 243 to 274. The fact that the PT curve can model $\frac{B^*}{B(0)}$ more generally than the Schaefer model lets the PT model reflect the shortcomings of these data to provide a more honest representation of RP estimates with wider uncertainty bounds as seen in Figure (1.2). Under the PT model MSY is estimated very similarly at 254 (verse the Schaefer model's 259) but with wider 95% confidence bounds ranging from 185 to 270. These models make similar point estimates of MSY, but understand the role of F^* differently by allowing $\frac{B^*}{B_0}$ to be estimated. Even with the small size of these data and the additional parameters of the PT, the PT model demonstrates evidence to explore models that allow $\frac{B^*}{B(0)}$ to be estimated below $\frac{1}{2}$, with only a 10% confidence that $\frac{B^*}{B(0)} \geq \frac{1}{2}$ marginally.

The bias-variance trade-off [63] makes it clear that the addition of a third parameter in the production function will necessarily reduce estimate bias. However the utility of

this bias reduction is still under debate because the particular mechanisms and behavior (direction and magnitude) of these biases for key management quantities are not fully understood or described [51]. Lee et. al. [39] provide some evidence that estimation of productivity parameters are dependent on changes in biomass trends through time (i.e. contrast) as well as model specification. Conn et. al. [11] come to similar conclusions via calibration modeling techniques. These studies indicate important factors that contribute to inferential failure. However they do not offer mechanisms of model failure, nor do their experimental designs allow for the control of different types of model misspecification.

In Chapters (2) and (3) of this thesis I consider the behavior of RP inference when index data are simulated from three-parameter PT and Schnute models of productivity, but the simulated data are fit using intentionally misspecified two-parameter Schaefer and BH models respectively. RP inference is simulated in the SPM setting, and the results are then extended to the context of models that include individual growth and maturity by developing a Schnute DDM in Chapter (4). In each simulation setting equations for RPs and associated quantities under the three-parameter models are derived. Under the PT model simulation design is entirely analytical. Under the Schnute model fully analytical designs are not possible. Thus in Chapter (3) a method is presented for generating simulation designs under the Schnute model that is based on the parametric form of RPs, but does not require analytical inversion of RPs. In Chapter (2) a Gaussian

Process (GP) metamodel [26, 56] is constructed for the analysis of Schaefer RP biases, and in Chapters (3) and (4) this model is extended for the exploration of BH RP biases in each of the SPM and DDM settings.

A key insight of this approach is that bias is considered broadly across RP-space to uncover patterns and correlations between RPs. Developing simulation designs broadly over RP space serves as a necessary control on the nature of the simulated model misspecification that other studies have not considered. Furthermore, the GP metamodel used to analyze RP biases is explicit about trade-offs between RPs so as to inform the full utility of reducing bias, as well as to suggest mechanisms for understanding what causes bias. Additionally, the effect of contrast on estimation is considered together with model misspecification.

Chapter 2

The Schaefer Model and

Pella-Tomlinson Generalization

2.1 Introduction

The Schaefer model is a canonical model in fisheries. The basis of the Schaefer model is ripe with debate [38], and the debate continues within modern fisheries modeling [57, 45, 58]. While the Schaefer model is based on a nonlinear ODE, it still manages to retain an appealing simplicity and instructive interpretability. The nonlinearity of the model gives the model its conceptual relevance to the biological systems, while retaining an approachable quadratic form that allows much of the analysis of the model to be closed form.

The Schaefer model is formed by choosing P, from Eq. (1.2), to be the logistic production function [43] parameterized by $\boldsymbol{\theta} = [r, K]$ so that the family of production functions take the following form,

$$P(B; [r, K]) = rB\left(1 - \frac{B}{K}\right). \tag{2.1}$$

r is a parameter controlling the maximum rate of net population growth (biomass production) for a population in the absence of competition for resources (i.e. the slope of production function at the origin). K is the so-called "carrying capacity" of the population. In this context the carrying capacity can be formally stated as steady state biomass in the absence of fishing (i.e. $\bar{B}(0) = K$). The model is typically stated without natural mortality, M, so that $Z(t) = F(t)$ (Appendix (B) shows a slightly more complicated

case where M may be included explicitly). The typical form of the model makes the logistic production interpretable as modeling surplus biomass production directly, and thus RPs may be visualized directly on the logistic curve.

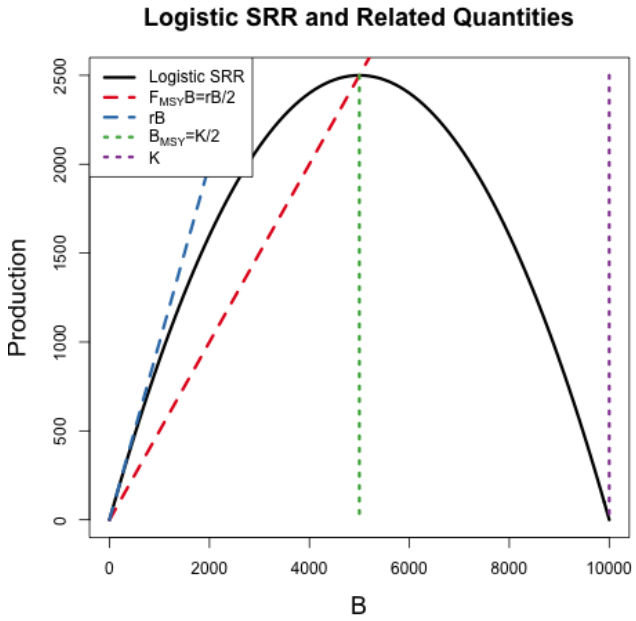

Figure 2.1:
The logistic production function in black plotted with depictions of the key biological parameters and reference points. The slope at the origin (and thus r) is shown in blue, catch resulting in MSY in red, biomass at MSY in green, and K in purple at the right x-intercept. MSY is seen at the peak of the parabola, and is attained with a fishing rate of $\frac{r}{2}$ and biomass equilibrating to $\frac{K}{2}$.

The logistic production function produces idealized parabolic production with RPs taking very simple forms that can be easily understood from the graphical construction seen in Figure (2.1). Positive productivity is observed when $B \in (0,K)$. Due to the parabolic shape of the logistic production function it is straightforward to see that yield is maximized by fishing the stock down to B^*, where the stock attains its peak productivity. By symmetry of the logistic parabola it is clear that this peak occurs at $B^* = \frac{K}{2}$. The fishing rate required to hold the stock at MSY is $F^* = \frac{r}{2}$, which is half of the stock's maximum rate of productivity. MSY is then the product of F^* and B^*so that $MSY = \frac{rK}{4}$.

While this idealized form is instructive, and convenient, these simplistic dynamics are also potentially problematic. The symmetry of the logistic functional form that provides its relatively straight-forward RP analysis also assumes very rigid dynamics. It assumes dynamics at smaller population sizes ($B \in (0, \frac{K}{2})$) mirror the dynamics of larger population sizes ($B \in (\frac{K}{2}, K)$). Maunder [45] argues that the Schaefer model is insufficient in large part due to the restriction it places on $\frac{B^*}{\bar{B}(0)}$, at $\frac{1}{2}$, and further argues that the three parameter Pella-Tomlinson (PT) model [55] should replace the Schaefer model to avoid biased parameter estimates.

The PT model is a three-parameter generalization of the Schaefer model that uses its extra parameter to explicitly control the location of $\frac{B^*}{\bar{B}(0)}$. In doing so, the PT model can model the entire space of RPs and does so in a way that retains much of the analytical appeal of the Schaefer model. While there are some oddities of the functional form [61, 21], the model has been very useful in generalizing the analysis of RPs [84].

In this chapter the PT model is used to generate index data simulated broadly in RP-space but fit with an intentionally misspecified Schaefer model. This parameterizes a broad set of misspecified situations for the Schaefer model where the simulated data have well understood dynamics in the fisheries community. A GP metamodel of the simulation is developed to demonstrate how misspecification of the Schaefer model forms biases in RP estimation. First, analytical expressions for RPs are derived under the PT model for use in deriving a fully analytical simulation design. Next, a GP

metamodel is developed and catch is parameterized in terms of contrast to demonstrate how the nature of bias is controlled by the information content in the data.

2.2 Methods

2.2.1 Model

The three-parameter Pella-Tomlinson (PT) family has a convenient form that includes, among others [23, 64], the logistic production function as a special case. PT production function is parameterized so that $\boldsymbol{\theta} = [r, K, \gamma]$ and the family takes the following form,

$$P_p(B; [r, K, \gamma]) = \frac{rB}{\gamma - 1}\left(1 - \left(\frac{B}{K}\right)^{(\gamma-1)}\right). \quad (2.2)$$

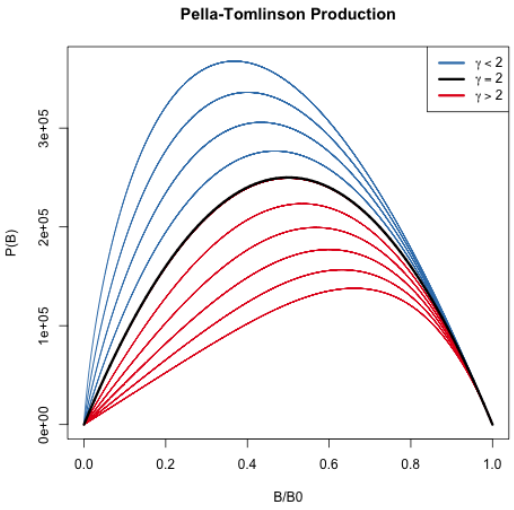

Figure 2.2: The Pella-Tomlinson production function plotted across a variety of parameter values. The special case of logistic production is shown in black, and the left-leaning and right-leaning regimes are shown in blue and red respectively.

The parameters r and K maintain the same interpretation as they do in the logistic production function. γ is a parameter which breaks PT out of the restrictive symmetry of the logistic curve. In this parameterization $\gamma \in (1, \infty)$, with the logistic model appearing in the special case of $\gamma = 2$ (the Fox

model [23] appears as a limiting case as $\gamma \to 1$). In Figure (2.2) PT production is shown for a range of parameter values so as to demonstrate the various productivity shapes that can be achieved under the PT model.

While the form of the PT curve produces some limitations [61, 21] importantly the introduction of a third parameter allows enough flexibility to fully describe the space of RPs. To see this, the reference points are analytically derived for the PT model below.

2.2.2 Reference Points

With $B(t)$ representing biomass at time t, under PT production, the dynamics of biomass are defined by the following ODE,

$$\frac{dB}{dt} = \frac{rB}{\gamma - 1}\left(1 - \left(\frac{B}{K}\right)^{\gamma - 1}\right) - FB. \tag{2.3}$$

An expression for the equilibrium biomass is attained by setting Eq (2.3) equal to zero, and rearranging the resulting equation to solve for B. Thinking of the result as a function of F gives,

$$\bar{B}(F) = K\left(1 - \frac{F(\gamma - 1)}{r}\right)^{\frac{1}{(\gamma - 1)}}. \tag{2.4}$$

At this point it is convenient to notice that $\bar{B}(0) = K$. The expression for B^* is given by evaluating Eq (2.4) at F^*. To get an expression for F^*, the equilibrium yield is

maximized with respect to F,

$$F^* = \underset{F}{\operatorname{argmax}}\, F\bar{B}(F). \tag{2.5}$$

In the case of PT production this maximization can be done analytically, by differentiating the equilibrium yield with respect to F as follows,

$$\frac{d\bar{Y}}{dF} = \bar{B}(F) + F\frac{d\bar{B}}{dF} \tag{2.6}$$

$$\frac{d\bar{B}}{dF} = -\frac{K}{r}\left(1 - \frac{F(\gamma-1)}{r}\right)^{\frac{1}{\gamma-1}-1}. \tag{2.7}$$

Setting Eq (2.6) equal to 0, substituting $\bar{B}(F)$ and $\frac{d\bar{B}}{dF}$ by Equations (2.4) and (2.7) respectively, and solving for F produces the following expression for the fishing rate required to produce MSY,

$$F^* = \frac{r}{\gamma} \tag{2.8}$$

Plugging the above expression for F^* back into Eq (2.4) gives the following expres-

sion for biomass at MSY,

$$B^* = K\left(\frac{1}{\gamma}\right)^{\frac{1}{\gamma-1}}. \tag{2.9}$$

The above derived expressions for $\bar{B}(0)$, B^*, and F^* can then be used to build a specific analytical form for the biological reference points in terms of only productivity parameters.

$$F^* = \frac{r}{\gamma} \qquad\qquad \frac{B^*}{\bar{B}(0)} = \left(\frac{1}{\gamma}\right)^{\frac{1}{\gamma-1}} \tag{2.10}$$

2.2.3 Simulation

Generating simulated indices of abundance from the PT model requires inverting the relationship between $\left(F^*, \frac{B^*}{\bar{B}(0)}\right)$, and (r,γ). It is not generally possible to analytically invert this relationship for many three-parameter production functions [61, 71]. Most three-parameter production functions lead to RPs that require expensive numerical methods to invert; more over the numerical inversion procedure can often be unstable. That said, for the case of PT this relationship is analytically invertible, and leads to

the following relationship

$$r = \gamma F^* \qquad\qquad \gamma = \frac{W\left(\frac{B^*}{\bar{B}(0)}\log\left(\frac{B^*}{\bar{B}(0)}\right)\right)}{\log\left(\frac{B^*}{\bar{B}(0)}\right)}. \tag{2.11}$$

Above W is the Lambert product logarithm function [40, 13]. More details about this derivation, and the Lambert product logarithm, are given in Appendix (A).

Using Eq. (2.11) to obtain production parameters, a PT production model can be fully defined for any combination of the RPs F^* and $\frac{B^*}{\bar{B}(0)}$. Since $\bar{B}(0)$ alone does not enter the RP calculation its value is fixed arbitrarily at 10000.

Indices of abundance are simulated from the three-parameter PT production model broadly over the space of F^* and $\frac{B^*}{\bar{B}(0)}$ via a space filling design as described in Section (2.2.4). A small amount of residual variation, $\sigma = 0.01$ in Eq. (1.1), is added to the simulated index, and these data are then fit with a Schaefer model, at various degrees of misspecification, so as to observe the effect of productivity model misspecification upon RP inference. Tests were performed with larger values of σ leading to similar overall results albeit requiring substantially more simulation runs.

2.2.4 Latin Hypercube Design

The goal of the space-filling design in this setting is to extend the notion of the random sample (and its desirable parameter estimation properties) across the simulated RP

domain so as to represent the simulated space as well as possible [26]. The simple random sample is the classical approach to unbiased parameter estimation, however simple randomness is patchy, often sampling some regions of design space quite densely, while leaving other regions of design space empty. Space-filling designs aim to preserve (or enhance) parameter estimation properties across the simulated domain [18, 79], while constraining samples to be spread over the entire space. Latin Hypercube Sampling [47, LHS] is among the most foundational methods of generating the designs for use in computer experiments. A Latin Hypercube Design [67, LHD] is thus an experimental design based on a LHS.

A LHS of size n distributes samples so as to spread points across a design region in a broadly representative way. A LHD extends the notion of a univariate random uniform sample across multiple dimensions so that each margin of the design space enjoys a uniform distribution. LHDs achieve this notion of uniformity by first partitioning each dimension of the design space into regular grids of size n. By intersecting the grids of each dimension, cells are produced that evenly partition the design space. In two dimensions n^2 cells are produced, from which a total of n samples are taken. Crucially only one point is randomly sampled from a given element of each grid in each dimension so as to reduce clumping of the n samples across the design space.

In the 2 dimensional space defined by the PT RPs a LHD is defined by first letting $\mathcal{F}$ and $\mathcal{B}$ be regular grids, of size $n = 150$, on $F^* \in (0.1, 0.7)$ and $\frac{B^*}{B_0} \in (0.2, 0.6)$

respectively. A LHS, of size 150, is then collected among the cells produced by $\mathcal{F} \times \mathcal{B}$.

Each of the sampled locations represent a unique PT model with the sampled RP values. Since the relationship mapping RPs analytically to productivity parameters can be found for the PT model, LHS designs for the PT model are computed directly in RP space and Eq. (2.11) is used to map the sampled RP design locations to PT productivity parameters.

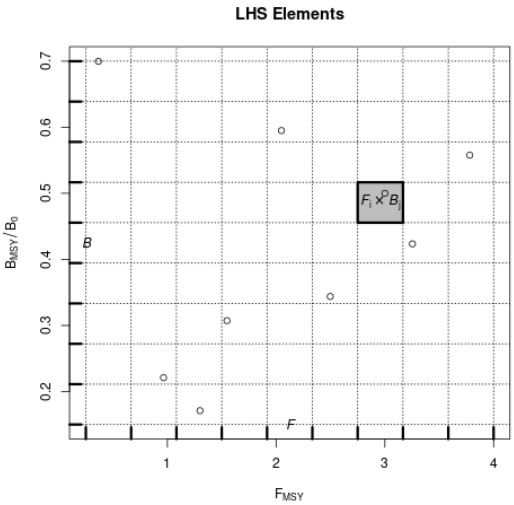

Figure 2.3: LHS grids with n=9. Intersecting $\mathcal{F}$ and $\mathcal{B}$ produces n^2 cells; a particular cell $\mathcal{F}_i \times \mathcal{B}_j$ is shown in grey. One point is in each of the marginal $\mathcal{F}_i$ and $\mathcal{B}_j$ grid elements.

2.2.5 Gaussian Process Metamodel

At its core, a metamodel is simply a model of some mapping of inputs to outputs (the mapping itself is typically defined by a computer model) [66]. By modeling the mapping with a statistical model (that explicitly defines the relevant features of the mapping) a metamodel defines a specific ontology for the mapping. By simulating examples of the mapping, the inferential infrastructure of the statistical model is used to empirically learn an effective emulation of the mapping within the ontology defined

by the statistical model [26]. The predictive infrastructure of the statistical model is then useful as an approximate abstraction of the system itself to better understand the system through further data collection, cheap approximation of the mapping, and/or study of the mapping itself [24].

In this setting, the aim of metamodeling is to study how well RPs are inferred when typical two-parameter models of productivity are misspecified for populations that are actually driven by more complicated dynamics. Thus the goal of metamodeling in this setting is not typical Bayesian calibration [37] of RPs, but rather to aid in the description (and simulation) of RP model misspecification consequences. Correcting these RP biases is clearly a goal, but the best estimates of RPs will likely be come from using the understanding developed by these metamodels to inform better, and more adequately flexible, models of productivity directly.

To that end the simulation design, $\boldsymbol{X}$, provides a sample of different population dynamics that are driven by three-parameter production functions broadly in RP space. By simulating index of abundance data from the three parameter model, and fitting those data with the two-parameter production model, we observe particular instances of how well RPs are inferred at the given misspecification of the two-parameter model relative to the true three-parameter production model. By gathering all of the simulated instances of how RPs are inferred under the two-parameter model, we form a set of example mappings to train a metamodel which represents the mapping of true RPs

(under the three-parameter model) to estimates of RPs under the misspecified two-parameter production model. The metamodel is essentially a surrogate for inference under the misspecified two-parameter production model that controls for the specific degree of model misspecification.

A flexible GP model is assumed for the structure of the metamodel to describe the mapping of RPs under misspecified two-parameter models of productivity. A GP is a stochastic process generalizing the multivariate normal distribution to an infinite dimensional analog. GP models are often specified primarily through the choice of a covariance (or correlation) function which defines the relationship between locations in the input space. Typically correlation functions are specified so that inputs closely related in space result in correlated effects in the model. In this setting the inputs to the GP metamodel are RPs from the full theoretical range of RPs under the three-parameter production model.

Indices of abundance are generated from three-parameter models; by fitting these data with the restricted two-parameter model maximum likelihood estimates (MLE; and associated estimation uncertainty) of each of the productivity parameters, and thus RPs, are obtained. To simplify the specification of the metamodel, let $\mathbf{y}$ be a vector collecting the fitted MLEs for $\log(F^*)$, and let $\boldsymbol{\omega}$ be a vector of estimates of the estimator variances (via the inverted Fisher information) at each $\mathbf{y}$. The transformed RP estimates are then modeled using the following GP metamodel.

$$\begin{aligned} \mathbf{y} &= \beta_0 + \boldsymbol{X}\boldsymbol{\beta} + \boldsymbol{v} + \boldsymbol{\epsilon} \\ \boldsymbol{v} &\sim N_n(\mathbf{0}, \tau^2 \boldsymbol{R}_\ell) \\ \boldsymbol{\epsilon} &\sim N_n(\mathbf{0}, \boldsymbol{\omega}' \boldsymbol{I}) \end{aligned} \tag{2.12}$$

$\boldsymbol{X}$ is the n x 2 LHS design matrix of RPs for each simulated three-parameter data generating model as described in Section (3.2.3.1). $\boldsymbol{\epsilon}$ models independent normally distributed error, which provides an ideal mechanism for propagating uncertainty from inference in the simulation step into the metamodel. By matching each y_i with an observed ω_i variance term, $\boldsymbol{\epsilon}$ serves to down weight the influence of each y_i in proportion to the inferred production model sampling distribution uncertainty. This has the effect of smoothing the GP model in a way similar to the nugget effect [28], although the application here models this effect heterogeneously.

The term, $\boldsymbol{v}$, contains spatially correlated GP effects. The correlation matrix, $\boldsymbol{R}_\ell$ describes how RPs close together in the simulation design are more correlated than those that are far away. This spatial effect is modeled with a squared exponential correlation function,

$$R(\boldsymbol{x}, \tilde{\boldsymbol{x}}) = \exp\left(\sum_{i=1}^{2} \frac{-(x_i - \tilde{x}_i)^2}{2\ell_j^2} \right). \tag{2.13}$$

R has an anisotropic separable form which allows for differing length scales, ℓ_1

and ℓ_2, in the different RP axes. The flexibility to model correlations separately in the different RP axes is key due to the differences in the extent of the RP domains marginally. The matrix $\boldsymbol{R}_\ell$ is filled out by evaluating the correlation function R at each pairwise combination of simulated design locations. The metamodel parameters β_0, $\boldsymbol{\beta}$, τ^2, ℓ_1 and ℓ_2 are fit via MLE against the observations $\mathbf{y}$, $\boldsymbol{X}$, and $\boldsymbol{\omega}$ from simulation fits.

Fitting the metamodel allows for a full predictive description of inference under the misspecified two-parameter model. Predictive estimates are obtained via kriging [14]

$$\hat{y}(\mathbf{x}^\star) = \beta_0 + \mathbf{x}^\star\boldsymbol{\beta} + \mathbf{r}(\mathbf{x}^\star)'\boldsymbol{R}_{\boldsymbol{\ell}}^{-1}\Big(\mathbf{y} - \big(\beta_0 + \boldsymbol{X}\boldsymbol{\beta}\big)\Big) \tag{2.14}$$

$\hat{y}(\mathbf{x}^\star)$ is the metamodel's predicted value of the modeled $\log(RP)$ estimates under the two-parameter production model, when the index of abundance is generated from the three-parameter production model at RP location $\mathbf{x}^\star$. Finally, $\mathbf{r}(\mathbf{x}^\star)$ is a vector-valued function of correlation function evaluations for the predictive location $\mathbf{x}^\star$ against all observations in $\boldsymbol{X}$(i.e. $\mathbf{r}(\mathbf{x}^\star) = \boldsymbol{R}(\mathbf{x}^\star, \boldsymbol{x}_i)\ \forall\ \boldsymbol{x}_i \in \boldsymbol{X}$).

Recall that under the Schaefer model $\frac{B^*}{B(0)} = 0.5$; by transforming metamodel predictions of $\log(F^*)$ back to F^*, metamodeled predictions of Schaefer RPs are obtained. By further subtracting the PT RPs from these predicted Schaefer RPs at each point in RP space a pattern of RP estimation biases, induced by model misspecification of the Schaefer model, can be visualized as will be seen in Figure (2.6).

In order to investigate metamodeled bias surfaces for B^* or MSY individually it is necessary to separate the quantity B^* from the ratio $\frac{B^*}{B_0}$. In order to do this, the additional metamodeled quantity $\log(B_0)$ was considered using the same structure as seen in this section. Ultimately those results were found to be consistent with the results presented throughout and thus were not included.

2.2.6 Catch

It is known that contrast in the observed index and catch time series can effect inference on the productivity parameters [32]. In this setting contrast refers to changes in the long term trends of index data. Figure (2.4, *right*) demonstrates an example of biomass that includes contrast induced by catch. It is not well understood how contrast may factor into inferential failure induced by model misspecification. Thus catch is parameterized so as to allow for a spectrum of possible contrast simulation settings.

Catch is parameterized so that $F(t)$ can be controlled with respect to F^*. Recall that catch is assumed to be proportional to biomass, so that $C(t) = F(t)B(t)$. To control $F(t)$ with respect to F^*, $C(t)$ is specified by defining the quantity $\frac{F(t)}{F^*}$ as the relative fishing rate. $B(t)$ is defined by the solution of the ODE, and F^* is defined by the biological parameters of the model. By defining $\frac{F(t)}{F^*}$, catch can then be written as $C(t) = F^* \left(\frac{F(t)}{F^*}\right) B(t)$.

Intuitively $\frac{F(t)}{F^*}$ describes the fraction of F^* that $F(t)$ is specified to for the current

$B(t)$. When $\frac{F(t)}{F^*} = 1$, $F(t)$ will be held at F^*, and the solution of the ODE brings $B(t)$ into equilibrium at B^*. When $\frac{F(t)}{F^*}$ is held constant in time biomass comes to equilibrium as an exponential decay from K approaching B^*. When $\frac{F(t)}{F^*} < 1$, $F(t)$ is lower than F^* and $B(t)$ is pushed toward $\bar{B} > B^*$. Contrarily, when $\frac{F(t)}{F^*} > 1$, $F(t)$ is higher than F^* and $B(t)$ is pushed toward $\bar{B} < B^*$; the precise values of $\bar{B}$ can be calculated from the steady state biomass equations provided above and depend upon the specific form of the production function.

For the simulations presented here, a family of fishing behaviors are considered where the fishing rate accelerates as technology and fishing techniques improve rapidly until management practices are applied, which ultimately brings fishing into equilibrium at F^*. This is parameterized as three distinct phases, over a total of 45 units of time, with each phase lasting 15 time units. The specific form is given below.

$$\frac{F(t)}{F^*} = ae^{bt}\mathbf{1}_{0\leq t<15} + (d-ct)\mathbf{1}_{15\leq t<30} + \mathbf{1}_{30\leq t\leq 45} \tag{2.15}$$

The first term of Eq (2.15) is an exponential increase in fishing, the second term is a linear decline in relative fishing as initial management practices are applied, and the third term, $\mathbf{1}_{30\leq t\leq 45}$, simply holds the fishing rate at F^* there after. These three phases are controlled by the four parameters a, b, c, and d. By enforcing that the interface of the phases meet at χ_{max} and 1 respectively the relative fishing series is reduced to a

two-parameter family.

$$a = e^{\log(\chi_{max})-15b} \qquad b = \frac{1}{t-15}\log\left(\frac{\chi_{min}}{\chi_{max}}\right) \tag{2.16}$$

$$c = \frac{\chi_{max}-1}{15-1} \qquad d = 15c+\chi_{max} \tag{2.17}$$

By further specifying $\chi_{max} = 1.6^{\chi}$ and $\chi_{min} = 0.4^{\chi}$ the two-parameters χ_{max}, and χ_{min} can be reduced to the single parameter χ. The tuning parameter χ then singularly controls contrast that appears in time series data. The constants 1.6 and 0.4 may be tuned to simulate more or less contrast, however the values chosen should be > 1 and < 1 respectively and should be chosen in coordination with the number of simulated epochs so at to avoid introducing an aliasing effect between the index sampling frequency and the higher frequency (i.e. sharp) features induced by fishing [74, 48]. For the 45 epoch simulation presented here the constants 1.6 and 0.4 are tuned to avoid aliasing high contrast features of index samples in the most dramatic simulations. By increasing the sampling frequency, or number of simulated time periods, the constants may be increased/decreased accordingly.

When $\chi = 0$, the relative fishing rate is a constant at 1 to create a low contrast simulation environment. As χ increases Eq (2.15) induces more and more contrast in the observed index and catch time series until $\chi = 1$ which produces a high contrast simulation environment. Figure (2.4) demonstrates a spectrum of contrast simulation

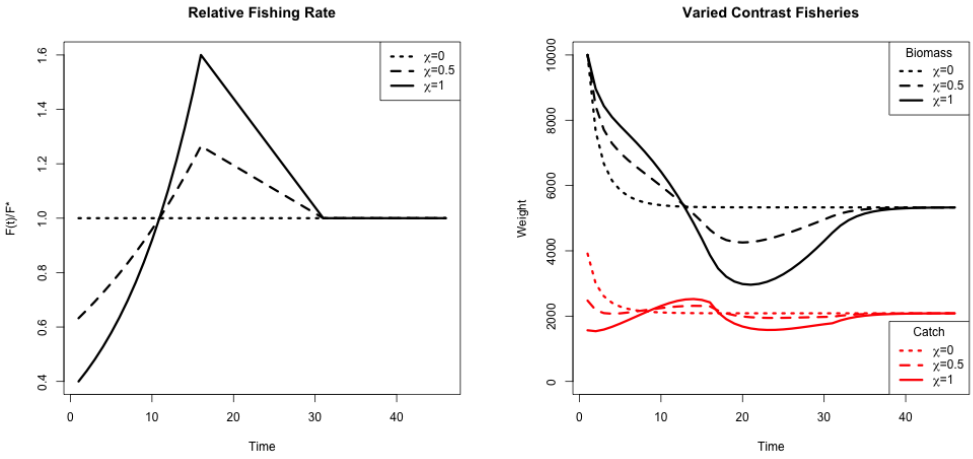

Figure 2.4: (*left*) Relative fishing with low, medium, and high contrast. (*right*) Population biomass and catch at each associated level of contrast.

environments as well as the time series data they induce in the solution of the production model ODE.

2.2.7 Two-Parameter Production Model Inference

The simulated mapping results from fitting an intentionally misspecified two-parameter production model to index of abundance data that are generated from a more complex three-parameter model of productivity. Thus, let I_t be an index of abundance simulated from the three-parameter PT model at time $t \in \{1,2,3,...,T\}$. However the fitted model is specified to be intentionally misspecified so that the fitted model is driven by a two-parameter Schaefer model.

The observation model for the fitted model is log-normal such that,

$$I_t|q,\sigma^2,\boldsymbol{\theta} \sim LN(qB_t(\boldsymbol{\theta}),\sigma^2). \tag{2.18}$$

$B_t(\boldsymbol{\theta})$ is defined by the solution of the ODEs defined by the Schaefer model with $\boldsymbol{\theta} = [r,K]$. From the perspective of the fitted model, the observed I_t are assumed independent conditional on q, σ^2, r, K and the two-parameter ODE model for biomass. Thus the log likelihood can be written as

$$\log \mathcal{L}(q,\sigma^2,\boldsymbol{\theta};I) = -\frac{T}{2}\log(\sigma^2) - \frac{1}{2\sigma^2}\sum_t \log\left(\frac{I_t}{qB_t(\boldsymbol{\theta})}\right)^2. \tag{2.19}$$

In this setting q is fixed at 0.0005 to focus on the inferential effects of model misspecification on biological parameters. Furthermore, estimating both q and K introduces identifiability issues in low contrast settings since both parameters are responsible for setting the scale of dynamics. In low contrast settings when $B_t \approx \bar{B}(\boldsymbol{\theta})$ for most t, the product $qB_t(\boldsymbol{\theta})$ is essentially $q\bar{B}(\boldsymbol{\theta})$. In turn, $q\bar{B}(\boldsymbol{\theta})$ can be written as $qK(1-F/r)$ to reveal the product qK. Since the likelihood will take the same value when swapping the values of K and q in these cases, only their product may be identified. This identifiability issue may be resolved by adding informative priors (i.e. essentially choosing a value for one of the parameters), or by adding enough contrast so as to inform the cor-

relation structure between the rest of the model parameters well enough to indirectly inform K and q individually.

Beyond these identifiability issues, the parameters σ^2 and $\boldsymbol{\theta}$ are reparameterized to the log scale and fit via MLE. Reparameterizing the parameters to the log scale improves the reliability of optimization, in addition to facilitating the use of Hessian information for estimating MLE standard errors. Given that the biological parameters enter the likelihood via a nonlinear ODE, and further the parameters themselves are related to each other nonlinearly, the likelihood function can often be difficult to optimize. A hybrid optimization scheme is used to maximize the log likelihood to ensure that a global MLE solution is found. The R package GA [72, 73] is used to run a genetic algorithm to explore parameter space globally. Optimization periodically jumps into the L-BFGS-B local optimizer to refine optima within a local mode. The scheme functions by searching globally, with the genetic algorithm, across many initial values for starting the local gradient-based optimizer. The genetic algorithm serves to iteratively improve hot starts for the local gradient-based optimizer. Additionally, optimization is only considered to be converged when the optimum results in an invertible Hessian at the found MLE.

2.2.8 Continuous Model Formulation

An important (and often overlooked) implementation detail is the solution to the ODE which defines the progression of biomass through time. As a statistical model it is of paramount importance that this ODE not only have a solution, but also that the solution be unique. Of primary concern, uniqueness of the ODE solution is necessary for well conditioned inference.

If the form of $\frac{dB}{dt}$ is at least Lipschitz continuous, then the Cauchy-Lipschitz-Picard theorem provides local existence and uniqueness of $B(t)$. Recall from Eq(1.2) that $\frac{dB}{dt}$ is separated into a term for biomass production, $P(B)$, and a term for removals, $Z(t)B(t)$. For determining Lipschitz continuity of $\frac{dB}{dt}$, the smallest Lipschitz constant of $\frac{dB}{dt}$ will be the sum of the constants for each of the terms $P(B)$ and $Z(t)B(t)$ separately. Typically any choice of $P(B)$ will be continuously differentiable, which implies Lipschitz continuity. At a minimum $Z(t)$ typically contains fishing mortality as a function of time $F(t)$ to model catch in time as $C(t) = F(t)B(t)$. $Z(t)$ may or may not contain M, but typically M is modeled as stationary in time and does not pose a continuity issue, unlike some potential assumptions for $C(t)$.

In practice $C(t)$ is determined by a series of observed, assumed known, catches. Catch observations are typically observed on a subannual basis, but in practice may not be complete for every epoch of the modeled period. It is overwhelmingly common to discretize the ODE in time. This is often computationally convenient when the underly-

ing species dynamics are reasonably well behaved, however when the dynamics model is used as a statistical model, with the goal of inferring the behavior of the underlying species dynamics, the regularity of the dynamics are not guaranteed. An implicit assumption of continuity of catch in time provides the necessary regularity for the statistical model. Furthermore a continuous handling of the dynamics provides improved accuracy in evaluating the ODE, particularly when inferring productivity parameters which largely control the regularity of the dynamics.

While there are many ways to handle catch continuity, here I assume that catches accrue linearly between observed catches. This assumption defines the catch function as a piecewise linear function of time, with the smallest Lipschitz constant for the catch term defined by the steepest time segment of the catch function. This assumption represents one of the simplest ways of handling catch, while retaining Lipschitz continuity overall. Furthermore linearly interpolated catch is adequately parsimonious for the typical handling of catches.

2.2.8.1 Integration and Stiffness

As previously mentioned, the overwhelming majority of implementations of stock assessment models discretize the ODE with the integration step sized fixed so as to match the observation frequency. In this setting we investigate model parameterizations that explore the full extent of biologically relevant reference points. This exercise

produces some combinations of parameters that result in numerically stiff ODEs.

The concept of stiffness in ODEs is hard to precisely characterize. Hairer and Wanner [83, p.2] describe stiffness in the following pragmatic sense, "Stiff equations are problems for which explicit methods don't work." It is hard to make this definition more mathematically precise, but due to the explicit discretization of the ODE this is a consistent issue for models of very productive species in the low contrast simulations. In these stiff regions it is necessary to integrate the ODE with an implicit integration method.

Several of the most common implicit methods were tried including the Livermore Solver for ODEs (lsode), and the Variable Coefficient ODE Solver (vode) as implemented in the deSolve package of R [76]. The difference between implicit solvers is negligible, while explicit methods result in wildly varying solutions to the ODE in stiff regions of parameter space. Results shown here are computed using the lsode integration since it runs relatively quickly and has a relatively smaller footprint in system memory.

2.3 Results

2.3.1 An *MSY*-Optimal Catch History

When $F(t)$ is held constant at F^*, as it is in the "low contrast" simulation setting, $B(t)$ comes to equilibrium as an exponential decay from K to B^*. Understanding model misspecification bias is simplified in this setting due to the relative simplicity that this induces in $B(t)$. However this simplicity is known to poorly inform estimates of r, and thus F^*, due to the limited range of the production function that is observed [32].

Figure (2.5) shows four of the most misspecified example production function fits as compared to the true data generating PT production functions. The rug plots below each set of curves show how the observed biomasses decay exponentially from K to B^* in each case. In particular, notice how observations only exist where the PT biomass is greater than B^*. Due to the leaning of the true PT curves, and the symmetry of the logistic parabola, the logistic curve only observes information about its slope at the origin

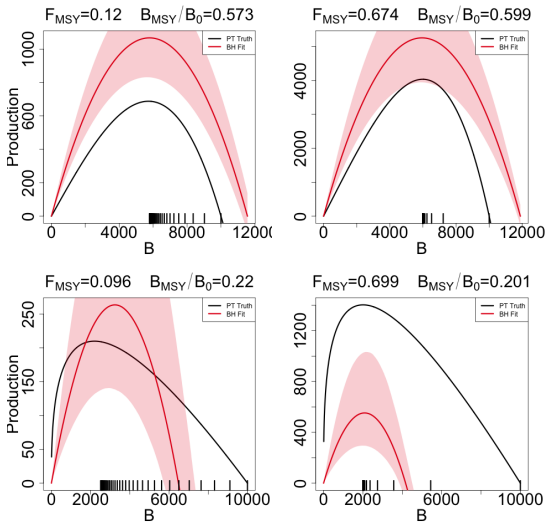

Figure 2.5: A comparison of the true PT production function (in black) and the estimated logistic curve (in red) with 95% CI shown. The examples shown represent the four corners of maximum model misspecification in the simulated RP-space. Observed biomasses are plotted in the rug plots below the curves.

from data observed on the right portion of the PT curves. The top two panels of Figure (2.5) show PT data generated such that $\frac{B^*}{\bar{B}(0)} > 0.5$; in these cases PT is steeper to the right of B^* than it is on the left, and so the the logistic curve overestimates r, and consequently also overestimates F^*. The bottom two panels of Figure (2.5) show PT data generated with $\frac{B^*}{\bar{B}(0)} < 0.5$ and where the vice versa phenomena occurs. PT is shallower to the right of B^* than it is on the left and so the logistic parabola estimate tends to underestimate F^*.

2.3.2 Metamodeled Trends

Each point in the space of the RPs F^* and $\frac{B^*}{\bar{B}(0)}$ uniquely identifies a complete PT model with different combinations of parameters values. Recall that when $\gamma = 2$ for the PT model, the PT curve becomes a parabola and is equivalent to the logistic curve of the Schaefer model. Since the logistic curve is symmetric about B^*, the Schaefer model must fix the value of $\frac{B^*}{\bar{B}(0)}$ at the constant 0.5 for any value of F^*. The line through RP space defined by $\frac{B^*}{\bar{B}(0)} = 0.5 \ \ \forall \ \ F^*$, defines the subset of RP space where $\gamma = 2$ and where the PT model is equivalent to the Schaefer model. For brevity this subset of RP where $\frac{B^*}{\bar{B}(0)} = 0.5$ will be referred to as the "Schaefer set". Thus simulated data that are generated along the Schaefer set will be the only data that are not misspecified relative to the Schaefer model; as PT data are simulated farther and farther away from this line at $\frac{B^*}{\bar{B}(0)} = 0.5$ model misspecification of the Schaefer model becomes worse and worse.

While Figure (2.5) demonstrates a real trend in simulation results, individual simulation runs will at best show jittery trends due to the stochastic nature of statistical inference. The GP metamodel accounts for this stochasticity to focus analysis on the signal in the simulation results.

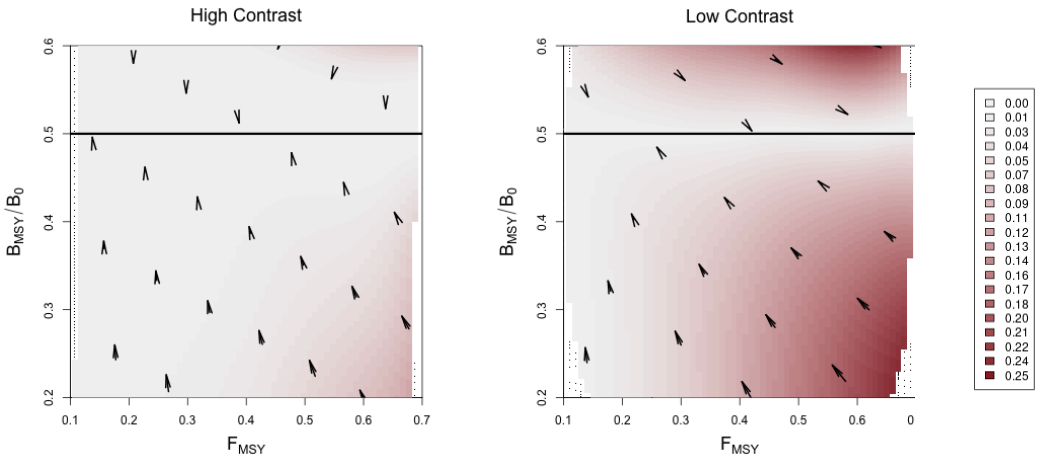

Figure 2.6: Joint bias direction for $(F^*, \frac{B^*}{B_0})$ estimates under the misspecified Schaefer Model. The intensity of color represents the excess bias relative to the shortest possible mapping. Results in the low contrast setting are shown (*right*), and the high contrast setting is shown ($left$).

Figure (2.6) shows the pattern of biases the Schaefer model creates when fit to PT data generated at each point of RP space. An equivalent way to think of Figure (2.6) is the mapping that is created by inferring RPs under a misspecified Schaefer model fit to PT data generated at each point over the pictured region. Since the Schaefer model must estimate RPs in the Schaefer set, the head of each arrow points to the location in the Schaefer set where the metamodel expects the Schaefer model to estimate its RPs. The tail of each arrow indicates the PT data generating RPs, and thus the location of

each arrow specifies a unique misspecification of the Schaefer model. The direction and magnitude of each arrow then indicates the combined bias in the Schaefer model's estimates of F^* and $\frac{B^*}{B_0}$ when measured jointly at each misspecified RP location to fully describe the mapping.

Since $\frac{B^*}{B_0}$ must be 0.5 under the Schaefer model, biases in the $\frac{B^*}{B_0}$ direction must simply map vertically onto the Schaefer set. Due to this simplified RP geometry under the Schaefer model, the degree of bias in $\frac{B^*}{B_0}$ estimation is defined solely by the degree of model misspecification irrespective of F^*. Furthermore, the closest possible point along the Schaefer set that Schaefer model inference could map RPs would be the perfectly vertical mapping. This pattern only contains the strictly necessary bias present in $\frac{B^*}{B_0}$, and zero bias in F^*. Any deviation from this minimal bias pattern is necessarily due to added bias in F^*.

The two simulation settings shown in Figure (2.6) are identical except for the amount of contrast present in the simulated index. The right panel of Figure (2.6) shows RP biases in the low contrast setting, while the left panel shows the high contrast setting. Notice that in the low contrast setting the RP bias pattern is far from the minimum distance mapping, however when contrast is added the mapping becomes much closer to a minimal vertical bias mapping. In the low contrast setting the observed bias is consistent with the pattern and mechanism described in Figure (2.5), where F^* is underestimated for data generated below the Schaefer line and overestimated above the

Schaefer set. In the high contrast simulation the mapping is nearly minimal distance with the exception of PT data generated with simultaneously low $\frac{B^*}{B_0}$ and high F^*.

2.3.3 Contrast & F^* Bias

Figure (2.7) demonstrates how bias in F^* estimation decreases as contrast is added to PT data as generated in the low $\frac{B^*}{B_0}$ and high F^* regime. By including additional contrast F^* bias is decreased. To fully extinguish F^* bias, additional contrast may be added by adjusting the time resolution to commensurately avoid sample aliasing issues as discussed in Section (2.2.6). Furthermore a more complex model of fishing may be necessary.

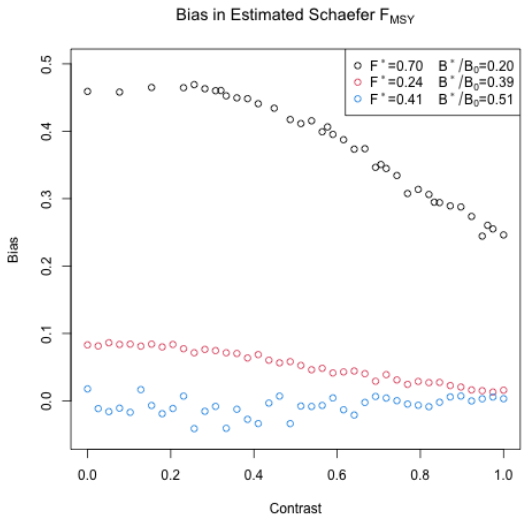

Figure 2.7: Bias in F^* as estimated under the Schaefer model when PT data are generated with increasing contrast at three select RP locations.

2.4 Discussion

The metamodeled trends in RP estimation under the Schaefer model are consistent with what is known about estimating population productivity parameters [39, 11, 42]. These studies focus on productivity parameters, but since RPs in the Schaefer model are entirely determined by population productivity parameters, there is a direct relationship between bias in RPs and productivity parameters. Previous studies do not directly control for the structure of model misspecification and as a result do not come to a complete mechanistic understanding of the model failure they observe. The LHD of this simulation adds to what is known about estimating RPs by organizing model misspecification so as to enlighten the mechanisms of how bias in productivity, and thus RPs, manifest under the Schaefer model. Figure (2.5) demonstrates that the observed RP biases are tied directly to the shape of the data generating PT production function relative to the symmetric case of the Schaefer model; a trend which is more generally described by the metamodel in Figure (2.6).

The metamodeled RP bias trends indicate that the Schaefer model may present systematic management risks that are yet unrecognized. It is understood that the Schaefer model will induce biases in $\frac{B^*}{B_0}$ so as to hold $\frac{B^*}{B_0} = 0.5$ [45, 58], but the structure of biases in F^* estimation is less well understood. These results suggest that populations coming from $\frac{B^*}{B_0} < 0.5$, will tend to have F^* underestimated by the Schaefer model. Complimentary, when the population comes from the RP regime where $\frac{B^*}{B_0} > 0.5$, these

results suggest that F^* is likely to be overestimated by the Schaefer model. The Schaefer model thus poses a risk for populations coming from $\frac{B^*}{B_0} > 0.5$, since overestimation of F^* may lead to management that results in overfishing. For the populations coming from $\frac{B^*}{B_0} < 0.5$ the underestimated F^* would make management based on Schaefer model estimates more conservative with respect to the possibility of overfishing, but would also reduce the expected long-term yield of the fishery. Our ultimate goals in modeling should be to provide an accurate summary of the stock with a complete contextualization of our models' deficiencies. To that end, this work contextualizes RP estimation under the Schaefer model, and suggests that understanding the degree of contrast in index data is important due to its influence on the degree of bias in F^* estimates.

This work reiterates the role of contrast [32] in estimating stock productivity. Since the structure of the Schaefer model does not induce strong correlations between RPs[1], it provides an exceptional modeling environment for understanding the estimation characteristics of F^*. In the presence of contrast, F^* estimation can enjoy very low bias even for a wide range of poorly specified models; conversely in the absence of contrast F^* estimation can suffer very large bias even for slightly misspecified models. This pattern is exemplified in the low-contrast setting where the Schaefer model imposes little a priori structure on F^* and the low contrast index data poorly informs F^*, through r, via a biased view of the upper biomass range of the PT curve. In the high contrast setting

[1] A luxury not granted under the BH model introduced in Chapter (3).

the GP metamodel demonstrates a straightforward vertical mapping of F^*, indicated minimal bias in F^* estimates.

The relative fishing rate parameterized in Section (2.2.6) is broadly representative of many California fisheries [53, 54]. The form used here captures a useful notion of contrast and provides a seamless form that reveals how model failure behaves as contrast is removed from the data. While the relative fishing rate parameterized in Section (2.2.6) captures a useful spectrum of relevant fishing behaviors, it is still limiting in the amount of information that it can induce. Generally improved methods for quantifying contrast in fisheries data, and/or methods of discovering more informative fishing behavior, could improve this analysis.

While the Schaefer model is among the simplest models in fisheries, the concepts it develops form the foundation of models that are commonly used in practice. In the following chapters the dynamics models considered layer in model complexity one piece at a time and the behavior of RP estimation is described in each case so as to understand the influence of each subsequent modeling component.

Chapter 3

The Beverton-Holt Model and

Schnute Generalization

3.1 Introduction

The perspective of Beverton-Holt [4] has been foundational to the structure of modern fisheries models [35]. Evolving from the work of von Bertalanffy [81] (and before that Baranov [3, 75]), alongside the Ricker [65] and Schaefer [68] models, the perspective of Beverton and Holt shaped the following decades of fisheries research. To this day, it is practically incumbent upon many stock assessments in the United States to view the BH model of recruitment as a default [49, 20].

Similarly to the Schaefer model, the Beverton-Holt (BH) model [4] is founded on a notion of density dependence [25] (albeit to a lesser extent). Unlike the Schaefer model, the BH approach to modeling productivity factors the density dependence related to recruitment separately from terms relating to natural mortality in the adult population, behooving a more explicit model of natural mortality [5]. Similarly to the Schaefer model, the derivation of the recruitment relationship assumes that density dependence appears as a quadratic logistic differential equation. However the BH model formulates this as a model of the change in recruitment over time, rather than as a direct model of net productivity as seen in the Schaefer model. They then solve this equation in discrete time and reparameterize to argue for the generality of the resulting recruitment relationship that we use today.

For purposes of this chapter their recruitment relationship is reparameterized as a

production function to model adult biomass production as,

$$P(B) = \frac{\alpha B}{1 + \beta B}. \tag{3.1}$$

The parameter α here has a similar interpretation as the r parameter, from the Schaefer model, in that it represents the slope at the origin of the production function. The β parameter here is also related to K, from the Schaefer model, however the BH model is not parameterized directly in terms of carrying capacity but rather $K \propto \frac{1}{\beta}$. The primary role of β in this parameterization is to scale the population, and β is largely responsible for controlling carrying capacity in practice.

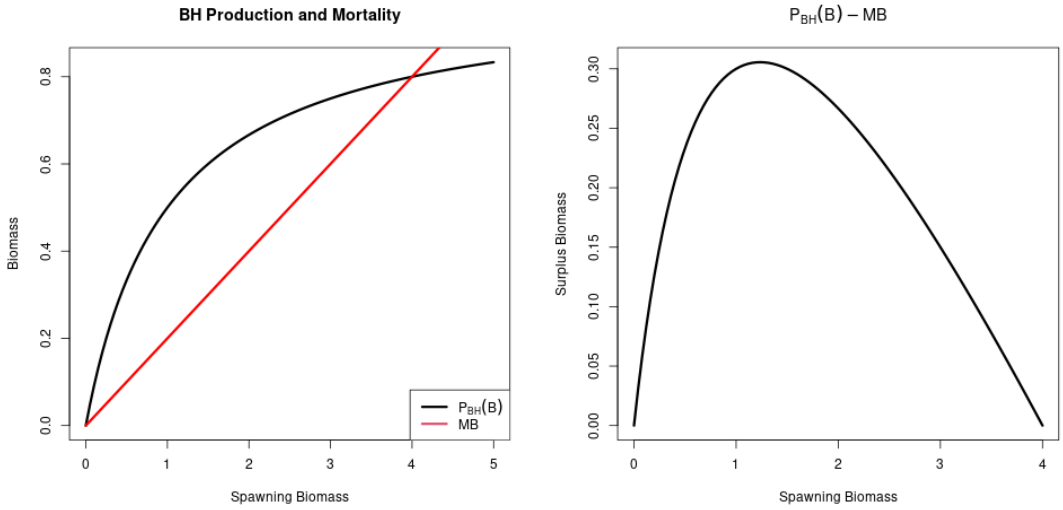

Figure 3.1: (*left*) BH production function plotted along side a linear model of natural mortality. (*right*) Surplus production implied by the combined BH model of production and linear natural mortality.

As seen in Figure (3.1, *left*) the BH model is an asymptoting curve, such that as

$\lim_{B\to\infty} P_{BH}(B) = \frac{\alpha}{\beta}$. This makes the inclusion of an explicit handling of natural mortality, M, pertinent for the modeling of surplus production. In this case, MB represents linear natural mortality, but it also constitutes a replacement line where biological production must exceed this rate of mortality to persist. Figure (3.1, *right*) demonstrates how when the typical linear handling of natural mortality is taken together with the BH model a left-leaning surplus production curve is produced that is reminiscent of PT curves for $\gamma_{PT} < 2$ as can be seen in Figure (2.2).

Under the PT model recall when $\gamma_{PT} \leq 2$ the RPs lie in the lower $\frac{B^*}{B_0} \leq 0.5$ region of RP space. Under the BH model this is also the case, although due to two-parameter form of the BH model, the set of BH RPs is a curve passing through $\frac{B^*}{B_0} \leq 0.5$. Myers et. al. [52], Brooks et. al. [8], and Mangel et. al. [44] show how this limitation arises analytically via steepness. Mangel et. al. [44], further demonstrates the generality of this phenomena, and shows how these functional limitations limit fisheries management based on MSY-based RPs.

Deriso [17] and Schnute [69] developed slightly different (but conceptually equivalent) three-parameter generalizations of the BH model[1]. This model generalizes the BH model by controlling the nature of density dependence; allowing production to increase or decrease beyond that of the BH model for large spawning biomass. The Schnute model not only generalizes the BH model, but in doing so it frees the RP lim-

[1]The later form in [69] is preferred here due its interpretability and the improved regularity of closed form RPs it produces.

itations presented above. The three-parameter Schnute model has the two-parameter BH, Ricker, and Schaefer models, as special cases. Each of the two-parameter models limits RPs similarly to the BH model, but in particular each of them models a different set of RPs. As the Schnute model transitions between these models it takes intermediate forms which can model all of the intervening RPs, thus representing all of the most biologically relevant hypotheses commonly discussed in stock assessments.

In this chapter the Schnute model is used to generate index data simulated broadly in RP-space but fit with an intentionally misspecified BH model. This parameterizes a broad set of misspecified situations for the BH model where the simulated data have well understood dynamics in the fisheries community. A GP metamodel of the simulation demonstrates how misspecification of the BH model forms biases in RP estimation. First, as many as possible of the necessary RP expressions are derived analytically under the Schnute model. The remaining RPs do not have analytical expressions. Therefore, a numerically stable method is then developed that allows an adaptive simulation design to be computed without the remaining closed-form RP expressions. The GP metamodel (as developed in Section (2.2.5)) is then used to demonstrate the nature of RP biases under the BH model.

3.2 Methods

3.2.1 Model

The Schnute production function is a three-parameter generalization of many of the most common two-parameter production functions [17, 69]. It can be written in the following form, with parameters α, β, and γ,

$$P_s(B;[\alpha,\beta,\gamma]) = \alpha B(1-\beta\gamma B)^{\frac{1}{\gamma}}. \tag{3.2}$$

The BH and Logistic production functions arise when γ is fixed to -1 or 1 respectively. The Ricker model is a limiting case as $\gamma \to 0$. For $\gamma < -1$ a family of strictly increasing Cushing-like [15] curves arise, culminating in linear production as $\gamma \to -\infty$. These special cases form natural regimes of similarly behaving production functions as seen in Figure (3.2).

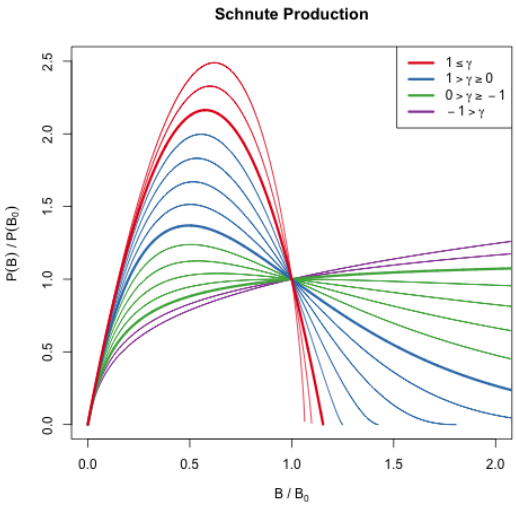

Figure 3.2: The Schnute production function plotted across a variety of parameter values. Regimes of similarly behaving curves are grouped by color.

The behavior of RP inference under the BH model is of particular interest due to

the overwhelming popularity of the BH assumption in stock assessment models. Since Schnute production models can represent a quantifiably wide variety of possible productivity behaviors, they present an ideal simulation environment for inquiry of the reliability of inference under the BH assumption.

Under Schnute production, biomass dynamics evolve according to the following ODE,

$$\frac{dB}{dt} = P_s(B;\theta) - (M+F)B. \tag{3.3}$$

This equation largely takes the same form as previously described, except that P_s is the Schnute production function and natural mortality, M, is modeled explicitly here. Natural mortality models the instantaneous rate of mortality from all causes outside of fishing. While Eq. (3.3) models M explicitly, natural mortality is implicit to the structure of the previously described Schaefer, Fox, and PT production models. Explicitly modeling natural mortality in this way allows P_s to model the production function in such a way so as to allow production to increase for large spawning biomass (or asymptote, e.g. BH production), and still retain well defined RPs so long as $\alpha > M$. This handling of M is typical for age structured models under BH or Ricker recruitment (or even BH/Ricker production models), but it is uncommonly used with the Schaefer model ($\gamma = 1$) as is possible in this setting. Appendix (B) shows that while explicit M

may not be typical under the Schaefer model, the assumption of linear natural mortality, $-MB$, produces a mathematically valid Schaefer model with an admissible interpretation.

The derivation of RPs under Eq. (3.3) follows a similar logic as under the PT model. An expression for equilibrium biomass is attained by setting $\frac{dB}{dt} = 0$ and rearranging the resulting expression to solve for B

$$\bar{B}(F) = \frac{1}{\gamma\beta}\left(1 - \left(\frac{M+F}{\alpha}\right)^{\gamma}\right). \tag{3.4}$$

The above expression quickly yields B_0, B^* by evaluation at $F = 0$ and F^* respectively,

$$B_0 = \frac{1}{\gamma\beta}\left(1 - \left(\frac{M}{\alpha}\right)^{\gamma}\right) \tag{3.5}$$

$$\frac{B^*}{B_0} = \frac{1 - \left(\frac{M+F^*}{\alpha}\right)^{\gamma}}{1 - \left(\frac{M}{\alpha}\right)^{\gamma}}. \tag{3.6}$$

Attaining an expression for F^* requires maximization of equilibrium yield, $\bar{Y} = F\bar{B}(F)$,

with respect to F. Analytically maximizing proceeds by differentiating $\bar{Y}$ to produce

$$\frac{d\bar{Y}}{dF} = \bar{B}(F) + F\frac{d\bar{B}}{dF} \tag{3.7}$$

$$\frac{d\bar{B}}{dF} = -\frac{1}{\beta}\left(\frac{\left(\frac{M+F}{\alpha}\right)^{\gamma}}{F+M}\right). \tag{3.8}$$

Setting $\frac{d\bar{Y}}{dF} = 0$, filling in the expressions for $\bar{B}(F)$ and $\frac{d\bar{B}}{dF}$, then rearranging to solve for F^* is less yielding here than it was in the case of the PT model. This procedure falls short of providing an analytical solution for F^* directly in terms of θ, but rather shows that F^* must respect the following expression,

$$0 = \frac{1}{\gamma} - \left(\frac{1}{\gamma} + \frac{F^*}{F^*+M}\right)\left(\frac{F^*+M}{\alpha}\right)^{\gamma}. \tag{3.9}$$

The lack of an analytical solution here is understood. Schnute & Richards [71, pg. 519] specifically point out that F^* cannot be expressed analytically in terms of productivity parameters, but rather give a partial analytical expression for the inverse relationship. Although parameterized slightly differently, Schnute & Richards derive expressions for α and β as a function of RPs and γ.

Since RPs are left without a closed form expression, computing RPs from productivity parameters amounts to numerically solving the system formed by collecting the expressions (3.9), (3.5), and (3.6).

3.2.2 Simulation

For the purpose of simulation, it is not necessary to completely know the precise relationships mapping RPs $\mapsto \theta$ or $\theta \mapsto$ RPs. Simulation only requires enough knowledge of these mappings to gather a list of (α, β, γ) tuples, for data generation under the Schnute model, and the corresponding RPs in some reasonable space-filling design over RP space.

Similarly to Schnute & Richards [71], expressions (3.9) and (3.5) are solved for α and β respectively. This leads to the partial mapping $\left(F^*, B_0\right) \mapsto \left(\alpha(\cdot,\gamma),\ \beta(\cdot,\cdot,\gamma)\right)$ in terms of RPs and γ. By further working with Eq. (3.6), to identify γ, the following system is obtained,

$$\begin{aligned} \alpha &= (M+F^*)\left(1+\frac{\gamma F^*}{M+F^*}\right)^{1/\gamma} \\ \beta &= \frac{1}{\gamma B_0}\left(1-\left(\frac{M}{\alpha}\right)^{\gamma}\right) \\ \frac{B^*}{B_0} &= \frac{1-\left(\frac{M+F^*}{\alpha}\right)^{\gamma}}{1-\left(\frac{M}{\alpha}\right)^{\gamma}}. \end{aligned} \tag{3.10}$$

For a population experiencing natural mortality M, by fixing F^*, B_0, and $\frac{B^*}{B_0}$ the above system can fully specify α and β for a given γ. Notice for a given γ a cascade of closed form solutions for α and β can be obtained. First $\alpha(\gamma)$ can be computed, and then $\beta(\alpha(\gamma),\gamma)$ can be computed. If $\alpha(\gamma)$ is filled back into the expression for $\frac{B^*}{B_0}$, the

system collapses into a single onerous expression for $\frac{B^*}{B_0}(\alpha(\gamma),\gamma)$. For brevity, define the function $\zeta(\gamma) = \frac{B^*}{B_0}\big(\alpha(\gamma),\gamma,F^*,M\big)$ based on Eq. (3.6).

Inverting $\zeta(\gamma)$ for γ, and computing the cascade of $\alpha(\gamma)$, and then $\beta(\alpha(\gamma),\gamma)$, fully defines the Schnute model for a given $(\frac{F^*}{M},\frac{B^*}{B_0})$. However inverting ζ accurately is difficult. Inverting ζ analytically is not feasible, and numerical methods for inverting ζ are unstable and can be computationally expensive. Rather than numerically invert precise values of $\zeta(\gamma)$, γ is sampled based on the form of ζ so that the overall simulation design is space filling. Ultimately this produces a similar LHD as described in Section (3.2.3), however bypassing inaccurate numerical methods.

Each design location defines a complete Schnute production model with the given RP values. B_0 and q are fixed as in Chapter (2), and M is fixed at a 0.2. Various values of M were tested leading to similar overall results. Indices of abundance are simulated from the Schnute model at each design location, a small amount of residual variation, $\sigma = 0.01$, is added to the simulated index, and the data are then fit with a misspecified BH production model. The design at large captures various degrees of model misspecification relative to the BH model, so as to observe the effect of productivity model misspecification upon RP inference.

3.2.3 Design

Due to the lack of an analytical relationship mapping RPs $\mapsto \theta$, analogous to the PT model's Eq. (2.11), producing a LHD over Schnute RPs requires a more tactful approach. The structured relationship between the RPs and productivity parameters, described in Section (3.2.2), allows an approximate LHD to be obtained by a careful navigation of the system of equations seen in Eq. (3.10).

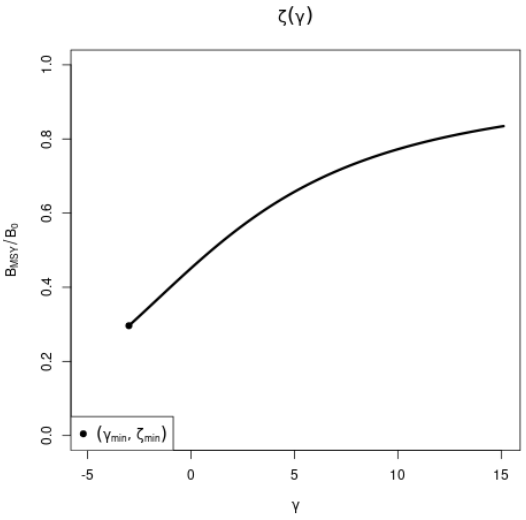

Figure 3.3: $\zeta(\gamma)$ Plotted for $F^* = 0.1$ and $M = 0.2$. The point $(\gamma_{min}, \zeta_{min})$ shows the lowest theoretical value of γ before surplus production becomes negative.

Under the Schnute model, let $\mathcal{F}$ and $\mathcal{B}$ represent regular grids on $\frac{F^*}{M} \in (0.25, 4)$ and $\frac{B^*}{B_0} \in (0.15, 0.7)$ respectively. Marginally this corresponds to $\frac{\alpha}{M} \in (2, 50)$ with the most typical values lying below 17. The grids $\mathcal{F}$ and $\mathcal{B}$ serve as the scaffolding for computing an approximate LHD. Furthermore, let the full design space be defined on the rectangle $R_{full} = (0.25, 4) \times (0.15, 0.7)$.

Since it is not practical to invert $\zeta(\gamma)$, a uniform sample in $\frac{B^*}{B_0}$ can be obtained by modeling γ as a random variable, with realization γ', and thinking of $\zeta(\gamma)$ as its cumulative distribution function (CDF). The aim is to model γ as an easily sampled

random variable with a CDF that closely approximates ζ, so that $\zeta(\gamma') \sim U(\zeta_{min}, 1)$ as closely as possible. The point $(\gamma_{min}, \zeta_{min})$ are the lowest theoretical values of γ and $\frac{B^*}{B_0}$ respectively (for a given $\frac{F^*}{M}$) before surplus production becomes negative[52, 61]. There may be many good models for the distribution of γ, but in this setting the following distribution is very effective,

$$\gamma' \sim \zeta_{min}\delta(\gamma_{min}) + (1 - \zeta_{min})t(\mu, \sigma, \nu)\mathbf{1}_{\gamma > \gamma_{min}}. \tag{3.11}$$

Above, $t(\mu, \sigma, \nu)\mathbf{1}_{\gamma > \gamma_{min}}$ is the density of the truncated location-scale family Student's t distribution with location μ, scale σ, and degrees of freedom ν. $\mathbf{1}_{\gamma > \gamma_{min}}$ is an indicator function truncating the Student's t distribution at the lower bound γ_{min}. $\delta(\gamma_{min})$ is the Dirac delta function evaluated at γ_{min}, which is scaled by the known value ζ_{min}; this places probability mass ζ_{min} at the point γ_{min}. Since sampling from a Student's t distribution is straightforward, sampling from a truncated Student's t mixture only requires slight modification.

Let T be the CDF of the modeled distribution of γ. Since the point $(\gamma_{min}, \zeta_{min})$ is known from the dynamics of the Schnute model at a given RP, full specification of Eq. (3.11) only requires determining the values for μ, σ, and ν which make T best approximate $\zeta(\gamma)$. Thus, the values of μ, σ, and ν are chosen by minimizing the L^2 distance between $T(\gamma)$ and $\zeta(\gamma)$.

$$[\hat{\mu},\hat{\sigma},\hat{\nu}] = \underset{[\mu,\sigma,\nu]}{\arg\min} \int_{\Gamma} \big(T(\gamma;\mu,\sigma,\nu) - \zeta(\gamma)\big)^2 d\gamma \tag{3.12}$$

The distribution $T(\gamma|\hat{\mu},\hat{\sigma},\hat{\nu})$ is fit for use in generating the random variates, γ', at specific values F^* and M. This approximation releases the need to invert ζ w.r.t. γ by using the γ' samples to generate approximately uniform samples of $\zeta(\gamma')$. By sampling approximately uniform $\zeta(\gamma')$ random variates in this way, and making use of the structure in Eq. (3.10), an approximate LHS can be collected via Algorithm (1).

Algorithm 1 LHS of size n on rectangle R.

procedure $LHS_n(R)$
  Define n-grids $\mathcal{F}, \mathcal{B} \in R$
  for each grid element i **do**
    Draw $\frac{F^*}{M} \sim Unif(\mathcal{F}_i)$
    Compute $[\hat{\mu},\hat{\sigma},\hat{\nu}]$ given F^* & M
    while $\mathcal{B}_j$ not sampled **do**
      Draw $\gamma' \sim T(\gamma|\hat{\mu},\hat{\sigma},\hat{\nu})$
      Compute $\zeta' = \zeta(\gamma')$
      Compute j such that $\zeta' \in \mathcal{B}_j$
    end while
    Compute $\alpha' = \alpha(\gamma', F^*, M)$
    Compute $\beta' = \beta(\alpha', \gamma', M, B_0)$
    Save $(\frac{F^*}{M}, \zeta') \Leftrightarrow (\alpha', \beta', \gamma')$ in $\mathcal{F}_i \times \mathcal{B}_j$
  end for
end procedure

For a given i, $\frac{F^*}{M}$ is drawn uniformly from within $\mathcal{F}_i$. Conditioning on the sample of F^*, and M, $T(\gamma|\hat{\mu},\hat{\sigma},\hat{\nu})$ is fit and γ' is sampled. ζ' is then computed and placed into the appropriate grid element $\mathcal{B}_j$. Given γ', the cascade $\alpha(\gamma')$, and $\beta(\alpha(\gamma'),\gamma')$, can be computed. The algorithm continues until all of the design elements, $(\frac{F^*}{M}, \zeta') \Leftrightarrow (\alpha', \beta', \gamma')$, have been computed for all $i \in [1,...,n]$. In the simulations presented here an initial design of size $n = 150$ is always collected.

3.2.3.1 Design Refinement

Since the behavior of RP inference, under misspecified models, will vary in yet-unknown ways, the exact sampling design density may be hard to know a priori. Several factors, including the particular level of observation uncertainty, high variance (i.e. hard to resolve) features of the response surface, or simply "gappy" instantiations of the initial LHD may necessitate adaptive design refinement, to accurately describe RP biases. Given the temperamental relationship between RPs and productivity parameters in the Schnute model, a recursive refinement algorithm that makes use of the previously described LHS routine, is developed.

While LHS ensures uniformity in the design margins, and a certain degree of spread, it is widely recognized that particular LHD instantiations may leave substantive gaps in the simulation design. To correct this, LHD are often paired with design elements of maximin design [50, 18]. Maximin designs sample the design space by maximizing the minimum distance between sampled points. This has the advantage of definitionally filling holes in the design, however because no points are ever drawn outside of the design domain, samples tend to clump around edges (particularly corners) of the design domain. Since LHS ensures uniformity in the margins and maximin designs enjoys a certain sense of optimality in how they define and fill gaps [36], the methods are quite complimentary when combined.

Making use of this complimentary relationship, holes in the existing RP LHD are

identified based on maximin design principles. New design points are collected based on areas of the RP design space which optimize the maximin distance between all pairs of points in the current design, based on the following distance function

$$d(\boldsymbol{x}, \boldsymbol{x'}) = \sqrt{(\boldsymbol{x} - \boldsymbol{x'})^T \boldsymbol{D}^{-1} (\boldsymbol{x} - \boldsymbol{x'})} \tag{3.13}$$

$$\boldsymbol{D} = \textbf{diag}\left[\left(max(\mathcal{F}) - min(\mathcal{F})\right)^2,\ \left(max(\mathcal{B}) - min(\mathcal{B})\right)^2 \right].$$

Above, d is a scaled distance function that defines the distance between points in the differing scales of $\frac{B^*}{B_0}$ and $\frac{F^*}{M}$. $\boldsymbol{D}$ is a diagonal matrix that measures the squared size of the domain in each axis of so as to normalize distances to a common scale.

If $\boldsymbol{X_n}$ is the initial design, computed on R_{full}, let $\boldsymbol{x_a}$ be the augmenting point which maximizes the minimum distance between all of the existing design points,

$$\boldsymbol{x_a} = \underset{\boldsymbol{x'}}{\text{argmax}}\ \ \min\{d(\boldsymbol{x_i}, \boldsymbol{x'}) : i = 1, ..., n\}. \tag{3.14}$$

The point $\boldsymbol{x_a}$ is used as an anchor for augmenting $\boldsymbol{X_n}$. An additional $LHS_{n'}$ (via Algorithm (1)) is collected, adding n' design points, centered around $\boldsymbol{x_a}$, to the overall design. The augmenting region , $R_{(x_a, d_a)}$, is defined based on the square centered at $\boldsymbol{x_a}$ with side length $2d_a$, where $d_a = \min\{d(\boldsymbol{x_i}, \boldsymbol{x_a}) : i = 1, ..., n\}$, in the space defined by the metric d.

Due to the tendency of maximin sampling to cluster augmenting points on the edges of the design space, $R_{(x_a,d_a)}$ is truncated by the outer most limits of R_{full} so as to focus design augmentation within the specified domain of the simulation. Furthermore, since the design space has a nonlinear constraint at low values of $\frac{B^*}{B_0}$, the calculation of $\boldsymbol{x_a}$ is further truncated based on a convex hull defined by the existing samples in the overall design.

Design refinement then proceeds as follows. An initial design is computed on the full RP design space, $X_n = LHS_n(R_{full})$. The maximin augmenting point, $\boldsymbol{x_a}$, is computed at a maximin distance of d_a from the existing samples. An augmenting design $X_{n'} = LHS_{n'}(R_{(x_a,d_a)})$ is collected and added to X_n. Design refinement carries on recursively collecting augmenting designs in this way until stability of the metamodel. Typically design refinement in Chapters (3) and (4) converged after the addition of about 60 augmenting designs of size $n' = 5$.

3.2.3.2 Metamodel Convergence

To demonstrate how convergence of the metamodel is identified Figure (3.4) shows the convergence process using the results from Section (2.3.2) as an example. The metamodel trends shown in the first column are made with an intentionally sparse initial design (50 samples) to exemplify an unconverged metamodel. As more samples are added to the initial sparse design, the pattern originally shown in Figure (2.6) emerges.

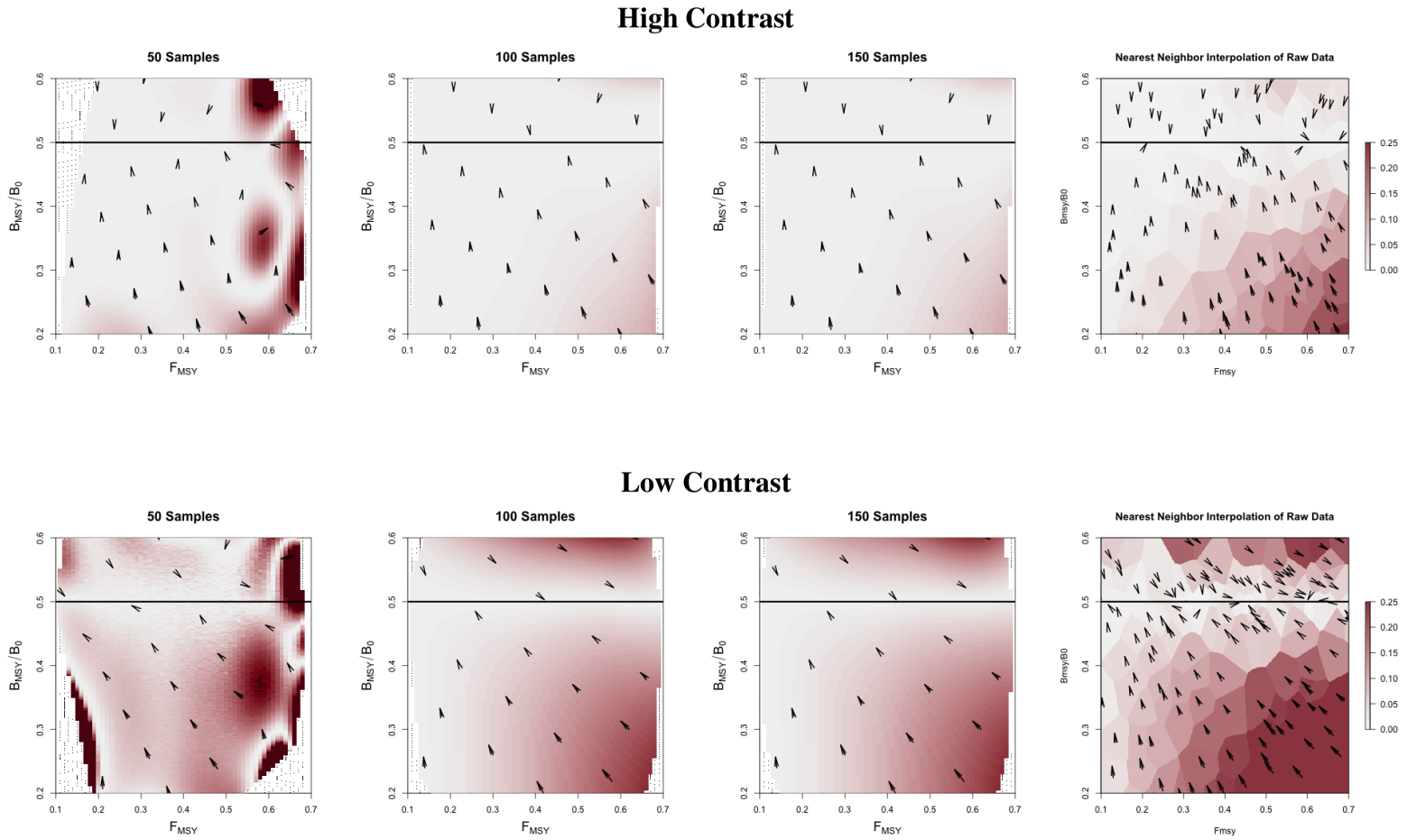

Figure 3.4: An example demonstrating convergence of the metamodeled trends describing RP biases of the Schaefer model in the high/low (*top*/*bottom*) contrast simulation settings as first shown in Figure (2.6). In each case, the first column demonstrates the unconverged metamodels with an initial 50 sample design. The second and third columns demonstrate the metamodel trends with progressively more dense designs. The final column shows the a nearest neighbor interpolation of the raw data of the most dense design.

As more samples are added beyond this point the metamodel trends are stable and do not change with additional densification of the underlying design. A nearest neighbor interpolation of the raw data from the densest design is shown to demonstrate that the converged metamodel follows the same basic mappings described by the simulated models.

3.2.4 Metamodeling

The GP metamodeling method previously developed in Section (2.2.5) is also applied in Chapters (3) and (4) for the analysis of BH RP inference with the following modifications.

Recall that each design location of the simulation uniquely represents a three-parameter Schnute model. Index of abundance data are generated from the Schnute model at each design location to be fit with a two-parameter BH model. For the specification of the metamodel in this case, let $\mathbf{y}$ be a vector collecting the fitted BH MLEs for $\log(F^*)$, and let $\boldsymbol{\omega}$ be a vector of estimates of the estimator variances (via the inverted Fisher information) at each $\mathbf{y}$. These quantities are then modeled by the GP metamodel described in Section (2.2.5) with all other details remaining the same.

Under the BH model $\frac{B^*}{\bar{B}(0)} = \frac{1}{\frac{F^*}{M}+2}$; by transforming metamodel predictions of $\log(F^*)$ to $\frac{F^*}{M}$ and $\frac{B^*}{\bar{B}(0)}$, via this relationship, metamodeled predictions of BH RPs are obtained. The deterministic restriction that the BH model places on RPs allows a GP with a one

dimensional response to model both BH RPs simultaneously through the $\frac{B^*}{\bar{B}(0)} = \frac{1}{\frac{F^*}{M}+2}$ RP relationship. By further subtracting the Schnute RPs from these predicted BH RPs at each point in RP space a pattern of RP estimation biases, induced by model misspecification of the BH model, can be visualized.

3.3 Results

3.3.1 Design

Algorithm (1) enforces uniform marginals in $\frac{F^*}{M}$ directly, as well as the adherence of the overall design to Latin squares. Figure (3.5) shows a uniform Q-Q plot for sampled ζ, using Algorithm (1), against theoretical uniform quantiles. As evidence by the excellent coherence to the theoretical uniform quantiles, the approximation in Section (3.2.3) for sampling γ (and therefore $\zeta(\gamma)$), is very effective. Furthermore since numerical inversion of $\zeta(\gamma)$ is costly and unreliable, the relative speed and accuracy that this approximate LHS sampling method provides is pivotal for the rest of the work presented here.

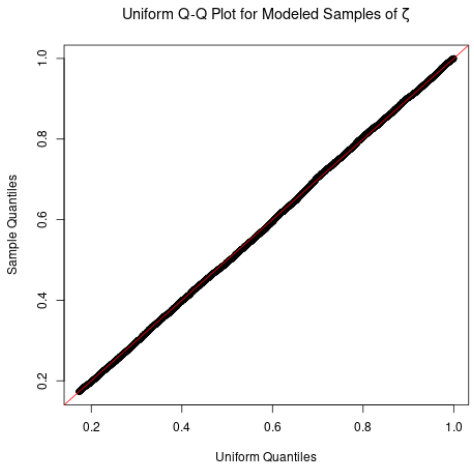

Figure 3.5: Uniform Q-Q plot for ζ plotted for $F^* = 0.1$ and $M = 0.2$.

Figure (3.6) shows how Schnute production has different behaviors in regimes of

RPs space that are entirely defined by the value of γ. When $\gamma \geq 1$ the Schnute model produces a family of Logistic-like curves that are increasingly right leaning as γ increases. For $0 < \gamma < 1$, Schnute production takes a family of left leaning Ricker-like curves that all approach the x-axis. For $-1 < \gamma < 0$ there are a family of BH-like curves that do not approach the x-axis but still have decreasing productivity for large biomass stocks. When γ is exactly -1 Schnute reduces to BH production which has asymptoting production for large biomass. Finally when $\gamma < -1$ Schnute produces a family of increasing Cushing-like curves that do not asymptote, and produces linear production as $\gamma \to -\infty$.

Modeling index data that are simulated broadly over the theoretical space of RPs with misspecified BH production greatly limits the range of possible RPs that can be inferred. Under BH production the full theoretical space of RPs are limited to the curve $\frac{B^*}{B_0} = \frac{1}{F^*/M+2}$. Going forward I refer to this curve as the "BH set". That is to say, the BH set is the set of RPs defined by $\left\{ \left(\frac{F^*}{M}, \frac{B^*}{B_0} \right) \middle| \frac{B^*}{B_0} = \frac{1}{F^*/M+2} \right\}$. The BH set is visualized by the green curve in Figure

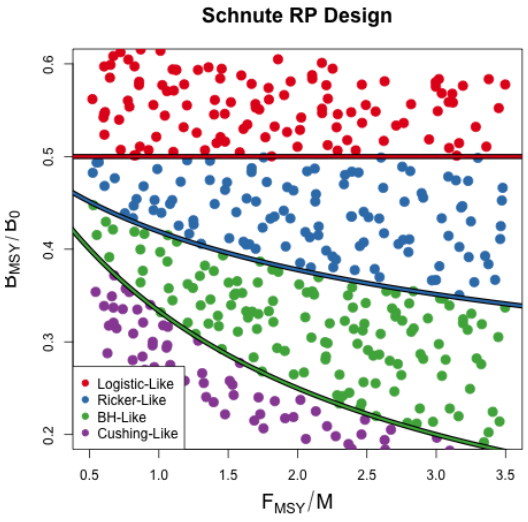

Figure 3.6: A Schnute RP design. Colors indicate different regimes of Schnute production. The black curve shows the BH set.

(3.6). The farther away from this set that Schnute data are simulated, the more the BH model is misspecified for those data.

3.3.2 Metamodeled Trends

Unlike the Schaefer model, the BH set is not a constant in $\frac{B^*}{B_0}$. Under the BH model, bias in $\frac{B^*}{B_0}$ is no longer entirely defined by the degree of model misspecification, but rather the structure of BH RPs allows bias in both $\frac{B^*}{B_0}$ and $\frac{F^*}{M}$ to interact as a function of contrast in the data.

3.3.2.1 High Contrast

Figure (3.7) shows metamodeled RP bias surfaces for inference under the BH model in the high contrast setting (i.e. $\chi = 1$ as defined in Section (2.2.6)). The (*left*) and (*bottom*) panels focus only on the $\frac{B^*}{\bar{B}(0)}$ and $\frac{F^*}{M}$ components of bias respectively. In these panels bias is shown as relative bias, $\frac{\widehat{RP}-RP}{RP}$, similar to a percent error calculation. Where RP represents the true value of the three-parameter RP, and $\widehat{RP}$ refers to the metamodel estimate.

Figure (3.7, *top-right*) combines the components of bias to show the overall mapping of RPs under BH inference in the high contrast simulation setting. Unlike high contrast RP inference under the Schaefer model, where mainly bias in $\frac{B^*}{\bar{B}(0)}$ occurred, the BH model shows bias in both RPs here. Despite the bias in $\frac{B^*}{\bar{B}(0)}$ and $\frac{F^*}{M}$ these re-

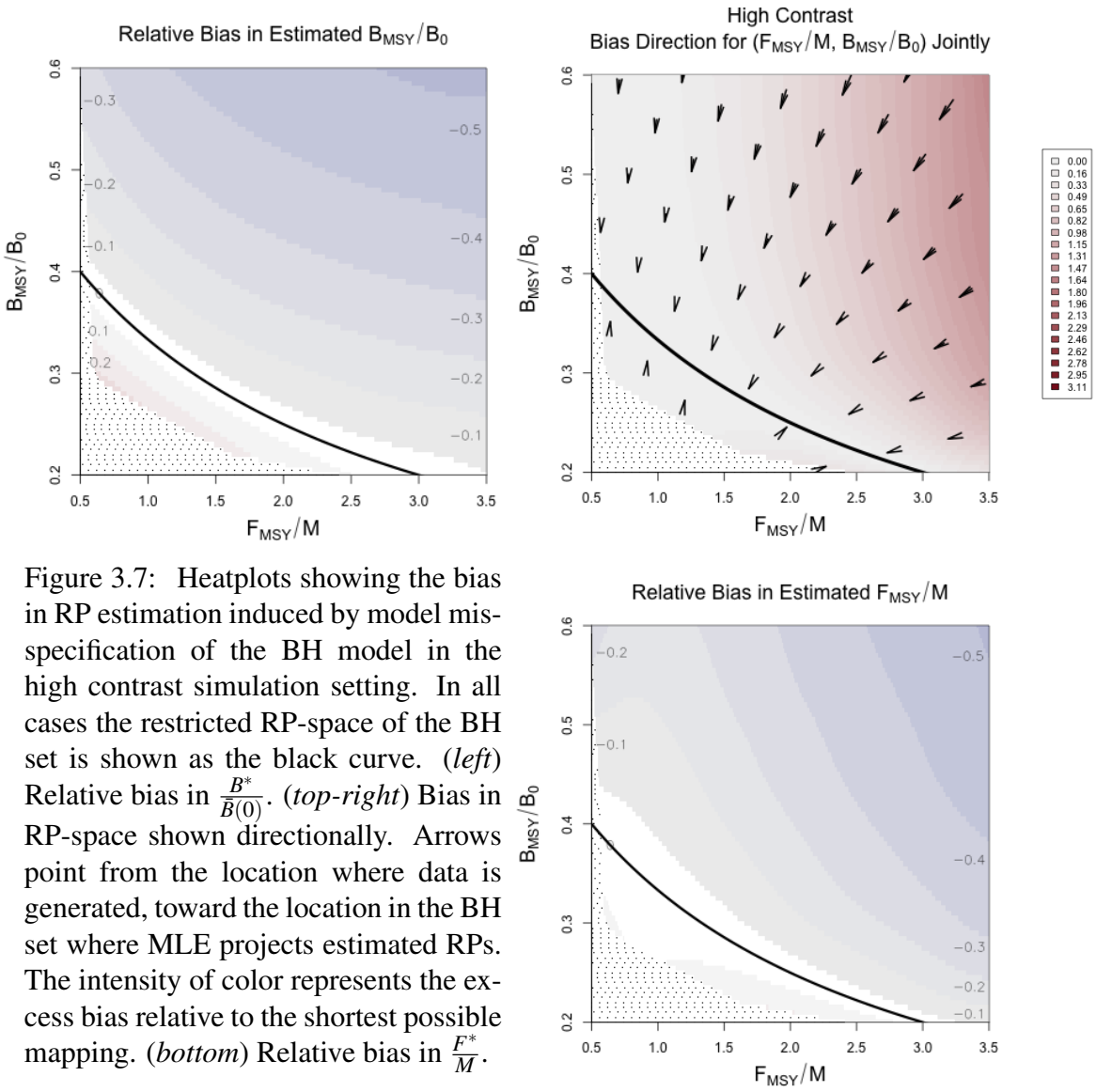

Figure 3.7: Heatplots showing the bias in RP estimation induced by model misspecification of the BH model in the high contrast simulation setting. In all cases the restricted RP-space of the BH set is shown as the black curve. (*left*) Relative bias in $\frac{B^*}{B(0)}$. (*top-right*) Bias in RP-space shown directionally. Arrows point from the location where data is generated, toward the location in the BH set where MLE projects estimated RPs. The intensity of color represents the excess bias relative to the shortest possible mapping. (*bottom*) Relative bias in $\frac{F^*}{M}$.

sults are similar to that of the Schaefer model in that the overall mapping of RPs is similar to a minimal distance mapping onto the constrained set of RPs. The primary difference between Schaefer model and BH RP inference is the geometry of their lim-

ited RP spaces. Unlike the Schaefer model the BH set encourages bias in both RPs for misspecified models even in very well informed setting.

The speckled region in the bottom left corner of each panel of Figure (3.7) represents RP combinations with negative surplus production [52, 61]. A theoretical stock governed by Schnute RPs in this region would have a vanishing small possibility of persisting to the point of being assessed. Thus these theoretical stocks are irrelevant to the study of RP bias beyond the recognition that the Schnute model includes the theoretical existence of such a stock.

3.3.2.2 Low Contrast

Figure (3.8) shows the mapping of RPs in the low contrast (i.e. $\chi = 0$ as defined in Section (2.2.6)) simulation setting. Figures (3.8) and (3.7, *top-right*) share a common scale for the intensity of color to facilitate comparison. In Figure (3.8) notice that the mildly misspecified area around the BH set produces mappings onto the BH set which resemble the minimal distance mapping seen in the

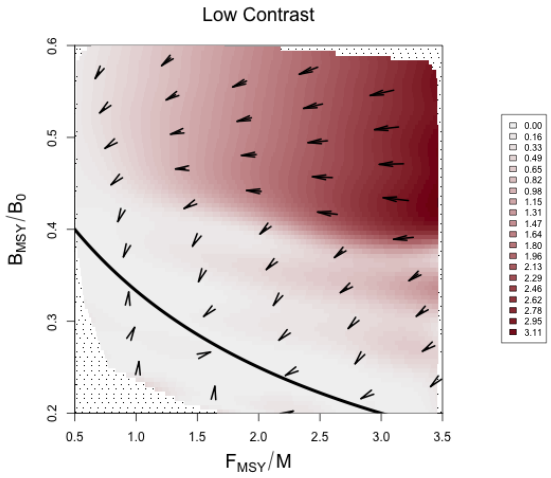

Figure 3.8: Joint bias direction of RP inference in the low contrast simulation setting. The intensity of color represents the excess bias relative to the shortest possible mapping.

high contrast setting. The primary difference in this low contrast setting, is the break point around $\frac{B^*}{B(0)} = 0.4$ above which $\frac{F^*}{M}$ is sharply underestimated.

The region of RPs where the BH model manages to recover the minimal distance mapping is a regime of dynamics where RP inference of remains "intact" for both RPs. That is to say both RPs are well enough modeled by a BH model in this intact region to recover the minimal distance mapping. Figure (3.9) demonstrates example yield curves of the intact minimal distance mapping in the high contrast simulation as compared with the catastrophic underestimation of $\frac{F^*}{M}$ in the low contrast simulation. By comparison of Figure (3.8), with Figure (3.6), the intact regime of the BH RP inference occurs for data simulated with Cushing-like or BH-like production. While bias of RPs estimation in this region can still become concerningly large, this region still produced RPs estimates where the data informs both RPs.

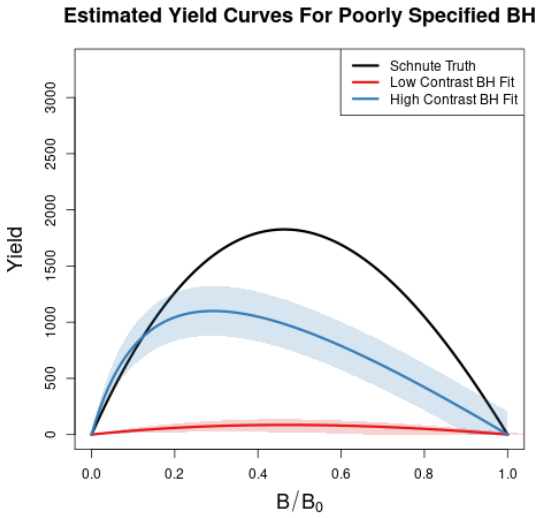

Figure 3.9: Yield curves for data generated with $\frac{F^*}{M} = 1.97$ and $\frac{B^*}{B(0)} = 0.46$.

Outside of this region of intact RP inference, RP estimation breaks from the minimal distance mapping around the interface between BH-Like and Ricker-Like regimes of

the Schnute model (see Figure (3.6)). The Ricker model lies along this regime interface, and represents the first model to approach the x-axis for large biomasses as γ increases. This markedly unBH-like productivity in the low information simulation setting breaks MLE inference from the minimal distance mapping and instead maps RPs to extremely low values of $\frac{F^*}{M}$; consequently $\frac{B^*}{B(0)}$ is estimated near the limiting value under the BH (i.e. $\lim_{F^*\to 0} \frac{1}{F^*/M+2} = 0.5$). Similarly the set of Ricker RPs (as well as the Schaefer set) include this trivial limiting point in common ($\frac{F^*}{M} = 0$, $\frac{B^*}{B(0)} = 0.5$).

Interestingly, in the high contrast setting this trivial mapping for highly misspecified BH models is not present. The fact that removing contrast produces larger biases in $\frac{F^*}{M}$ for the sake of preserving $\frac{B^*}{B(0)}$ (as best as possible within the BH set) suggests that contrast is fundamental to informing $\frac{F^*}{M}$ under the BH model. A similar observation was made under the Schaefer model and the mechanism driving this phenomenon is established in Section (2.3.1). Due to the lack of symmetry of the BH yield curve such explicit mechanisms are more difficult to access in the BH setting, however extending this notion under the BH model is consistent with existing analyses under BH ASMs [11, 39]. Thus when contrast is present, improved estimates of $\frac{F^*}{M}$ drive compromised estimates of $\frac{B^*}{B(0)}$ in accordance with $\frac{B^*}{B(0)} = \frac{1}{F^*/M+2}$. This phenomenon balances RP estimation within the constrained BH set as mediated by the information content of the data and the degree of model misspecification. When not enough contrast is present in the data to drive a compromised RP estimate, inference completely disregards accurate

estimation of F^* in order to better estimate $\frac{B^*}{B(0)}$ by exploiting the common limiting behavior of the BH set and that of Ricker/Logistic-like models.

3.4 Discussion

This chapter reinforces and expands the understanding of how RPs are estimated and demonstrates a vexing risk profile to BH RP inference. Similar to the Schaefer model, contrast clearly plays an important role in estimating RPs, but under the BH model the geometry of the RP set complicates the role of model misspecification in biasing RP estimates. The approximate LHD methods presented in this chapter extend the scope of the simulation methodology to handle the analysis of models where fully analytical designs are not possible, and the design refinement methods further allow the GP to resolve more complicated response surfaces. The GP metamodeling approach when applied in this setting generalizes the RP bias pattern previously observed under the Schaefer model to demonstrate how RP inference is oriented to the geometry of the two-parameter BH model.

As seen in all of the metamodeled trend figures (3.7 and 3.8), even with weakly informative data, when data are generated from RPs immediately around the BH set RP estimates are unbiased and well estimated. Thus contrast alone is not the only factor leading to inferential failure. The particular RP bias depends on the RP geometry of the

fitted model relative to the data, and the degree of contrast present in the data directs the mapping. The available information in the data produces a region of intact RP estimation for misspecified models with an approximately shortest distance map on to the BH set. Outside of this intact region the observed contrast cannot overcome the degree of model misspecification resulting in catastrophic failure of RP estimation as observed in the low contrast simulation setting. This catastrophic failure mode is akin to self regulation of RPs where $\frac{F^*}{M}$ is almost completely ignored for the purposes of preserving $\frac{B^*}{\bar{B}(0)}$ estimates as best as possible within the BH set. This failure mode produces models that attempt to only focus on high-level biomass tends in the data. Within the intact region the geometry of the BH set and the nearly shortest distance map onto the BH set correlates $\frac{F^*}{M}$ and $\frac{B^*}{\bar{B}(0)}$ inference in a way that is not observed for the Schaefer model. Under the BH model this not only makes contrast important for the estimate of $\frac{F^*}{M}$, but also means that the observed contrast will influence the estimate of $\frac{B^*}{\bar{B}(0)}$ (as opposed to the Schaefer model where $\frac{B^*}{\bar{B}(0)} = \frac{1}{2}$ for all $\frac{F^*}{M}$.

If the utility of RP estimation is measured in terms of minimizing the total joint RP bias, the observed approximately minimal distance RP mapping might be considered a nearly best-case scenario. However when combined with the geometry of the BH RP set this behavior may lead to unintuitive implications in RP estimation. For example, due to the shape of the BH RP set a minimal distance mapping ensures that if there is bias in one of $\frac{B^*}{B_0}$ or $\frac{F^*}{M}$, there will necessarily be bias in the other RP. This is an issue

that the Schaefer model[2] does not encounter.

When one considers the implications of RP bias, overestimation of $\frac{F^*}{M}$ carries the severe implication of management recommendations potentially leading to overfishing, while underestimation leads to overly cautious management. In this sense, when the true model is not known the geometry of the BH set together with the metamodeled bias trends makes the BH model a naturally cautious model for most of the stocks modeled here. The one notable exception to this tend stands for data generated in the Cushing-like regime of Schnute RPs. In this regime the BH model tends to be fairly unbiased overall, however the bias that is present for these populations tends to overestimate $\frac{F^*}{M}$. These stocks have relatively small surplus production compared with most stocks outside of this regime. This leads to the regrettable situation where some of the more vulnerable stocks simulated here are subject to subtle but systematic overestimation of $\frac{F^*}{M}$, while more productive stocks are managed in an overly cautious way.

It is important to fully recognize the limitations that the BH model of productivity poses structurally, but also how statistical inference interfaces with those structural limitations. We should not merely accept the potentially cautious RP estimation regimes as a rational of accepting the pervasive use of the BH model in American fisheries. By moving toward three-parameter models we can release these underlying structural limitations [44]. While three-parameter production functions have their own complicating factors [61], the flexibility that three-parameter production functions offer may be used

[2]Or any PT model with a fixed value of γ.

in a number of ways outside of direct parameter estimation. For example, Appendix (C) describes a method of using the Schnute model to solve a structural inconsistency presented by RP proxies. Furthermore, the Schnute model analyzed here makes an intuitive bridge model for developing the use of three-parameter models going forward.

Chapter 4

A Delay Differential Model

4.1 Introduction

The simplified dynamics of SPMs capture a broad range of RP variation, however RP behavior can be complicated by the inclusion of individual growth. The SPM captures the net effect of biomass production by assuming all aspects of biomass production (i.e. maturity, recruitment, growth, etc.) are modeled by the the production function. There are a number of approaches to model these dynamics to explicitly tease out these processes [62, 32], but for the purpose of stock assessment, when data limitations are not too severe, age structured models, ASM, [49] are often considered best practice.

ASMs separate the dynamics of the population into cohorts moving between age classes through time. Cohorts are governed by a system of equations such that each cohort is modeled in a way that resembles the SPM in time. By tracking the average size, and relative contribution to production, of individuals in the population as they age, ASMs inform models of individual growth. ASMs require the specification of many parametric forms for describing the recruitment, growth, maturity, selectivity, etc. that enmesh the system of equations at their core. These complex structures allow ASMs to capture a wide range of dynamics, however the simultaneous accurate specification, implementation, and estimation of all of these forms, and the parameters they imply, requires a lot of expensive data of many different types to fit.

Delay differential models, DDMs (or delay difference models in discrete time)

are an intermediate approach between SPMs and ASMs. At their simplest, DDMs do not necessarily model individual growth [19, 1], but still these models are beneficial in modeling the lag between egg production and recruitment into the reproducing population. By linking selectivity and maturity together with a simplified knife-edge lagged model, more complex DDMs are capable of exactly representing simple ASMs [17, 22, 69, 70]. When information about individual growth is available these DDMs have enough growth, lagged maturity, and lagged selectivity modeling infrastructure to make use of the information without requiring the use of heavily parameterized ASMs. The relatively smaller size, and yet flexible dynamics, of DDMs makes them ideal for modeling "data-limited" stocks, while still entertaining varied hypotheses that relate growth and maturity.

DDMs are effective and flexible data-limited models, however there use in stock assessments have been limited by the accessibility of RP calculations [51]. This chapter expands the previous chapters' analyses of RP biases under the two-parameter BH model using the DDM outlined by Walters [82] to account for RP bias as individual growth and maturity dynamics vary. The simulation design using this DDM requires a derivation of analytical RPs that account for individual growth and maturity dynamics under a Schnute model of recruitment. Munyandorero [51] gives RP expressions using this same DDM under BH, Ricker, and Shepard recruitment. My work in this chapter adds to that work by deriving RP calculations under the Schnute model. The

Munyandorero results are reiterated by the BH and Ricker model special cases of the Schnute DDM. The Schnute model further unifies these results with a single analytical form that also extends RP results to include Schaefer and Cushing-like models. These analytical expressions form the basis of the simulation-based inquiry of RP biases as they are influenced by individual growth and maturity dynamics.

These analytical expressions form the basis of the simulation-based inquiry of RP biases under BH recruitment, when the data are generated broadly under the Schnute model. Additionally, the DDM setting allows for a probe into how recruitment and growth interact to effect RP estimation. This work begins with a derivation of RPs under the three-parameter Schnute DDM. Analytical RP calculations are then structured so as to fit into the simulation design methods presented in Section (3.2.3), and RP biases are then analyzed via the GP metamodel developed in Sections (2.2.5) and (3.3.2).

4.2 Methods

4.2.1 Delay Differential Model

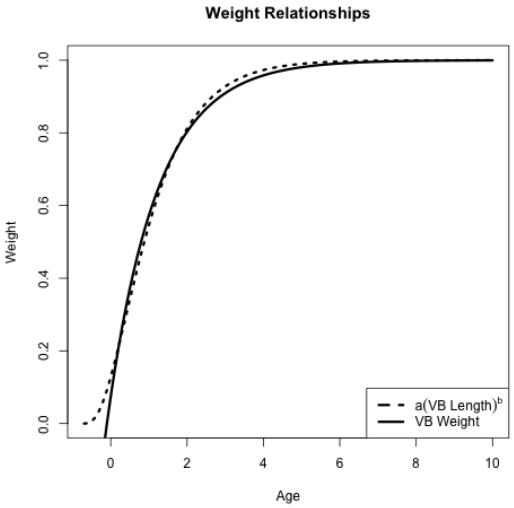

Figure 4.1: The typical composition of allometric weight ($b = 3$) with VB growth in length, as approximated by VB growth in weight directly.

ASMs typically assume von Bertalanffy [81, VB] growth in length with age. To model weight the assumption of VB growth in length, $l(a) = l_\infty(1 - e^{-\kappa(a-a_0)})$, is composed with a power law relating length to weight, $w = al^b$. Since weight is typically proportional to volume, b is usually ~ 3. When b takes a value around 3 this composition of assumed functional forms results in a monotonically increasing sigmoidal curve of weight with age. When $b \leq 1$ weight at age takes a VB-like form with $b = 1$ resulting in an exact correspondence of simultaneous VB-growth in length and weight.

The DDM slightly abridges these relationships by directly assuming VB growth in weight as follows,

$$w(a) = w_\infty(1 - e^{-\kappa(a-a_0)}). \tag{4.1}$$

Here κ is a parameter that controls the instantaneous rate of individual growth (in weight) with age. w_∞ is the maximum weight of individuals in the population, and $w(a)$ is the average weight of an individual at age a. The parameter a_0 controls the age at which individuals are assumed to have zero weight; by letting $a_0 < 0$ this allows fish of age zero to have positive weight. Rather than taking a sigmoidally increasing function, VB growth directly in weight results in a monotonically increasing curve that asymptotes with a strictly decreasing growth rate with age. This results in a curve that can approximate the composite VB-allometric growth assumption very well except at very young ages, see Figure (4.1).

Together with VB growth, the DDM is derived from the assumption that both natural mortality and fishing selectivity are both proportional to a common Heaviside step function with age. That is to say, before a threshold age of selectivity, a_s, no explicit mortality is modeled outside of what is implied by the stock-recruitment relationship, but all fish older then a_s experience the same rate of natural mortality. Simultaneously all fish older than a_s are equally vulnerable to fishing (i.e. knife edge selectivity at age a_s), although fishing effort may vary through time. Maturity is also assumed to be knife edge at age a_s, with only mature fish recruiting into the population.

Together the parameters κ and a_s control individual growth and maturity of the stock. Larger values of κ represent faster growing individuals; in the limiting case where $\kappa \to \infty$ individuals recruit at w_∞. Since this DDM ties maturity and selectivity

together, a_s can also be thought of as controlling the average age of maturity into the reproducing stock. Since faster growing stocks tend to mature at younger ages, κ and a_s tend to be negatively correlated. Furthermore when $\kappa \to \infty$ simultaneously with $a_s \to 0$, as consistent with the negative correlation between the parameters, the DDM converges to the previously studied SPM.

Walters [82] (preceded with similar discrete time models by Deriso [17] and Schnute [69]) shows that within the above assumptions, the following delay-differential system of equations describes the population dynamics of the total mature, exploitable biomass $B(t)$ and number of individuals $N(t)$ through time.

$$\frac{dB}{dt} = w(a_s)R(B;\theta) + \kappa[w_\infty N - B] - (M+F)B \tag{4.2}$$

$$\frac{dN}{dt} = R(B;\theta) - (M+F)N \tag{4.3}$$

This formulation separates the number of individuals in the population from the biomass of the population. The dynamics of N, as seen in Eq (4.3), are very similar to that of the production model in Section (3.2.1), however the role of the production function is now filled by a "recruitment" function, $R(B)$, which describes the number of new individuals recruiting into the exploitable population as a function of exploitable biomass. In turn, the biomass dynamics are coupled to the numbers dynamics by the assumption of VB growth with growth parameters appearing in Eq (4.2), converting

population numbers into biomass and accounting for the growth of biomass with age.

Eq (4.2) of the above model expands the notion of biomass production into the processes of recruitment, individual growth, and maturity. The term $w(a_s)R(B;\theta)$ represents the biomass of new recruits; with $w(a_s)$ representing the weight of individuals at the age of maturity/selectivity, a_s, and $R(B;\theta)$ representing the number of new recruits entering the exploitable population at time t. The negative term, $(M+F)B$, represents all causes of mortality as it is applied to biomass. Finally, the term $\kappa[w_\infty N - B]$ accounts for the net growth of the existing biomass by discounting the limiting maximal individual growth rate by metabolic weight loss proportional to $B(t)$. This structure, as derived from the assumption of simultaneous knife-edge maturity and selectivity, and the delay structure in R, provides the major computational savings of the delay differential setting, as compared with full ASMs. The mean size and growth associated with changes in recruitment as cohorts mature into the population are automatically described by the DDM equations rather than the numerous numerical arrays used by ASMs to track quantities across all age classes in time.

Often a BH functional form is assumed for the stock recruitment relationship, but many families of functions may model this relationship. For the sake of evaluating the adequacy of assumed BH recruitment, the simulation described in the following sections is derived for the DDM under the assumption of generalized three-parameter

Schnute recruitment,

$$R(B;[\alpha,\beta,\gamma]') = \alpha B(t-a_s)(1-\beta\gamma B(t-a_s))^{\frac{1}{\gamma}}. \tag{4.4}$$

The parameters $\boldsymbol{\theta}' = [\alpha,\beta,\gamma]$ function similarly in this setting as previously described in Section (3.2.1). That said, since the DDM explicitly parses out growth in its dynamics, these parameters only describe the net processes of reproduction where as the production model uses these parameters to also model the net effects of growth on biomass production. The γ parameter generalizes the family to model varying degrees of decreasing recruitment for large biomasses as γ increases. The Schnute function is again exactly equivalent to BH recruitment at the special case when $\gamma = -1$, it passes through the Ricker model as $\gamma \to 0$, and Logistic recruitment occurs when $\gamma = 1$.

Since the DDM assumes knife edge selectivity, at age a_s, the term $B(t-a_s)$ appears in R. That is to say, fish recruiting into the exploitable population are the result of larval production of biomass a_s time units in the past. This is because fishing selectivity is only assumed to occur for fish that are at least a_s time units old and thus fish younger than a_s are not exploitable. This waiting period requires that new recruits be the result of spawning biomass a_s time units in the past. Modeling maturity and selectivity in this way results in dynamics equations which are a system of delay differential equations as opposed to the simple ODEs that arise in the production model setting.

4.2.2 Reference Points

Deriving reference points for the DDM under Schnute recruitment is conceptually similar to the SPM setting. The additional nonlinear VB growth assumption, alongside Schnute recruitment, quickly makes the expressions look somewhat unwieldy. Although complicated by growth parameters, analytical solutions can still be derived for most of the same quantities as was done in Chapter (3).

Starting from Eqs. (4.2) and (4.3), setting both $\frac{dB}{dt}$ and $\frac{dN}{dt}$ simultaneously equal to zero, and solving for B and N as a function of fishing, gives the equilibrium biomass and numbers equations.

$$\bar{B}(F) = \frac{1}{\beta\gamma}\left(1 - \left(\frac{(F+M)(F+M+\kappa)}{\alpha w(a_s)(F+M+\frac{\kappa w_\infty}{w(a_s)})}\right)^{\gamma}\right) \tag{4.5}$$

$$\bar{N}(F) = \frac{\alpha\bar{B}(F)(1-\beta\gamma\bar{B}(F))^{1/\gamma}}{F+M} \tag{4.6}$$

Eq. (4.6) is just $\frac{R(\bar{B})}{F+M}$, and is coupled to $\bar{B}(F)$ where most of the dynamics appear. Eq. (4.5) resembles Eq (3.4) from the simple production model setting although the growth parameters κ, w_∞ and $w(a_s)$, make slight adjustments to the balance of the maximum rate of recruitment and mortality rate to give an expression for equilibrium biomass that accounts for the factors of individual growth.

Expressions for B_0 and B^* are attained by evaluating $\bar{B}(F)$ at $F = 0$ and $F = F^*$ respectively. The calculation of F^* typically involves maximization of equilibrium

yield, $\bar{Y} = F\bar{B}(F)$. Just as was the case under the Schnute SPM in Chapter (3), it is again not possible to analytically maximize $\bar{Y}$ under the Schnute model in the DDM setting. However stable numerical solutions for calculating F^* were obtained by numerically solving for the roots of the analytical derivative of equilibrium yield with respect to F. Below a greatly simplified expression for $\frac{d\bar{Y}}{dF}$ is shown; the substitution $Z = F + M$ (total mortality rate) has been made to produce a more compact expression.

$$\frac{d\bar{Y}}{dF} = \frac{1}{\beta\gamma}\left[1 - \left(\frac{Z(Z+\kappa)}{\alpha w(a_s)(Z+\frac{\kappa w_\infty}{w(a_s)})}\right)^{\gamma} - \left(\frac{\gamma F}{\alpha w(a_s)}\right)\left(\frac{Z(Z+\kappa)}{\alpha w(a_s)(Z+\frac{\kappa w_\infty}{w(a_s)})}\right)^{\gamma-1}\left(1 + \frac{\left(\frac{\kappa w_\infty}{w(a_s)}\right)\left(\kappa - \frac{\kappa w_\infty}{w(a_s)}\right)}{(Z+\frac{\kappa w_\infty}{w(a_s)})^2}\right)\right] \tag{4.7}$$

F^* is calculated as the numerical root, w.r.t. F, of the above expression. The numerical root is calculated using the base R uniroot function which employs a derivative free search given by [7].

4.2.2.1 BH Constraint

In the SPM the BH constrained RPs are fixed to $\frac{1}{x+2}$, where $x = \frac{F^*}{M}$. In the DDM the constrained BH RP set is complicated by the growth parameters a_s and κ. Under BH recruitment these parameters slightly influence this relationship as seen in Figure (4.2). That said, the influence of a_s and κ on RPs is still largely limited to a confined region of reference point space which resembles the $\frac{1}{x+2}$ form. In fact the confined region of RPs is bounded above by $\frac{1}{x+2}$. In Figure (4.2) notice that for values of a_s and κ that result in high $w(a_s)$ (high values of κ and small values of a_s

seen in red) the BH RP space converges to $\frac{1}{x+2}$ as derived in the simple production model setting. Opposing the SPM limit, when $w(a_s)$ is low (as seen in the more blue region of Figure(4.2)), RPs decrease as the influence of growth in the dynamics increases (i.e. slower individual growth). This is another way (this time in RP space) of noticing that the DDM converges to the previously studied SPM as $\kappa \to \infty$ and $a_s \to 0$ simultaneously.

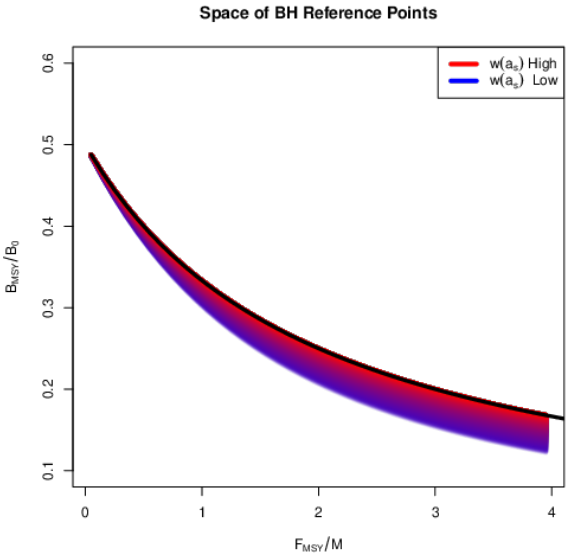

Figure 4.2: The space of BH RPs for the delay model as a function of κ and a_s. The RP space is plotted for 80×80 combinations of $\kappa \in [0.1, 2]$ and $a_s \in [0.1, 10]$. The color drawn is the resulting value of $w(a_s)$ mapped between blue and red. $\frac{1}{x+2}$ is plotted in black for reference.

4.2.3 Simulation Design

Similarly as previously described in Section (3.2.2) the relationship between RPs $\mapsto \theta$ cannot be fully expressed analytically for the Schnute DDM. However, just as in the SPM setting, simulation only requires enough knowledge of these mappings to gather a list of (α, β, γ) tuples and the corresponding RPs in some reasonable space-filling design over RP space.

In the DDM a partial mapping for $\left(F^*, B_0\right) \mapsto \left(\alpha(\cdot, \gamma),\ \beta(\cdot, \cdot, \gamma)\right)$ can be derived

analytically in terms of RPs and γ. The substitution $Z^* = F^* + M$ is made where F^* and M appear together to produce a more compact expression.

$$\alpha = \left[\left(\frac{Z^*(Z^*+\kappa)}{w(a_s)(Z^*+\frac{\kappa w_\infty}{w(a_s)})} \right)^\gamma + \left(\frac{\gamma F^*}{w(a_s)} \right) \left(\frac{Z^*(Z^*+\kappa)}{w(a_s)(Z^*+\frac{\kappa w_\infty}{w(a_s)})} \right)^{\gamma-1} \left(1 + \frac{\left(\frac{\kappa w_\infty}{w(a_s)}\right)\left(\kappa - \frac{\kappa w_\infty}{w(a_s)}\right)}{(Z^*+\frac{\kappa w_\infty}{w(a_s)})^2} \right) \right]^{\frac{1}{\gamma}} \tag{4.8}$$

$$\beta = \frac{1}{\gamma B_0} \left(1 - \left(\frac{M(M+\kappa)}{\alpha w(a_s)(M+\frac{\kappa w_\infty}{w(a_s)})} \right)^\gamma \right) \tag{4.9}$$

Above Eq. (4.8) results from setting Eq. (4.7) equal to zero and solving for α, and Eq. (4.9) results from solving the $\bar{B}(0)$ expression, as derived from Eq. (4.5), for β. The system is completed by further working with the $\frac{\bar{B}(F^*)}{\bar{B}(0)}$ expression, as seen below, to identify γ.

$$\frac{B^*}{B_0} = \frac{1 - \left(\frac{(F^*+M)(F^*+M+\kappa)}{\alpha w(a_s)(F^*+M+\frac{\kappa w_\infty}{w(a_s)})} \right)^\gamma}{1 - \left(\frac{M(M+\kappa)}{\alpha w(a_s)(M+\frac{\kappa w_\infty}{w(a_s)})} \right)^\gamma} \tag{4.10}$$

The system formed by collecting Eqs. (4.8), (4.9), and (4.10) can be navigated similarly to Eq. (3.10) in the Schnute production model setting. For a population experiencing natural mortality M, VB growth with parameters κ and w_∞, and age of selectivity a_s the above system can fully specify α and β for a given γ, by fixing F^*, B_0, and $\frac{B^*}{B_0}$. For a given γ a cascade of closed form solutions for α and β can be obtained, just as in Section (3.2.2). First $\alpha(\gamma)$ can be computed, and then $\beta(\alpha(\gamma),\gamma)$ can be computed. If $\alpha(\gamma)$ is filled back into the expression for $\frac{B^*}{B_0}$, the system collapses into a single onerous expression for $\frac{B^*}{B_0}(\alpha(\gamma),\gamma)$. For brevity, define the function $\zeta(\gamma) = \frac{B^*}{B_0}\big(\alpha(\gamma),\gamma,F^*,M\big)$

based on Eq. (4.10).

Again rather than inverting $\zeta(\gamma)$ for γ, γ is the sampled so that the overall simulation design is space filling as described in Section (3.2.3). Given the sampled γ, the cascade of $\alpha(\gamma)$, and then $\beta(\alpha(\gamma),\gamma)$, can be computed, and the Schnute DDM is fully defined by a given $(\frac{F^*}{M}, \frac{B^*}{B_0})$. While conceptually this framing is similar to the Schnute SPM, the analytical expressions are more complex, and numerically treacherous, since growth parameters appear explicitly here. Other ways of navigating the RPs $\mapsto \theta$ system are possible, but for the sake of numerical stability this strategy has proven the most reliably accurate by limiting exposure to numerical error propagation which quickly becomes significant using other schemes.

Each design location defines a complete Schnute DDM with the given RP values. Just as in Chapter (3), B_0 is fixed at 10000, q is fixed at 0.0005, and M is fixed at 0.2; furthermore a_0 and w_∞ (of VB growth) were fixed to -1 and 1 respectively throughout. The values of κ and a_s are varied roughly along the line $w(a_s) = w_\infty - \frac{a_s}{3}$ so as to produces a negatively correlated relationship between κ and a_s representing fast ($\kappa = 10$, $a_s = 0.1$), medium ($\kappa = 0.5$, $a_s = 1$) and slow ($\kappa = 0.1$, $a_s = 2$) individual growth simulation settings. Indices of abundance are simulated from the Schnute model at each design location, a small amount of residual variation, $\sigma = 0.01$, is added to the simulated index, and the data are then fit with a misspecified BH model. σ is later relaxed to 0.12 in Section (4.3.5). The design captures various degrees of model misspecification

relative to the BH model, so as to observe the effect of recruitment misspecification upon RP inference.

4.2.4 Metamodeling

The GP metamodeling method previously developed in Section (2.2.5), and later adapted for analysis of the BH model in Chapter (3), is also used in the DDM setting here.

4.2.5 Delay Differential Integration

The delay model belongs to a class of differential equations known as delay differential equations (DDE). The delay arises from the $B(t-a_s)$ terms found in the recruitment function. Solving DDEs require special care which depends on the nature of the time delay. The addition of time-varying delays, many different delays, or very small delays (delays below the step size of the numerical integrator) results in some of the more challenging settings for solving DDEs. However with a single stationary model of the age of selectivity and maturity, the DDM used here represents one of the most straightforward numerical DDE settings. The most numerically challenging case presented here arises in the case of the limiting SPM when $a_s \to 0$ while $\kappa \to \infty$. That said the limiting SPM can be approximated for values of $a_s \approx 0.1$, and it was straightforward to ensure that the step size of the integrator remained reasonably below 0.1.

The DDE presented here is integrated with the initial values fixed at B_0 and N_0 as

given by Eqs. (4.5) and (4.6) with $F = 0$ at any given configuration of $\boldsymbol{\theta}$ and growth parameters. The system given in Eqs. (4.2) and (4.3) are then solved numerically using the implicit Livermore Solver (lsode) as implemented in the `dede` function of the R package `deSolve` [76]. The `dede` solver provides many methods for integrating DDEs, but lsode was chosen because it is an implicit method that runs relatively quickly with a relatively smaller footprint in system memory as compared with other methods. The radau method was also tried in more computationally challenging settings with good results (albeit running more slowly that lsode). Ultimately the simulated parameter space did not produce DDEs that require the more expensive radau integrator to solve accurately.

4.2.6 Parameter Estimation

Let $I_t, t \in \{1,2,3,...,T\}$, be a series of indices of abundance, proportional to biomass, as simulated from the Schnute DDM. These data are modeled with the following log-normal observation model that has been intentionally constrained to BH recruitment,

$$I_t \sim LN(qB_t(\boldsymbol{\theta},\boldsymbol{\phi}),\sigma^2). \tag{4.11}$$

$B_t(\boldsymbol{\theta},\boldsymbol{\phi})$ is the biomass solution of the BH constrained DDE system. The BH constraint is implemented by fixing $\gamma = -1$ so that $\boldsymbol{\theta}' = [\alpha,\beta,\gamma = -1]$. $\boldsymbol{\phi}$ is a vector of growth

and maturity parameters, $\phi' = [\kappa, w_\infty, a_0, a_s]$. The nuisance parameter q models the proportionality constant of the index with process biomass, and σ^2 models residual variation of the index.

In this setting, ϕ is fixed to focus on the inferential effects of model misspecification on recruitment parameters and RPs. Typically ϕ is not well informed by index data and would be estimated externally to the DDM for data-limited stocks.

σ^2 and θ are reparameterized to the log scale and fit via MLE. Transforming the parameters to the log scale improves the reliability of optimization, in addition to facilitating the use of Hessian information for estimating MLE standard errors. Given that the biological parameters enter the likelihood via a nonlinear differential equation, and further the parameters themselves are related to each other nonlinearly, the likelihood function can often be difficult to optimize. A hybrid optimization scheme is used to maximize the log likelihood to ensure that a global MLE solution is found. The R package GA [72, 73] is used to run a genetic algorithm to explore parameter space globally. Optimization periodically jumps into the L-BFGS-B local optimizer to refine optima within a local mode. The scheme functions by searching globally, with the genetic algorithm, across many initial values for starting the local gradient-based optimizer. The genetic algorithm serves to iteratively improve hot starts for the local gradient-based optimizer. Additionally, optimization is only considered to be converged when the optimum results in an invertible Hessian at the found MLE.

4.2.6.1 Numbers Indices

While not utilized here, ASMs may model indices as proportional to numbers rather than (or simultaneously to) biomass. When solving the DDE, Eq. (4.3) points out that the full DDE solution will expose a numbers solution simultaneously with a biomass solution that may be used for these purposes. These solutions are often quite similar since the main driver of process behavior comes from the form of R which is shared among N and B. However, it is common on the west coast of the US that indices derived from commercial fisheries are measured as weights while indices derived from recreational fisheries are often measured as counts. If a numbers index, J_t, is observed alongside the previously mentioned biomass index, the following likelihood component can be added as a conditionally independent component of the likelihood,

$$J_t \sim LN(pN_t(\boldsymbol{\theta}, \boldsymbol{\phi}), \tau^2). \tag{4.12}$$

$N_t(\boldsymbol{\theta}, \boldsymbol{\phi})$ is the numbers solution of the DDE system. $\boldsymbol{\theta}$ and $\boldsymbol{\phi}$ are the productivity and growth parameters shared in common with the biomass component. p and τ^2 are then the analogous proportionality constant and residual variation of the numbers index respectively.

There may be many other useful ways to build observation models from the numbers and biomass DDE solutions. For example, one may develop models around the quantity $\frac{B(t)}{N(t)}$ to model the average size of individuals in the population through time. By including average size data, with stationary models of mortality, this model may resolve uncertainty around latent recruitment in time. That said, for the purposes of the simulations run here the observation model is expressed only in terms of biomass as stated in Eq. (4.11) of the previous section.

4.3 Results

Figure (4.3) shows the VB growth curves in weight described at the end of Section (4.2.3). The larger values of $w(a_s)$ correspond to larger recruits relative to maximum size; by comparing the RPs of models with larger values of $w(a_s)$ in Figure (4.5) we can see that these models result in SPM-like RPs. When $w(a_s)$ is large, recruits are near maximum size and thus there is little growth left to be

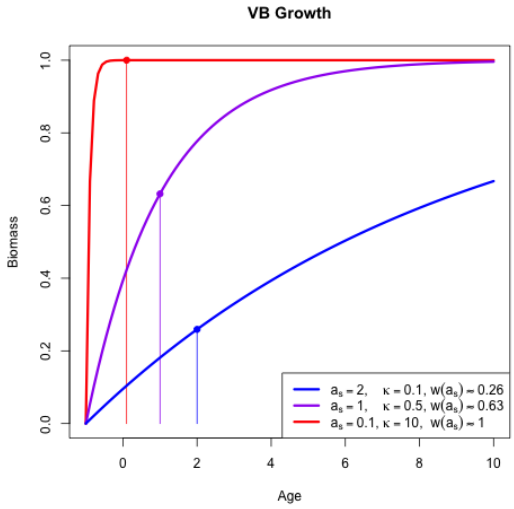

Figure 4.3: Three hypothetical individual-growth curves, demonstrating fast (i.e. SPM limit), medium and slow individual growth in red, purple, and blue respectively.

evaluated by the biomass dynamics equations. In Figure (4.3) the red curve demonstrates a stock with fast growing individuals that provides an example of the SPM limit ($a_s \to 0$ and $\kappa \to \infty$). In this setting individuals recruit so near maximum size that growth does not meaningfully effect the biomass dynamics in this setting (i.e. $w(a_s) \approx w(a_s+1) \approx w(a_s+2)...$). The cases shown with smaller $w(a_s)$ values (the purple and blue curves) correspond to incrementally slower growth behaviors. The slowest growth stock simulated is the blue curve, where $a_s = 2$ and $\kappa = 0.1$, emphasizing the effect of growth on the biomass dynamics.

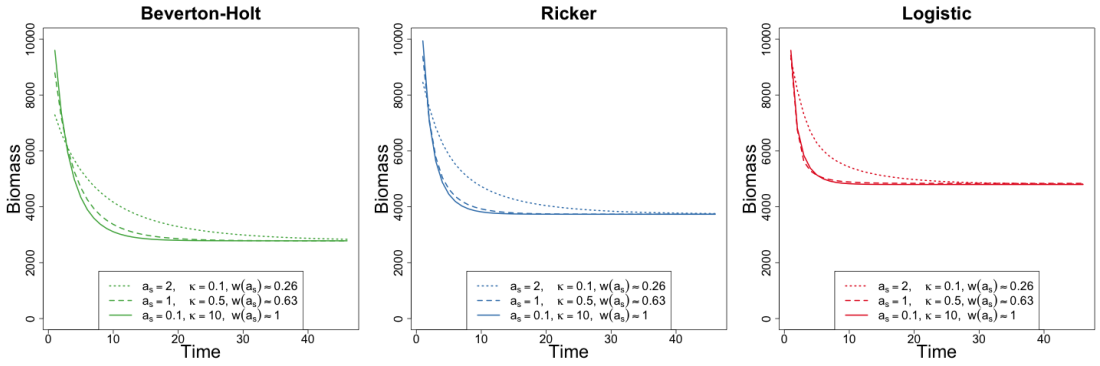

Figure 4.4: Biomass dynamics of BH (*left*), Ricker (*center*), and Logistic (*right*) DDMs in the low contrast simulation setting. In all cases $\alpha = 1.2$ and β is chosen so that each model shares the same B^* within each given γ.

Figure (4.4) demonstrates a range of biomass dynamics that the Schnute DDM can display under this spectrum of growth behaviors with fishing held consistent at F^*. The three special cases of $\gamma = -1$ (BH), $\gamma \to 0$ (Ricker), and $\gamma = 1$ (Logistic) recruitment are shown in each of the above growth configurations.

Figure (4.5) shows the range of RPs that can be modeled with each of the BH, Ricker, and Logistic recruitments over the spectrum of individual-growth/maturity models simulated here. Notice for smaller values of $\frac{w(a_s)}{W_\infty}$ the further the RP curve lies from the SPM, and each recruitment model reacts slightly differently under each of the given growth parameters. The Ricker and BH RP-spaces are qualitatively similar in shape with smaller values of $w(a_s)$ decreasing $\frac{B^*}{B_0}$ relative to the SPM. The Logistic model on the other hand increases $\frac{B^*}{B_0}$ relative to the SPM as $w(a_s)$ decreases. It is also worth noting that the Ricker model's RPs are much less influenced by growth parameters as compared with that of the BH or Logistic model.

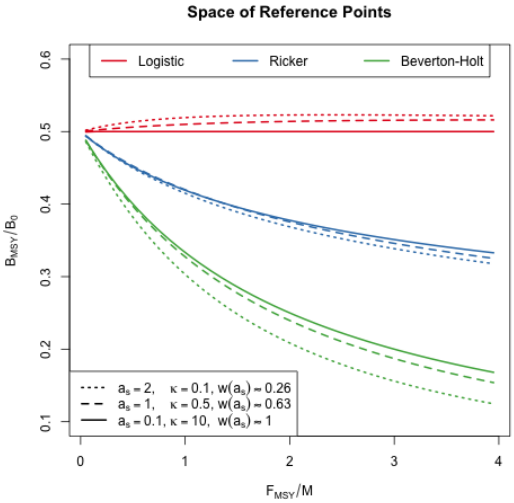

Figure 4.5: Restricted RP-space under each recruitment models, with each growth curve.

4.3.1 Fast Individual Growth (SPM Limit)

Under the delay differential's limiting SPM ($a_s = 0.1$ and $\kappa = 10$), the expectation is that RP inference should be identical to that of the model seen in Chapter (3). By way of verifying this equivalence, Figure (4.6) demonstrates a virtually identical pattern of RP biases as previously seen in Figures (3.7) and (3.8) (under both of the high and low

contrast settings).

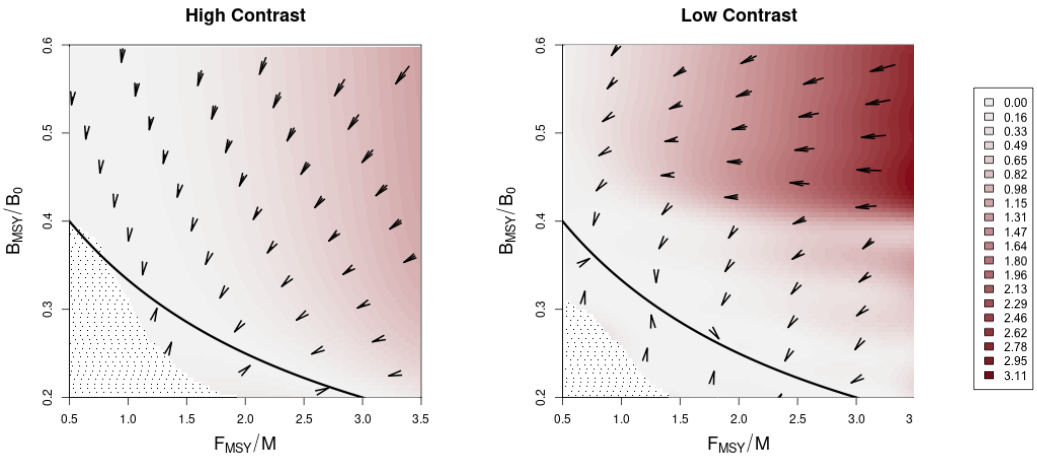

Figure 4.6: RP mapping of BH DDM fit to Schnute DDM data under the fast individual growth setting (SPM limit) $(left)$ High contrast simulation. $(right)$ Low contrast simulation.

Indeed in the high contrast setting, Figure (4.6, $left$) shows how the BH model induces the same pattern of bias as seen in Chapter (3). There is bias in both RPs (in accordance with the $\frac{B^*}{\bar{B}(0)} = \frac{1}{F^*/M+2}$ RP-set) so as to produce a nearly minimal distance mapping of RPs onto the constrained BH set of RPs. Similarly, in the low contrast setting, Figure (4.6, *right*) again shows the same two regime pattern of RP inference. Firstly, there is a region of relatively small model misspecification where a similar nearly minimal distance mapping is preserved. Secondly, as model misspecification becomes greater (around the Ricker set) $\frac{F^*}{M}$ begins to be sharply underestimated. Above this break point in RP estimation inference appears to be driven toward the trivial RP $\frac{F^*}{M} = 0$, $\frac{B^*}{\bar{B}(0)} = 0.5$) that is shared in common among all of the two-parameter models described here.

These results confirm that the expected theoretical limiting dynamics do indeed behave nearly identical to RP inference patterns previously described. Given the implementation differences between the DDM and the SPM this result also provides replicability of the results in Chapter (3).

4.3.2 Moderate Individual Growth

Moving past the SPM, other values of a_s and κ provide a probe into the effects individual growth dynamics may have on RP inference. Individual growth is a multifaceted phenomena that is not easily reduced to a single number, but for the purposes here $w(a_s)$ serves as a decent proxy for the extent of the model dynamics that are due to individual growth. This follows from the intuition that individuals maturing at a smaller fraction of w_∞ demonstrate the dynamics of growth during an observable (to the model) phase rather than growth occurring prior to selection.

That said, $w(a_s)$ is not a one-to-one map of κ and a_s. A level curve of $w(a_s;\kappa) = c$ is attained by increasing the value of a_s and decreasing κ correspondingly, or vice versa. The case where $a_s = 1$ and $\kappa = 0.5$ (resulting in $w(a_s) \approx 0.6$) represents a reasonable example of moderate individual growth. Similar examples of the $w(a_s) = 0.6$ level curve result in much larger lags (discussed in Section (4.3.5)) or larger κ's which quickly tend toward behaviors previously described in the SPM setting.

The RP mappings seen in Figure (4.7) show very similar RP mappings to that of

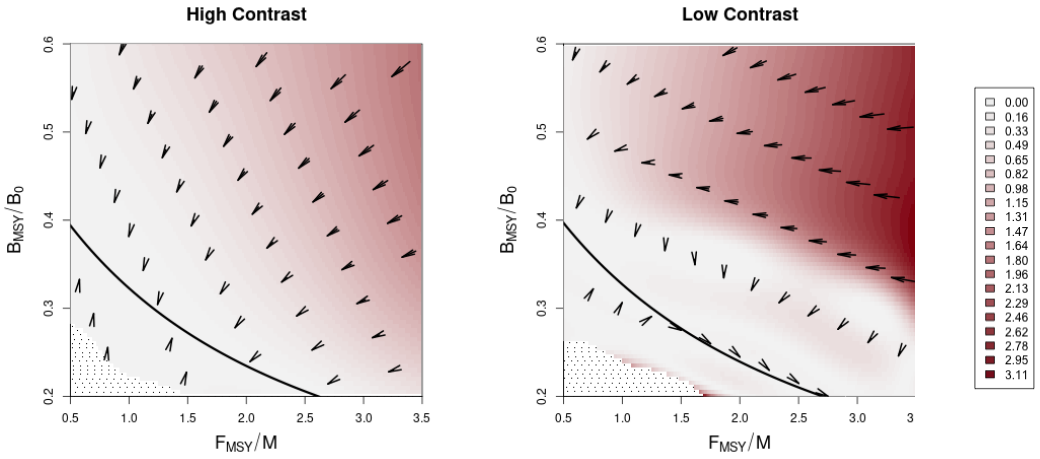

Figure 4.7: RP mapping of BH DDM fit to Schnute DDM data under moderate growth ($a_s = 1$ and $\kappa = 0.5$). $(left)$ High contrast simulation. $(right)$ Low contrast simulation.

the SPM, with the biggest differences occurring around the location of the break point where the low contrast model begins to dramatically underestimate $\frac{F^*}{M}$. In the high contrast simulation setting Figure (4.7; $left$) shows the RP mappings again demonstrate a similar nearly minimal distance mapping of RPs onto the constrained BH RP set. In the low contrast setting Figure (4.7; *right*) shows a very similar two regime pattern of RP inference is observed, however the location of the break between these regimes appears at lower values of $\frac{B^*}{B(0)}$. In this moderate growth setting the break point occurs around values of $\frac{B^*}{B(0)}$ just below 0.4 as opposed to the SPM where the break point occurs at values of $\frac{B^*}{B(0)}$ just above 0.4.

4.3.3 Slow Individual Growth Dynamics

The slow individual growth setting simulated here fixes $a_s = 2$ and $\kappa = 0.1$, to simulate a species that grows quite slowly and matures into the reproducing stock relatively later than the previously describe simulations. This combination has the effect of exaggerating the components of the model dynamics which are related to individual growth since individuals recruit at a smaller size and slowly grow over the extent of the modeled period.

The slow growth of these dynamics oppose the simple production model setting in the sense that they move the constrained RP set a large distance (largest among the spectrum of decreasing $w(a_s)$ populations simulated here) away from the $\frac{1}{x+2}$ limiting case.

Despite the heavily growth influenced biomass dynamics in this setting, the RP mappings seen in Figure (4.8) obviously bear a huge resemblance to the previously seen RP mappings. Again the biggest differences in the RP mappings occur around the location of the break point where the low contrast model begins to dramatically underestimate $\frac{F^*}{M}$. In this low contrast setting the break point in RP estimation occurs around values of $\frac{B^*}{\bar{B}(0)}$ well below 0.4 with the behavior extending as far down as $\frac{B^*}{\bar{B}(0)} = 0.3$. This regime shift occurs well below that of the Ricker set, as initially observed in the production model setting. This reduced range of acceptable RP inference indicates that for slow growing stocks misspecified BH models becomes increasingly brittle with

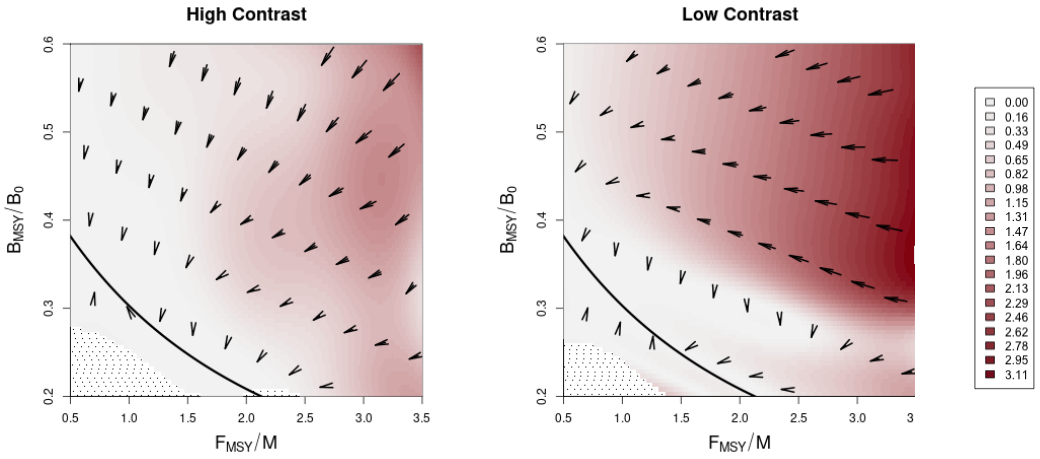

Figure 4.8: RP mapping of BH DDM fit to Schnute DDM data under dramatic growth ($a_s = 2$ and $\kappa = 0.1$). $(left)$ High contrast simulation. $(right)$ Low contrast simulation.

respect to RPs.

Interestingly this pattern only follows for the low contrast setting. In the high contrast setting inference returns to a pattern resembling the minimal distance mapping onto BH RP set, further pointing to the importance of contrast for informing these models.

4.3.4 Clustering Catastrophic Model Failure

Considering the behavior observed in Sections (4.3.1-4.3.3), where $\frac{F^*}{M}$ is dramatically underestimated, it is natural to ask where specifically in RP space we might expect to see this catastrophic failure of the BH model as growth assumptions change. Below a hypothesis testing inspired classifier is derived in terms of the GP predictive structures for identifying where BH inference fails in this way.

Recall that the metamodel models MLEs of $log(F^*)$ under the misspecified BH model. Thus, for a given predictive set of RPs, $\mathbf{x}^\star$, the BH metamodeled quantity is given by kriging prediction as $N(\hat{y}(\mathbf{x}^\star), \hat{\sigma}^2(\mathbf{x}^\star))$, where $\hat{y}(\mathbf{x}^\star)$ is the kriging mean (as previously described in Eq. (2.14)) and $\hat{\sigma}^2(\mathbf{x}^\star)$ provides estimate uncertainty via the kriging predictive variance given by,

$$\hat{\sigma}^2(\mathbf{x}^\star) = \mathbf{R}(\mathbf{x}^\star, \mathbf{x}^\star) - \mathbf{r}(\mathbf{x}^\star)' \boldsymbol{R}_\ell^{-1} \mathbf{r}(\mathbf{x}^\star). \tag{4.13}$$

Model failure with respect to estimating $\frac{F^*}{M}$ under the BH model is measured by the percent error as previously described in Section (3.3.2.1). When the BH model estimates $\frac{F^*}{M}$ well, the percent error is expected to be small in the following sense,

$$\frac{\frac{F^*}{M} - \frac{\hat{F}^*}{M}}{\frac{F^*}{M}} \leq P. \tag{4.14}$$

P defines the extent of model failure on the scale of percent error. For measuring catastrophic model failure P was chosen to be 0.5, but smaller values of P may be chosen to emphasize regions of more subtle model failure. Since $\frac{F^*}{M}$ is generally underestimated for stocks above the BH set, a one-sided test is used to identify model failure. Thus, when the percent error is statistically greater than P the notion that the BH model estimates $\frac{F^*}{M}$ well (in the sense defined by P) is rejected.

For statistical evaluation, it is convenient to rearrange Eq. (4.14) as $\hat{F}^* \geq (1-P)F^*$.

$\hat{F}^*$ is then distributed as $LN(\hat{y}(\mathbf{x}^\star), \hat{\sigma}^2(\mathbf{x}^\star))$, and catastrophic model failure is predicted in regions of RP space where the 5^{th} percentile of the Log-normal distribution falls below $(1-P)F^*$.

Figure (4.9) shows the clustering thresholds for the low contrast simulations of each of the fast, medium, and slow growth simulation settings. Each line separates hypothetical stocks where simulations would expect the BH model to catastrophically fail in RP estimation. A percent error of 50% was chosen to represent the threshold of catastrophic model failure so that the nearly minimal distance mapping occurs below the lines and dramatic underestimation of $\frac{F^*}{M}$ occurs for data generated above each line.

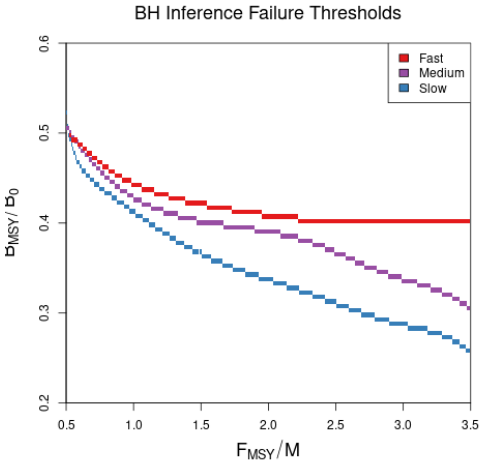

Figure 4.9: BH RP estimation catastrophic model failure ($P = 0.5$) thresholds with decreasing individual growth dynamics.

In general clustering thresholds are oriented to the shape of the BH RP set in each of the simulated individual growth settings. As individual growth slows from the SPM limit (in red) to the most emphatically slow growing simulation in blue, the BH model fails catastrophically for an increasingly large range of RP space. This indicates that the slower growing simulation makes the BH model more brittle to model misspecification.

In particular the fragility of the BH model is exacerbated most for high $\frac{F^*}{M}$ stocks as individual growth slows. For low $\frac{F^*}{M}$ stocks the failure thresholds for each simulated individual growth setting converges around the common value $\frac{B^*}{B_0} = 0.5$.

Model misspecification of the BH model is compounded in the slower individual growth settings, indicating an interaction between the functional form of recruitment and growth dynamics. In the following section, this interaction is exemplified by exploring oscillatory dynamics that arise outside of the more biological regimes explored here.

4.3.5 Oscillatory Growth. The Road to Chaos.

While the above patterns of RP estimation follow for the negatively correlated growth and maturity parameters (i.e. $corr(a_s, \kappa) < 0$), as a_s increases to weaken (and eventually reverse) this negative correlation between a_s and κ, a regime of oscillatory dynamics appear. While RP estimation behaves somewhat similar in this oscillatory regime there are unique features in this setting. Below consider the oscillatory example of a logistic DDM with $a_s = 10$, $\kappa = 0.1$ and fishing fixing at F^* (i.e. low contrast: $\chi = 0$).

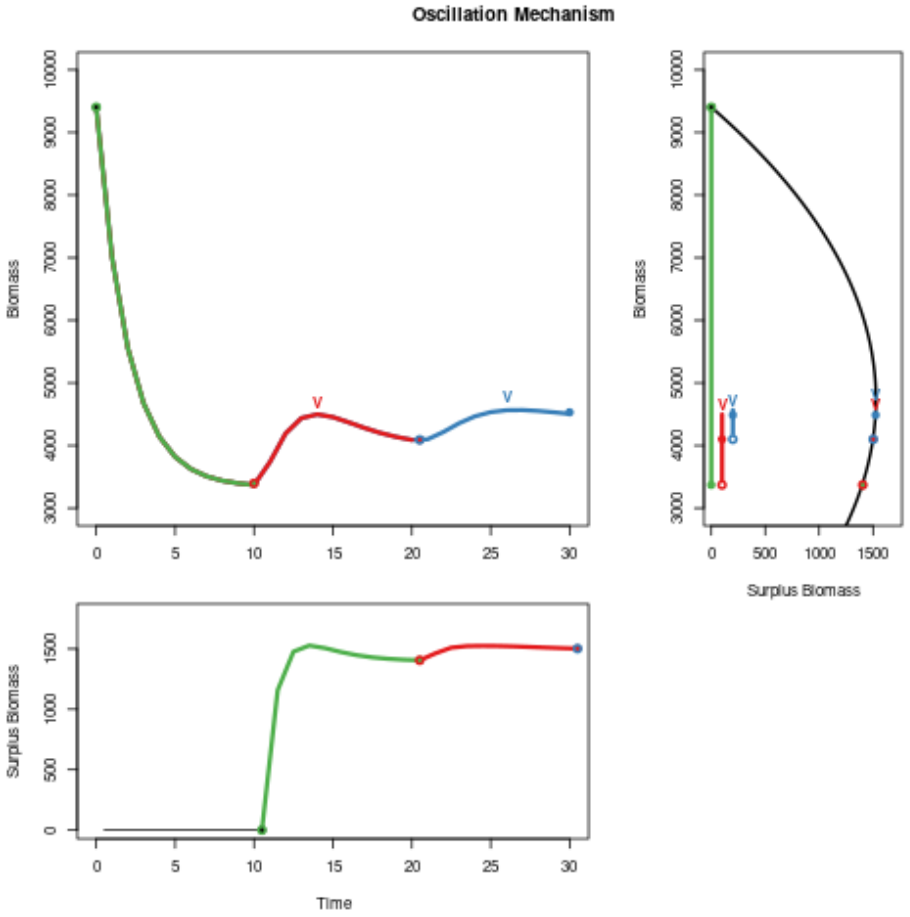

Figure 4.10: *top left* : Logistic DDM biomass over 30 epochs of time with $a_s = 10$. Green, red, and blue colors indicate three 10 epoch long windows of biomass. v indicates local biomass oscillation maxima. *top right* : Surplus biomass production plotted over the range of biomasses shown. The biomass range of each 10 epoch window is shown in the vertical colored lines. *bottom left* : Surplus biomass production plotted through time. Colors correspond to the lagged biomass region that results in the evaluated yield. The black horizontal line demonstrates the pre-model assumption of biomass fixed at B_0.

Figure (4.10) demonstrates the mechanism of how these oscillatory dynamics form. Oscillatory dynamics appear when fishing pushes biomass past B^* within the lagged a_s window. When $t \leq 0$ the delay model assumes that biomass is fixed in equilibrium at B_0. Therefore in the green region of the biomass series, $0 < t < 10$, the population recruits at $R(B_0)$. Figure (4.10) shows that in this initial period $R(B_0)$ results in zero surplus yield for that period, and biomass falls as a result.

Once t exceeds a_s, the lagged recruitment refers to the integrated biomass series to evaluate recruitment based on B_{t-a_s}. The red region of the biomass series is the result of surplus biomass production (i.e. evaluation of the yield curve) over the initial green biomasses. Figure (4.10) shows that the surplus biomass production over the green biomass series first increases, as biomass decreases to approach B^* ($B^* \approx 5000$ here). As biomass decreases below B^*, surplus biomass then decreases to create the local maximum in the red biomass series.

Furthermore, the blue region of the biomass series is then based on surplus biomass over the red biomasses. Notice that since the red biomasses first increase and then decrease, surplus biomass increases as the red biomass increases and surplus biomass subsequently decreases following the descending leg of the red biomass series. This surplus biomass pattern carries the oscillation of the red biomass region forward into the blue region despite the red biomasses never increasing past B^*.

This process of biomass oscillation carries on in this manner nonetheless approach-

ing equilibrium at B^*. Equilibrium is reached in an oscillatory manner set off by the green biomass series crossing over from above B^* to below it. The example shown in Figure (4.10) exemplifies the oscillatory phenomena simulated here, but the mechanism that produces these oscillations may occur with other forms of recruitment, or fishing, outside of logistic recruitment whenever fishing causes biomass to cross over B^* within the lagged recruitment window. By repeatedly forcing the population biomass over the B^* threshold, in this manner, the dynamics can quickly resemble the behavior of chaotic equations [2, 77].

4.3.5.1 RP Estimation

Statistical inference in the oscillatory regimes of individual growth can be challenging. Depending on the parameters inferred, the likelihood can have multiple local modes which require global optimization techniques to distinguish. Furthermore, parameter estimation is more uncertain in this setting as the likelihood may confuse oscillations with residual noise.

Figure (4.11) shows the BH RP mapping fixing $w(10;0.1) \approx 0.6$ in the high contrast simulation setting. This places the dynamics firmly in the oscillatory regime, but the high contrast setting provides significant information for inferring recruitment parameters.

Interestingly in this high contrast setting, a very similar two regime pattern of RP inference is observed as previously seen in low contrast settings. That said the boundary between the regimes in this setting is much smoother and the location of the break between these regimes appears around higher values of $\frac{B^*}{\bar{B}(0)}$.

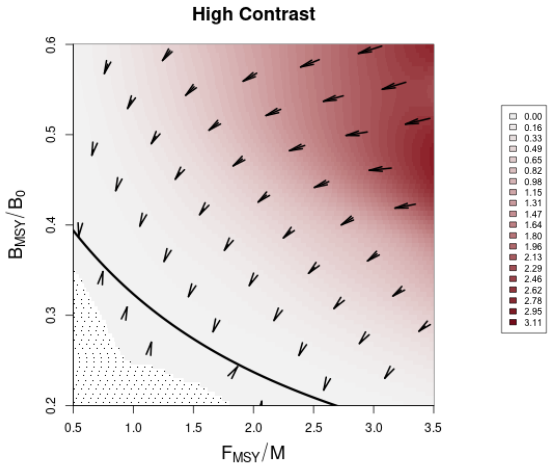

Figure 4.11: RP mapping of BH DDM fit to high contrast Schnute DDM data under oscillatory growth ($a_s = 10$ and $\kappa = 0.1$).

This higher $\frac{B^*}{\bar{B}(0)}$ break point, hovering around 0.5, is consistent with the mechanism which induces oscillation. For fixed B_0 increased $\frac{B^*}{\bar{B}(0)}$ will tend to exacerbate oscillatory behavior by increasing B^* so that biomass is more easily pushed past B^* by fishing within the initial lagged window of recruitment. This produces more dramatic oscillations in the higher $\frac{B^*}{\bar{B}(0)}$ region of RP space. This phenomena may also be understood in terms similar to the notion of elasticity described by Yeakel and Mangel [85] and its relationship with γ and B^*.

The fitted BH model does not produce significant oscillations because under the BH model $\frac{B^*}{B(0)}$ is constrained below 0.5 with the majority of the simulation BH $\frac{B^*}{B(0)}$ RPs falling between 0.4 and 0.2. Therefore, the fitted BH model will not tend to push biomass past B_{MSY} and thus is incapable of modeling oscillatory biomass series. Figure (4.12) shows a subset of example BH fits, which demonstrates the limited oscillatory capacity of the BH fits. Furthermore, since the BH model has a limited oscillatory capacity in this setting, the BH model tends to explain the oscillations with artificially high residual variation and artificially low α, focusing fits on overly simplistic trends in the data.

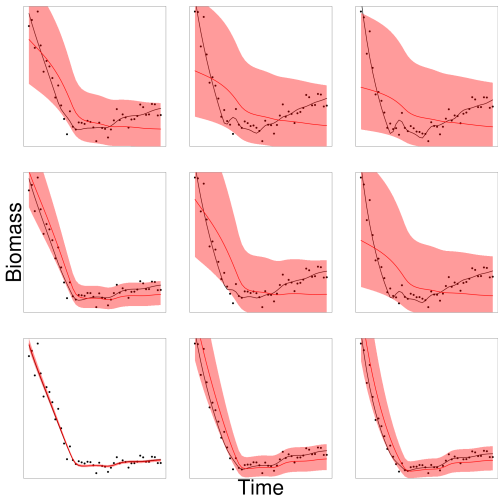

Figure 4.12: Example BH fits (*red*) to Schnute data (*black*). Each example plot is arranged to mirror its location in RP space.

4.3.5.2 Estimating More

Figure (4.13) shows a subset of example model fits to Schnute data simulated broadly over RP space with residual variation, $\sigma = 0.12$, resulting in a CV of about 6%. Model fits are shown both under the two-parameter BH model as well as under the three-parameter Schnute model, each model estimating all of its recruitment parameters as well as the individual growth and maturity parameters κ and a_s.

While estimating κ and a_s is not typically done in practice, these parameters are estimated here to demonstrate the interaction that can be present between recruitment and growth parameter estimation. Notice that the BH model, even when additionally estimating κ and a_s, does not gain the flexibility to properly model Schnute data.

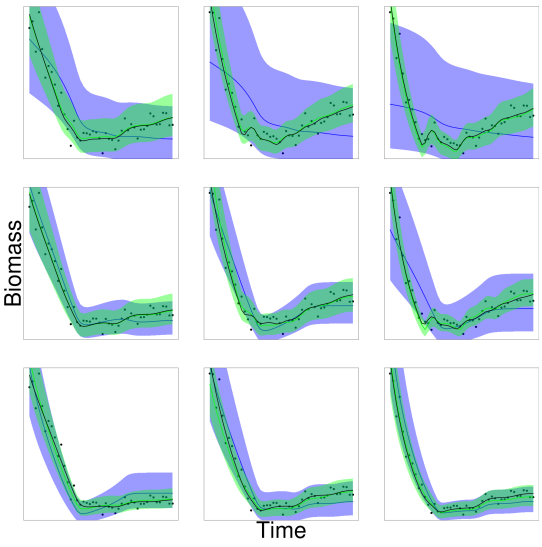

Figure 4.13: κ and a_s estimation under BH (*blue*) and Schnute (*green*) fits to Schnute data (*black*) arranged to mirror RP space.

On the one hand the lack of oscillatory dynamics produced by the BH model causes the misspecified BH fits in Figure (4.13) to largely estimates κ and a_s so as to approximate the SPM limiting case. The fitted Schnute model on the other hand, can produce the oscillatory dynamics and thus the information in the oscillatory data well inform estimates of κ and a_s under the Schnute model. Furthermore, the Schnute model has no issue learning its γ parameter.

While statistical inference in the oscillatory regime can be challenging in the highly constrained BH model, the Schnute model can easily estimate its extra γ parameter. The flexibility of estimating γ simplifies inference by correctly specifying RPs, and also by opening up the model dynamics to reveal additional information about κ and a_s in the data.

4.4 Discussion

The addition of individual growth, lagged maturity and selectivity dynamics, via the DDM, to the previous SPM results further reiterates the general patterns observed in Chapter (3). The added individual growth dynamics, and the modest effect they have on modifying the BH RP set as seen in Figure (4.2), expands the notion that RP estimation under two-parameter recruitment models are largely oriented to the geometry induced by the restricted recruitment model rather than adult growth. Furthermore, the added individual growth dynamics of the DDM demonstrates that the BH model can become very brittle for slower growing species, most notably resulting in underestimation of F^* in low contrast settings.

The general behavior of the RP mapping in the DDM setting is very similar to that observed under the SPM in Chapter (3). In the presence of contrast RPs consistently map onto the BH set in a manner resembling a shortest distance map inducing bias in both $\frac{F^*}{M}$ and $\frac{B^*}{\bar{B}(0)}$. In the low contrast setting the RP mapping has two primary regimes, a region of relatively minor BH model misspecification with intact nearly shortest distance RP estimation, and a region of catastrophic failure of RP estimation where $\frac{F^*}{M}$ is dramatically underestimated outside of the intact region. This poses the same general risk profile for fisheries management with BH RP estimates in the DDM setting as for the SPM. The primary difference in RP estimation of the DDM as compared with the SPM is the degree of allowable model misspecification of the BH model before the

catastrophic failure mode of RPs sets in. As growth becomes a larger component of the dynamics, the BH model becomes more brittle with a decreased range of model misspecification resulting in intact RP estimation.

The flexibility of the recruitment function is the primary driver of the space of RPs that can be modeled by these fisheries models. While individual growth contributes to RP flexibility, the effects of growth dynamics on the range of modeled RPs is secondary to the model of recruitment. By specifying a BH model of recruitment, we a priori reduce the space of RPs dramatically and the RP flexibility offered by individual growth and maturity dynamics is heavily influenced by the model of recruitment. Furthermore the mapping that statistical inference produces onto these restricted spaces is a function of this interaction between individual growth and recruitment. The brittleness observed under the BH model in the slower individual growth settings indicates that not only does the BH model limit the space of RPs, but even when a_s and κ are correctly specified an incorrect specification of the BH model dampens the effects of those growth dynamics.

The analysis of oscillatory dynamics demonstrate how individual growth interacts with the form of recruitment. This interaction under the BH model exacerbates model misspecification by dampening the information that individual growth contributes to biomass dynamics. At this time it is not best practice to estimate individual growth parameters from index of abundance data as done in Section (4.3.5.2). This analysis is consistent with that practice when the BH model of recruitment is misspecified (as

it so often may be). However if recruitment is made more flexible by the use of a three-parameter model, such as the Schnute curve, not only is the γ parameter possible to estimate, but the flexibility that this adds to the model of recruitment is vital to tapping into the information about a_s and κ that may be available in index data. Of course if index data is sufficiently noisy there may not be much discernible information available about a_s and/or κ since the features they control in biomass dynamics may easily be confused with residual variation, and the observed behavior of the BH model demonstrates that overly restricted models of recruitment worsen this effect.

The results presented here suggest that future work should be done to investigate the feasibility of using three-parameter recruitment models in stock assessments. Firstly, this study makes it clear that two-parameter recruitment models can induce significant biases in RPs, and the use of three-parameter models of recruitment can certainly contribute to better RP estimates. Three-parameter models of recruitment can be directly estimated to allow better estimates of RPs (even when growth dynamics are dominant in the model). Alternatively, the increased flexibility of three-parameter models can be used to improve RP estimation without direct estimation of γ by resolving structural inconsistencies presented by RP proxies as seen in Appendix (C). Secondly, the results presented here suggest that better specification of recruitment may make models less brittle. Particularly for slow growing, data-limited stocks, where the available data does not demonstrate good contrast, the use of three-parameter models may improve the reg-

ularity of parameter estimation and allow stock assessment models to better access the information that is available in limited datasets. Furthermore, results presented here suggest that three-parameter recruitment models may be useful for supplementing the inference of individual growth and maturity parameters beyond the external analysis of age data.

The DDE structure given in [82, 17, 69], together with Schnute three-parameter recruitment, makes the DDM presented here an extraordinarily general, and compact, model for analysis of a wide range of dynamics. This one DDE can exactly represent everything from the simplest Schaefer model, to Ricker, BH, or Cushing-like models, all with a wide range of individual growth and maturity dynamics ranging from simple SPMs, lag-only models (similar to [19]), ranging up to simple ASMs. While not all RPs can be represented analytically, under many common models the RPs are analytical. The methods presented here for navigating RPs across the variety of different models representable by this compact DDM open the door to countless future uses in stock assessment.

Chapter 5

Conclusion

This thesis develops a metamodeling simulation framework for evaluating RP estimation under misspecified two-parameter models of productivity. By developing three-parameter models in the SPM and DDM settings, analytical and numerical methods are provided for generating data broadly in RP space under the Schnute and PT models. A GP metamodel is presented for explicit analysis of RP biases under two-parameter models. The analytical methods for navigating the relationship between three-parameter models and RPs form the foundation of a paper under review based on the work presented in Appendix (C). The implementation and analytical results for the DDM is particularly novel and contributes to further expansion of the use of DDM models in data-limited stock assessment. Additionally involvement in these projects have lead to my contributions in recent stock assessments[20].

The simulation setting under the PT/Schaefer models in Chapter (2) demonstrates a simplified and fully analytical setting for developing the conceptual basis of how two-parameter productivity models may bias RP estimation. A useful notion of contrast is developed here, and the simplified geometry of the Schaefer model aids in understanding mechanisms by which a lack of contrast contributes to RP biases. The simulation and metamodel developed in this setting forms the basis of the metamodeling analysis to be extended into the more challenging simulation settings presented in the following chapters.

Chapter (3) generalizes the simulation framework to handle SPMs where F^* is not

analytical by extending the LHD methods to generate data under the Schnute production function. Furthermore, due to the relatively more complicated RP response surface induced by the BH geometry an adaptive method of augmenting the simulation design is developed for refining hard to resolve features. The metamodel analysis of RP estimation under the BH model generalizes the RP mapping developed under the Schaefer model to more complex RP sets. Under the BH model RP inference demonstrates an approximately shortest distance mapping onto the constrained RP space as mediated by the information content provided by the available contrast in the data. For the BH RP geometry (unlike the Schaefer model) this shortest distance mapping ensures that if there is bias in one of $\frac{B^*}{B_0}$ or $\frac{F^*}{M}$, there will necessarily be bias in the other RP. These biases would tend to result in potentially overly cautious management for stocks that are more density dependent than the BH model, but leads to overestimation of $\frac{F^*}{M}$ for stocks that are less density dependent than the BH model. Furthermore, the low contrast simulation setting demonstrates that heavily misspecified BH models demonstrate a catastrophic failure mode that dramatically underestimations $\frac{F^*}{M}$ so as to prioritize high level biomass tends in the data.

The development of the DDM in Chapter (4) further extends the simulation-based analysis of RPs to account for the effects of individual growth and lagged maturity/selectivity dynamics. While F^* is not analytical under the general Schnute DDM, many of the special cases of the Schnute model do provide analytical RP calculations for the

DDM. Furthermore the analytical results derived under the general Schnute DDM provide stable methods for navigating RP space to describe RP behavior for general density dependence simultaneously accounting for individual growth and maturity. The effects of individual growth and maturity on RPs are found to be small relative to the form of recruitment, but differ by the level of density dependence. The behavior of BH RP estimation in the DDM setting is generally very similar to the SPM setting. The relationship between the form of recruitment and individual growth interact under the BH model to make RP estimation more brittle for slower growing stocks. This indicates that better, and/or more flexible, models of recruitment may be required to develop more complex DDMs as useful and practical models in stock assessment.

In most of the simulation settings described, the stationarity of the GP is a reasonable and well motivated assumption of the metamodel structure. In both the high and low contrast settings, RP estimates under the Schaefer model are smoothly varying over RP space with a steady linear mean and spatial correlation structure. Similar well motivated stationarity is observed in the high contrast BH simulations in both of the SPM and DDM settings. However, in the low contrast BH simulations the catastrophic failure mode in $\frac{F^*}{M}$ results in a distinct behavior that likely implies a different mean and correlation structure than the intact mode implies. The flexibility of the GP still accurately captures the very distinct RP estimation pattern in these regions, but due to the change in the underlying mechanism of model failure in these cases, the simu-

lation requires more design samples to produce convergence of the metamodel when the catastrophic failure mode in $\frac{F^*}{M}$ is present. While nonstationary metamodels could improve the modeling of these situations, nonstationary metamodels will themselves become more expensive to fit. For the stock assessment models considered here, it is likely that this added expense may be more costly than simply simulating a denser design, as was done.

5.1 Future Work

While the work presented here provides a novel understanding of how RPs are biased by two parameter models of productivity, there are always improvements that can be made in future study. There are two major directions for interrelated future work. Firstly, there is always a desire to study additional biology dynamics. Secondly, the results presented here suggest that studying these more complex biologies would be aided by extensions to the metamodeling techniques.

Given the role of contrast for informing productivity parameters, and thus RPs, improved notions of understanding contrast could improve this analysis. This analysis develops some mechanisms by which the lack of contrast fails to inform RPs, but developing a deeper understanding of how contrast informs parameters, or at least developing methods of quantifying observed contrast, more generally is clearly important

for contextualizing model fit. The notion of contrast developed in Section (2.2.6) is representative of many California fisheries and is useful for the simulation purposes here, but methods of understanding the notion more generally would be extremely valuable.

The catchability parameter, q, is fixed throughout this work due to the weak identifiability between q and K (or β as the case may be). As described in Section (2.2.7), this issue arises when estimating both quantities in low contrast simulations. This work explores the lower extent of contrast by fixing q to focus on the estimation properties of θ, and therefore RPs, in the weakest information settings. That said, many stock assessments enjoy more informative data than the minimal contrast setting simulated here, and often q is not known. By tuning χ to the lowest value that allows identification of q over the range of simulated RPs, one may extend this work to estimate q, albeit over a smaller range of contrast. This is a natural direction for future work and would also contribute to developing a more specific understanding of the role of contrast in fisheries models.

While the DDM developed in Chapter (4) parsimoniously develops the most foundational biological processes in fisheries management, further developing RP analyses that account for additional biological processes are always desired. The addition of recruitment deviations to the DDM is clear a next step. Thorson et. al. [80] show that modeling recruitment deviations as a random effect composed with BH recruitment can reduce bias in estimates of depletion and improve uncertainty quantification

for data-limited models of Pacific hake. The methods presented in this thesis are an ideal framework for understanding those results more broadly in terms of RP model misspecification. Furthermore, the simulation framework developed here provides a straightforward path for extending into the analysis of more complex ASMs such as Stock Synthesis [49] or FIMS [78].

The metamodeling structures developed here have proven effective tools for understanding RP biases in the SPM and DDM settings presented. That said, several improvements may be made to the metamodeling simulation framework itself to facilitate this analysis in more complex settings. Improving the speed of simulations would allow for more easily relaxing the simulation assumptions around estimating q and increasing the simulated values of residual variation. Decreasing simulation run time to the order of days in more complex settings would allow the analysis to condition on specific stock assessment models and data (i.e. catches, ages, lengths) to consider how RP model misspecification may manifest in a given stock assessment. It was not considered a priority for the work presented in this thesis but by more effectively refining the simulation design through the use of more pointed acquisition functions[56], fewer simulations may be collected [1]. In particular, since optimization is not a goal of the metamodel in this setting, developing entropy-based acquisition functions [30, 31] could be useful here. Furthermore, given the catastrophic model failure that was observed under low contrast BH models, particularly in the slower growing examples, it

[1]The primary factor for determining the run time of these simulations

could be valuable to consider nonstationary GP metamodels [27, 6, 29]. These metamodels will come with much more complexity and expense on the metamodeling side of this framework, but for the analysis of more computationally expensive stock assessments these costs may be outweighed by a more efficient identification of catastrophic failure modes.

Appendix A

Inverting $\frac{B^*}{\bar{B}(0)}$ and γ for the PT Model

Under the PT model, as parameterized in Chapter (2), an expression for $\frac{B^*}{B(0)}$ in terms of γ is given by Eq. (2.10). Letting $\zeta = \frac{B^*}{B(0)}$, and inverting Eq. (2.10) to express γ in terms of ζ proceeds as follows,

$$\begin{aligned}
\zeta &= \left(\frac{1}{\gamma}\right)^{\frac{1}{\gamma-1}} \\
\zeta &= \gamma\zeta^{\gamma} \\
\zeta &= \gamma e^{\gamma\log(\zeta)} \\
\zeta\log(\zeta) &= \gamma\log(\zeta)e^{\gamma\log(\zeta)}.
\end{aligned}$$

The Lambert product logarithm, W, is defined as the inverse function of $z = xe^x$ such that $x = W(z)$ [40, 13]. Applying this definition allows for the isolation of γ,

$$\begin{aligned}
\gamma\log(\zeta) &= W\left(\zeta\log(\zeta)\right) \\
\gamma &= \frac{W\left(\zeta\log(\zeta)\right)}{\log(\zeta)}.
\end{aligned} \tag{A.1}$$

The Lambert product logarithm is a multivalued function with a branch point at $-\frac{1}{e}$. The principal branch, $W_0(z)$, is defined on $z \in \left(-\frac{1}{e}, \infty\right)$, and the lower branch, $W_{-1}(z)$, is defined on $z \in \left(-\frac{1}{e}, 0\right)$. Taken individually, each respective branch is analytic, but cannot be expressed in terms of elementary functions.

When $\zeta \in \left(0, \frac{1}{e}\right)$ the solution of interest in Eq. (2.11) comes from W_0. When $\zeta \to \frac{1}{e}$,

the Fox Model emerges as $\gamma \to 1$. When $\zeta \in \left(\frac{1}{e}, 1\right)$ the solution of interest comes from W_{-1}. For the use case presented here, Eq. (2.11) is to be interpreted as,

$$\gamma = \begin{cases} \frac{W_0(\zeta \log(\zeta))}{\log(\zeta)} & \zeta \in \left(0, \frac{1}{e}\right) \\ \\ \frac{W_{-1}(\zeta \log(\zeta))}{\log(\zeta)} & \zeta \in \left(\frac{1}{e}, 1\right) \end{cases} . \tag{A.2}$$

Appendix B

A Schaefer Model with Explicit *M*

The Schaefer model is typically stated as discussed in Chapter (2)

$$\frac{dB}{dt} = rB\left(1 - \frac{B}{K}\right) - FB. \tag{B.1}$$

However under model 3.3, when $\gamma = 1$, $P_s(B;[\alpha,\beta,1])$ reduces to quadratic logistic production and draws a parallel to the logistic production of the typical Schaefer model. The typical Schaefer model does not explicitly include M, but rather natural mortality is assumed to be implicit in the quadratic form of surplus production. That said, if natural mortality is explicitly included in a model with logistic production, as seen in Chapter (3) under the Schnute model when $\gamma = 1$, it is straight forward to show that the result is in fact a Schaefer model with updated parameters that explicitly model M.

$$\begin{aligned}
\frac{dB}{dt} &= \alpha B(1-\beta B) - (M+F)B \\
&= \alpha B - \alpha\beta B^2 - MB - FB \\
&= (\alpha - M)B - \alpha\beta B^2 - FB \\
&= (\alpha - M)B\left(1 - \frac{\alpha\beta}{\alpha - M}B\right) - FB
\end{aligned} \tag{B.2}$$

The linear MB term naturally combines with the quadratic form of $P_s(B;[\alpha,\beta,1])$ to simplify into another quadratic form that is now directly analogous with the typical Schaefer model seen in Eq. (B.1). This process produces a Schaefer model with the

following updated parameters

$$\frac{dB}{dt} = r'B\left(1 - \frac{B}{K'}\right) - FB \tag{B.3}$$

$$r' = \alpha - M \qquad K' = \left(\frac{\alpha - M}{\alpha}\right)\frac{1}{\beta}. \tag{B.4}$$

$P_s(B;[\alpha,\beta,1])$ represents the biomass production independent of mortality. By combining MB into the quadratic form, a new intrinsic population growth rate, r', is derived which represents the maximum rate of biomass production less natural mortality. Similarly, carrying capacity is shrunk by the factor $\frac{\alpha-M}{\alpha}$ which can be interpreted as the percent decrease of α by removing M.

Furthermore working with $\gamma = 1$ in the analytical expression of Schnute RPs, as given in Chapter (3), analytical RPs take the expected values. For example, working with the equation for α from Eq. (3.10), with $\gamma = 1$, F^* is shown to takes the expected form for a Schaefer model.

$$\begin{aligned}\alpha &= (M + F^*)\left(1 + \frac{F^*}{M + F^*}\right)\\ &= M + 2F^*\\ F^* &= \frac{\alpha - M}{2} = \frac{r'}{2}\end{aligned} \tag{B.5}$$

Working with Eq. (3.5) from the text gives the expected carrying capacity.

$$
\begin{aligned}
B_0 &= \frac{1}{\beta}\left(1-\frac{M}{\alpha}\right) \\
&= \frac{\alpha - M}{\alpha\beta} = K'
\end{aligned}
\tag{B.6}
$$

Furthermore, Eq. (3.5) for B^* gives,

$$
\begin{aligned}
B^* &= \frac{1}{\beta}\left(1-\frac{M+\frac{\alpha-M}{2}}{\alpha}\right) \\
&= \frac{1}{\beta} - \frac{M+\alpha}{2\beta\alpha} \\
&= \frac{\alpha - M}{2\alpha\beta} = \frac{K'}{2}.
\end{aligned}
\tag{B.7}
$$

Finally $\frac{B_{MSY}}{B_0}$ in the case of explicit mortality is indeed also $\frac{1}{2}$,

$$
\frac{B^*}{B_0} = \frac{K'/2}{K'} = \frac{1}{2}.
\tag{B.8}
$$

This is a similar model as the logistic model discussed by Aalto et. al. [1], albeit their model includes additional dynamics. In terms of the complexity of dynamics, the model presented by Aalto et. al. prioritizes differing lags of recruitment and mortality to increase complexity over the SPM presented in Chapter (3). The special case of logistic recruitment in the DDM presented in Chapter (4) has a simplified lag structure as compared with the Aalto et. al. model but would be similar to their logistic model albeit with an explicit handling of individual growth.

Appendix C

The Schnute Model's Relationship to

RP Proxies

Due to the difficulty of calculating RPs, in particular F^* as exemplified by the Schnute model as seen in Sections (3.2.1) and (4.2.2), proxies of RPs have been developed [9, 41, 10]. One such proxy is the fishing rate that brings the *Spawning Potential Ratio* (SPR) to $x\%$ of B_0, also known as F_{SPR_x}. This definition implies the following relation between total mortality, B_0 and R_0.

$$(F_{SPR_x} + M)xB_0 = R_0$$

By setting x appropriately the hope is that F_{SPR_x} is a easily calculable proxy for F^*. Calculating F_{SPR_x} is relatively more straightforward than F^* because it is independent of the functional form of productivity. Since R_0 is defined as $R_0 = MB_0$, F_{SPR_x} can then be written as,

$$\begin{aligned} F_{SPR_x} &= \frac{R_0}{xB_0} - M \\ &= \frac{MB_0}{xB_0} - M \\ &= M\left(\frac{1}{x} - 1\right). \end{aligned} \tag{C.1}$$

Another proxy used manages fishing so as to target an equilibrium biomass that is $y\%$ of B_0, denoted B_y. When B_y is combined with the F_{SPR_x} proxy (of F_{MSY}), B_y is thought of as a proxy for $\frac{B_{MSY}}{B_0}$. Enforcing both proxies simultaneously implies

	x	$\frac{F_{SPR_x}}{M}$	$\left[\frac{F^*(y)}{M}\right]_{BH}$	y (of B_y)	$\left[\frac{\bar{B}(F_{SPR_x})}{B_0}\right]_{BH}$
RF	0.50	1	0.5	0.40	0.33
GF	0.45	1.22	0.5	0.40	0.31
FF	0.30	2.33	2	0.25	0.23

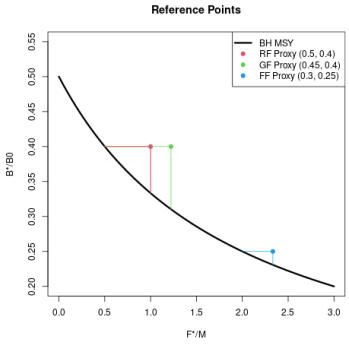

Figure C.1: Management targets and BH RP projections for Rockfish, Groundfish, and Flatfish management categories.

$\frac{\bar{B}(F_{SPR_x})}{B_0} = y$. By managing the population so as to target these two proxies simultaneously it is thought that the population is approximately managed to a state of *MSY* (erring conservatively).

Under a two parameter BH SPM, enforcing these two proxies uniquely specifies a single BH α parameter to make the recruitment relationship consistent with both proxies. As a statistical model, this only leaves β free to estimate the scale of the population B_0 with no additional degrees of freedom to learn anything about RPs from data. Furthermore, fixing α to match the management proxies over-constrains *MSY* RPs. The table in Figure (C.1) lists the current proxy targets, along with BH RPs projected from the proxies, for Rockfish (RF), Groundfish (GF) and Flatfish (FF) management categories.

In Figure (C.1) notice that $y > \left[\frac{\bar{B}(F_{SPR_x})}{B_0}\right]_{BH}$ consistently for all categories. This is a conservative management approach from the BH perspective since species are managed to biomasses that are greater than the BH B^*, but it also admits that proxy values are inconsistent with the underlying dynamics used to estimate biomass in the first place.

Furthermore the BH SPM necessitates that the chosen proxy values will never equal the RPs they are intended to approximate.

Under the three-parameter Schnute model the γ parameter provides an additional degree of freedom that can be used to resolve the limiting issues presented by the BH model in any of a number of ways. One potentially compelling use of this extra degree of freedom is to engineer the values of α and γ to demand consistency of the proxies and *MSY*. This necessitates that RPs are always equal to their measurable proxy approximations, and it resolves the inconsistency between proxies and the underlying dynamics used to estimate the biomasses to which they are compared. The Schnute model can do this by using γ to tie proxies directly to the true RPs that they are intended to approximate. This makes the proxies easily calculable quantities that truly represent Schnute *MSY* RPs.

To derive the values of α and γ that will result in consistency of the proxies with *MSY* we first consider the expression of $\frac{\bar{B}(F)}{B_0}$ under the Schnute SPM (similar to Eq.(3.6)) evaluated at F_{SPR_x} (as given in Eq. (C.1))

$$\begin{aligned}\frac{\bar{B}(F_{SPR_x})}{B_0} &= \frac{1-\left(\frac{M+\left[M\left(\frac{1}{x}-1\right)\right]}{\alpha}\right)^{\gamma}}{1-\left(\frac{M}{\alpha}\right)^{\gamma}} \\ y &= \frac{1-\left(\frac{M}{x\alpha}\right)^{\gamma}}{1-\left(\frac{M}{\alpha}\right)^{\gamma}}. \end{aligned} \tag{C.2}$$

Solving Eq. (C.2) for α gives a relation between α, and γ that defines an infinite

family of Schnute curves that respect the proxy values x and y.

$$\alpha = M\left[\frac{\frac{1}{x^{\gamma}} - y}{1-y}\right]^{1/\gamma} \qquad \text{(C.3)}$$

Now to align the proxy α-γ values given by Eq. (C.3) with *MSY* RPs we recall Eq.(3.10) from the text,

$$\alpha = (M+F^*)\left(1+\frac{\gamma F^*}{M+F^*}\right)^{1/\gamma}. \qquad \text{(C.4)}$$

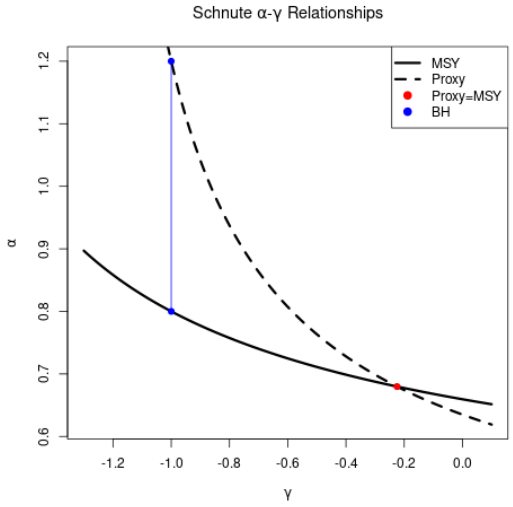

Figure C.2: α-γ relationships between Schnute MSY RPs, Eq. (C.5), and proxies, Eq. (C.3), for the Rockfish management category. The discrepancy that the BH model presents between MSY RPs and proxies is shown by the difference in the implied values of α respectively (shown in blue) when $\gamma = -1$ under the BH model.

While this expression for α was previously used in simulation design, here it is used as a relation between α and γ that defines an infinite family of Schnute curves that respect a given value of F^*. Eqs. (C.3) and (C.4) each define different sub-families of Schnute curves that respect the proxies and *MSY* respectively. When taken together, the curves intersect to uniquely identify a single pair (α, γ) that both respect the proxies and *MSY* simultaneously. With the aim of isolating this point, Eq. (C.3) and Eq. (C.4) can be equated to find the value of γ that brings proxies into agreement with *MSY*. When RPs and proxies are in agreement, $F^* = F_{SPR_x}$ and thus F^* in Eq. (C.4) may be replaced by

Eq. (C.1) to write the MSY relation in terms of x and y as,

$$\alpha = \frac{M}{x}\Big(1+\gamma(1-x)\Big)^{1/\gamma}. \tag{C.5}$$

Now equating Eqs. (C.3) and (C.5) and then simplifying with the aim of solving for γ gives,

$$\begin{aligned}
\left[\frac{\frac{1}{x^{\gamma}}-y}{1-y}\right]^{1/\gamma} &= \frac{1}{x}\Big(1+\gamma(1-x)\Big)^{1/\gamma} \\
1-yx^{\gamma} &= \Big(1+\gamma(1-x)\Big)(1-y) \\
1 &= \left[1-\gamma\frac{(1-x)(1-y)}{y}\right]x^{-\gamma}.
\end{aligned}$$

At this point it convenient to make the substitution $r(x,y) = \frac{y}{(1-x)(1-y)}$. Making this substitution, and factoring, simplifies the above form as,

$$r(x,y) = \Big(r(x,y)-\gamma\Big)x^{-\gamma}. \tag{C.6}$$

Recall the Lambert product logarithm, W, is defined as the inverse function of xe^x such that $x = W(xe^x)$ [40, 13]. Isolating γ requires that the above expression be placed into the form xe^x to apply the definition of W.

$$
\begin{aligned}
r(x,y)x^{r(x,y)} &= \Big(r(x,y)-\gamma\Big)x^{r(x,y)-\gamma} \\
r(x,y)x^{r(x,y)}\log(x) &= \Big(r(x,y)-\gamma\Big)\log(x)e^{\Big(r(x,y)-\gamma\Big)\log(x)} \\
W_{-1}\Big(r(x,y)x^{r(x,y)}\log(x)\Big) &= \Big(r(x,y)-\gamma\Big)\log(x) \\
\gamma &= r(x,y) - \frac{W_{-1}\Big(r(x,y)x^{r(x,y)}\log(x)\Big)}{\log(x)} \qquad \text{(C.7)}
\end{aligned}
$$

The solution of interest for the γ (bringing proxies into agreement with MSY) comes from W_{-1} branch of the Lambert product logarithm. To complete the point (α,γ), α may be computed by substituting γ from Eq. (C.7) into either of Eqs. (C.3) or (C.5) to give α in terms of only the proxies and the Lambert product logarithm.

Figure (C.3) demonstrates how the BH RPs can be generalized by the three parameter Schnute model to bring *MSY* RPs into alignment with the proxy values. The colored curves show Schnute RPs with γ's fixed by Eq. (C.7). Notice that the proxy values fall along the colored curves, with the specific location of the the proxy point given by the α as derived by plugging γ back into either of Eqs. (C.3) or (C.5).

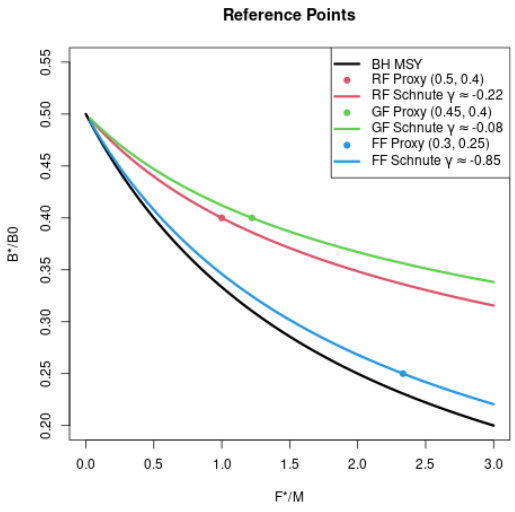

Figure C.3: BH MSY RP curve, along side Schnute MSY RP curves with γ chosen to match the management proxies.

In concept, other three-parameter models should allow similar flexibility, but the results may not be analytical as given here for the Schnute model. While other three-parameter models should be able to bring RPs into correspondence with their proxies, the differing functional forms of various three-parameter models may result in yield curves that behave in unexpected ways. A beautiful feature of the Schnute model used in this way is that the derived γ values generalize the BH model in a way that results in familiar production models such as the Cushing-like, BH, Ricker, or Logistic models each with well studied risk characteristics and dynamics.

Appendix D

Delay Differential Replacement Line

The replacement line is the rate of productivity which exactly balances biomass loss in the absence of fishing. In the SPM, productivity must simply balance biomass loss due to M. Thus when $R(B;\theta) > MB$ there will be some surplus productivity to enable fishing.

In the DDM, productivity is complicated by biomass changing, both with the recruitment of young into the reproducing population, as well as biomass accumulation due to the growth of existing individuals in the population. To derive the replacement line in the case of the DDM in Chapter (4) the equilibrium equations in the absence of fishing are considered and the $R(B)$ that this implies is then isolated.

$$0 = \frac{dB}{dt} = w(a_s)R(B) + \kappa[w_\infty N - B] - MB \tag{D.1}$$

$$0 = \frac{dN}{dt} = R(B) - MN. \tag{D.2}$$

Eq(D.2) quickly gives $\bar{N} = R(B)/M$. Substituting this equilibrium value into Eq(D.1) to rewrite N in terms of B,

$$0 = w(a_s)R(B) + \kappa\left[w_\infty \frac{R(B)}{M} - B\right] - MB. \tag{D.3}$$

Collecting like terms,

$$R(B)\left[w(a_s)+\frac{\kappa w_\infty}{M}\right]=[M+\kappa]\,B. \tag{D.4}$$

Finally solving for $R(B)$, and simplifying, gives the equation of the replacement line as,

$$R(B)=\left[\frac{M(M+\kappa)}{w(a_s)M+\kappa w_\infty}\right]B. \tag{D.5}$$

Bibliography

[1] Emilius A. Aalto, E.J. Dick, and Alec D. MacCall. Separating recruitment and mortality time lags for a delay-difference production model. *Canadian Journal of Fisheries and Aquatic Sciences*, 72(2):161–165, February 2015.

[2] Marcel Ausloos and Michel Dirickx. *The logistic map and the route to chaos: From the beginnings to modern applications*. Springer Science & Business Media, 2006.

[3] Fedor I. Baranov. *On the question of the biological basis of fisheries*. 1918.

[4] Raymond JH Beverton and Sidney J. Holt. *On the dynamics of exploited fish populations*, volume 11. Springer Science & Business Media, 1957.

[5] Raymond JH Beverton and Sidney J. Holt. *A review of the lifespans and mortality rates of fish in nature, and their relation to growth and other physiological characteristics.* Novartis Foundation Symposia. John Wiley & Sons, Ltd, Chichester, UK, January 1959.

[6] Mickaël Binois and Robert B. Gramacy. **hetGP** : Heteroskedastic Gaussian Process Modeling and Sequential Design in *R*. *Journal of Statistical Software*, 98(13), 2021.

[7] Richard P. Brent. Chapter 4: An Algorithm with Guaranteed Convergence for Finding a Zero of a Function. In *Algorithms for minimization without derivatives*. Courier Corporation, 1973.

[8] Elizabeth N. Brooks, Joseph E. Powers, and Enric Cortés. Analytical reference points for age-structured models: application to data-poor fisheries. *ICES Journal of Marine Science*, 67(1):165–175, January 2010.

[9] William G. Clark. Groundfish exploitation rates based on life history parameters. *Canadian Journal of Fisheries and Aquatic Sciences*, 48(5):734–750, 1991. Publisher: NRC Research Press Ottawa, Canada.

[10] William G. Clark. F 35% Revisited Ten Years Later. *North American Journal of Fisheries Management*, 22(1):251–257, February 2002. Publisher: Taylor & Francis _eprint: https://doi.org/10.1577/1548-8675(2002)022<0251:FRTYL>2.0.CO;2.

[11] Paul B. Conn, Erik H. Williams, and Kyle W. Shertzer. When can we reliably estimate the productivity of fish stocks? *Canadian Journal of Fisheries and Aquatic Sciences*, 67(3):511–523, 2010.

[12] Jason M. Cope, Natalie A. Dowling, Sybrand A. Hesp, Kristen L. Omori, Pia Bessell-Browne, Leandro Castello, Rowan Chick, Dawn Dougherty, Steven J. Holmes, and Richard McGarvey. The stock assessment theory of relativity: deconstructing the term "data-limited" fisheries into components and guiding principles to support the science of fisheries management. *Reviews in Fish Biology and Fisheries*, 33(1):241–263, 2023. Publisher: Springer.

[13] R. M. Corless, G. H. Gonnet, D. E. G. Hare, D. J. Jeffrey, and D. E. Knuth. On the LambertW function. *Advances in Computational Mathematics*, 5(1):329–359, December 1996.

[14] Noel Cressie. *Statistics for spatial data*. John Wiley & Sons, 2015.

[15] D. H. Cushing. The Dependence of Recruitment on Parent Stock in Different Groups of Fishes. *ICES Journal of Marine Science*, 33(3):340–362, May 1971.

[16] D. H. Cushing. Dependence of Recruitment on Parent Stock. *Journal of the Fisheries Research Board of Canada*, 30(12):1965–1976, December 1973. Publisher: NRC Research Press.

[17] R. B. Deriso. Harvesting Strategies and Parameter Estimation for an Age-Structured Model. *Canadian Journal of Fisheries and Aquatic Sciences*, 37(2):268–282, February 1980.

[18] C. Devon Lin and Boxin Tang. Latin Hypercubes and Space-filling Designs. In *Handbook of Design and Analysis of Experiments*. 2015.

[19] E. J. Dick and Alec D. MacCall. Depletion-based stock reduction analysis: a catch-based method for determining sustainable yields for data-poor fish stocks. *Fisheries Research*, 110(2):331–341, 2011. Publisher: Elsevier.

[20] E.J. Dick, Cheryl Barnes, Aaron Berger, Fabio Caltabellotta, Julia Coates, Jason Cope, Nick Grunloh, Lisa Hillier, Kristen Hinton, Melissa Monk, Corey Niles, Lief Rasmuson, Tanya Rogers, Clair Rosemond, Theresa Tsou, and Alison Whitman. Stock Assessment Review Panel Review of 2023 Stock Assessments

for Black Rockfish off Washington, Oregon and California (ID475) | National Oceanic and Atmospheric Administration. July 2023.

[21] R. I. Fletcher. On the restructuring of the Pella-Tomlinson system. *Fish. Bull*, 76(3):515–521, 1978.

[22] David A. Fournier and Ian J. Doonan. A length-based stock assessment method utilizing a generalized delay-difference model. *Canadian Journal of Fisheries and Aquatic Sciences*, 44(2):422–437, 1987. Publisher: NRC Research Press Ottawa, Canada.

[23] William W. Fox Jr. An Exponential Surplus-Yield Model for Optimizing Exploited Fish Populations. *Transactions of the American Fisheries Society*, 99(1):80–88, 1970. _eprint: https://onlinelibrary.wiley.com/doi/pdf/10.1577/1548-8659%281970%2999%3C80%3AAESMFO%3E2.0.CO%3B2.

[24] Linda Weiser Friedman. *The Simulation Metamodel*. Springer Science & Business Media, December 2012. Google-Books-ID: covTBwAAQBAJ.

[25] Nicholas J. Gotelli. *A primer of ecology.* 1995.

[26] Robert B. Gramacy. *Surrogates: Gaussian process modeling, design, and optimization for the applied sciences*. Chapman and Hall/CRC, 2020.

[27] Robert B. Gramacy and Herbert K. H. Lee. Bayesian Treed Gaussian Process Models with an Application to Computer Modeling. *Journal of the American Statistical Association*, 103(483):1119–1130, 2008. Publisher: [American Statistical Association, Taylor & Francis, Ltd.].

[28] Robert B. Gramacy and Herbert KH Lee. Cases for the nugget in modeling computer experiments. *Statistics and Computing*, 22(3):713–722, 2012. Publisher: Springer.

[29] Markus Heinonen, Henrik Mannerström, Juho Rousu, Samuel Kaski, and Harri Lähdesmäki. Non-Stationary Gaussian Process Regression with Hamiltonian Monte Carlo. In *Proceedings of the 19th International Conference on Artificial Intelligence and Statistics*, pages 732–740. PMLR, May 2016. ISSN: 1938-7228.

[30] Philipp Hennig and Christian J. Schuler. Entropy search for information-efficient global optimization. *Journal of Machine Learning Research*, 13(6), 2012.

[31] José Miguel Hernández-Lobato, Matthew W Hoffman, and Zoubin Ghahramani. Predictive Entropy Search for Efficient Global Optimization of Black-box Functions. In *Advances in Neural Information Processing Systems*, volume 27. Curran Associates, Inc., 2014.

[32] R. Hilborn and C. J. Walters. Quantitative Fisheries, Stock Assessment: Choice Dynamics, and Uncertainty Chapman and Hall. *New York*, 1992.

[33] Ray Hilborn. Pretty good yield and exploited fishes. *Marine Policy*, 34(1):193–196, 2010. Publisher: Elsevier.

[34] Ray Hilborn and Marc Mangel. *The Ecological Detective: Confronting Models with Data*. Princeton University Press, March 1997.

[35] Mike Holden. Beverton and Holt revisited. *Fisheries Research*, 24(1):3–8, July 1995.

[36] Mark E. Johnson, Leslie M. Moore, and Donald Ylvisaker. Minimax and maximin distance designs. *Journal of statistical planning and inference*, 26(2):131–148, 1990. Publisher: Elsevier.

[37] Marc C. Kennedy and Anthony O'Hagan. Bayesian calibration of computer models. *Journal of the Royal Statistical Society: Series B (Statistical Methodology)*, 63(3):425–464, 2001.

[38] Sharon Kingsland. The refractory model: the logistic curve and the history of population ecology. *The Quarterly Review of Biology*, 57(1):29–52, 1982. Publisher: Stony Brook Foundation, Inc.

[39] Hui-Hua Lee, Mark N. Maunder, Kevin R. Piner, and Richard D. Methot. Can steepness of the stock–recruitment relationship be estimated in fishery stock assessment models? *Fisheries Research*, 125-126:254–261, August 2012.

[40] Jussi Lehtonen. The Lambert W function in ecological and evolutionary models. *Methods in Ecology and Evolution*, 7(9):1110–1118, September 2016.

[41] Pamela M. Mace. Relationships between Common Biological Reference Points Used as Thresholds and Targets of Fisheries Management Strategies. *Canadian Journal of Fisheries and Aquatic Sciences*, 51(1):110–122, January 1994. Publisher: NRC Research Press.

[42] Arni Magnusson and Ray Hilborn. What makes fisheries data informative? *Fish and Fisheries*, 8(4):337–358, 2007. Publisher: Wiley Online Library.

[43] Marc Mangel. The Theoretical Biologist's Toolbox: Quantitative Methods for Ecology and Evolutionary Biology. 2006.

[44] Marc Mangel, Alec D. MacCall, Jon Brodziak, E.j. Dick, Robyn E. Forrest, Roxanna Pourzand, and Stephen Ralston. A perspective on steepness, reference points, and stock assessment. *Canadian Journal of Fisheries and Aquatic Sciences*, 70(6):930–940, April 2013.

[45] Mark N. Maunder. Is it time to discard the Schaefer model from the stock assessment scientist's toolbox? *Fisheries Research*, 61(1-3):145–149, 2003.

[46] Mark N. Maunder and André E. Punt. A review of integrated analysis in fisheries stock assessment. *Fisheries Research*, 142:61–74, May 2013.

[47] Michael D. McKay, Richard J. Beckman, and William J. Conover. A comparison of three methods for selecting values of input variables in the analysis of output from a computer code. *Technometrics*, 42(1):55–61, 2000. Publisher: Taylor & Francis.

[48] R. F. McLean, S. H. Alsop, and J. S. Fleming. Nyquist—overcoming the limitations. *Journal of Sound and Vibration*, 280(1):1–20, February 2005.

[49] Richard D. Methot and Chantell R. Wetzel. Stock synthesis: A biological and statistical framework for fish stock assessment and fishery management. *Fisheries Research*, 142:86–99, May 2013.

[50] Max D. Morris and Toby J. Mitchell. Exploratory designs for computational experiments. *Journal of Statistical Planning and Inference*, 43(3):381–402, February 1995.

[51] Joseph Munyandorero. Analytical expressions of sustainable benchmarks generic for all two-stage-structured models of exploited fish populations. *Canadian Journal of Fisheries and Aquatic Sciences*, 80(9):1425–1435, 2023.

[52] Ransom A Myers, Keith G Bowen, and Nicholas J Barrowman. Maximum reproductive rate of fish at low population sizes. *Canadian Journal of Fisheries and Aquatic Sciences*, 56(12):2404–2419, December 1999.

[53] Donald Edgar Pearson and Glenn Almany. The effectiveness of California's commercial rockfish port sampling program. 1995.

[54] Donald Edgar Pearson, Brenda Erwin, and Meisha Key. Reliability of California's groundfish landing estimates from 1969-2006. 2008.

[55] Jerome J. Pella and Patrick K. Tomlinson. A generalized stock production model. *Inter-American Tropical Tuna Commission Bulletin*, 13(3):416–497, 1969.

[56] Tony Pourmohamad and Herbert Lee. *Bayesian Optimization of Computer Experiments*. Springer, 2021.

[57] Michael H. Prager. Comparison of logistic and generalized surplus-production models applied to swordfish, Xiphias gladius, in the north Atlantic Ocean. *Fisheries Research*, 58(1):41–57, 2002. Publisher: Elsevier.

[58] Michael H Prager. Reply to the Letter to the Editor by Maunder. *Fisheries Research*, 61(1):151–154, March 2003.

[59] André E. Punt. *Model selection for the dynamics of southern African hake resources*. PhD Thesis, University of Cape Town, 1988.

[60] André E. Punt, Doug S. Butterworth, Carryn L. de Moor, José A. A. De Oliveira, and Malcolm Haddon. Management strategy evaluation: best practices. *Fish and Fisheries*, 17(2):303–334, 2016.

[61] André E. Punt and Jason M. Cope. Extending integrated stock assessment models to use non-depensatory three-parameter stock-recruitment relationships. *Fisheries Research*, 217:46–57, September 2019.

[62] Terrance J. Quinn and Richard B. Deriso. *Quantitative fish dynamics*. oxford university Press, 1999.

[63] Karthik Ramasubramanian and Abhishek Singh. *Machine learning using R*. Number 1. Springer, 2017.

[64] Peter Sheldon Rankin and Ricardo T. Lemos. An alternative surplus production model. *Ecological Modelling*, 313:109–126, October 2015.

[65] William Edwin Ricker. Stock and recruitment. *Journal of the Fisheries Board of Canada*, 11(5):559–623, 1954. Publisher: NRC Research Press Ottawa, Canada.

[66] Thomas J. Santner, Brian J. Williams, and William I. Notz. Space-Filling Designs for Computer Experiments. In Thomas J. Santner, Brian J. Williams, and William I. Notz, editors, *The Design and Analysis of Computer Experiments*, Springer Series in Statistics, pages 121–161. Springer, New York, NY, 2003.

[67] Thomas J. Santner, Brian J. Williams, William I. Notz, and Brain J. Williams. *The design and analysis of computer experiments*, volume 1. Springer, 2003.

[68] Milner B. Schaefer. A study of the dynamics of the fishery for yellowfin tuna in the eastern tropical Pacific Ocean. 1957.

[69] Jon Schnute. A General Theory for Analysis of Catch and Effort Data. *Canadian Journal of Fisheries and Aquatic Sciences*, 42(3):414–429, March 1985.

[70] Jon Schnute. A general fishery model for a size-structured fish population. *Canadian Journal of Fisheries and Aquatic Sciences*, 44(5):924–940, 1987. Publisher: NRC Research Press Ottawa, Canada.

[71] Jon T Schnute and Laura J Richards. Analytical models for fishery reference points. *Canadian Journal of Fisheries and Aquatic Sciences*, 55(2):515–528, February 1998.

[72] Luca Scrucca. GA: A Package for Genetic Algorithms in R. *Journal of Statistical Software*, 53:1–37, April 2013.

[73] Luca Scrucca. On Some Extensions to GA Package: Hybrid Optimisation, Parallelisation and Islands EvolutionOn some extensions to GA package: hybrid optimisation, parallelisation and islands evolution. *The R Journal*, 9(1):187–206, 2017.

[74] Claude E Shannon. Communication in the Presence of Noise. *PROCEEDINGS OF THE IEEE*, 86(2), 1998.

[75] Alexei Sharov. The unknown Baranov. Forty years of polemics over the formal theory of the life of fishes. *ICES Journal of Marine Science*, 78(2):743–754, 2021. Publisher: Oxford University Press.

[76] Karline Soetaert, Thomas Petzoldt, and R. Woodrow Setzer. Solving Differential Equations in R: Package deSolve. *Journal of Statistical Software*, 33:1–25, February 2010.

[77] J.C. Sprott. A simple chaotic delay differential equation. *Physics Letters A*, 366(4-5):397–402, July 2007.

[78] Christine Stawitz, Andrea Havron, Bai Li, Matthew Supernaw, Kathryn Doering, Nathan Vaughan, Kelli Johnson, Jane Sullivan, Jon Kenton Tarsus Brodziak, Ian Taylor, Meg Oshima, Jim Ianelli, Tim Miller, Peter Kuriyama, and KyleShertzer-NOAA. The Fisheries Integrated Modeling System (FIMS), December 2023.

[79] Michael Stein. Large sample properties of simulations using Latin hypercube sampling. *Technometrics*, 29(2):143–151, 1987. Publisher: Taylor & Francis.

[80] James T. Thorson, Merrill B. Rudd, and Henning Winker. The case for estimating recruitment variation in data-moderate and data-poor age-structured models. *Fisheries Research*, 217:87–97, September 2019.

[81] Ludwig Von Bertalanffy. A quantitative theory of organic growth (inquiries on growth laws. II). *Human biology*, 10(2):181–213, 1938. Publisher: JSTOR.

[82] Carl J. Walters. The continuous time Schnute-Deriso delay-difference model for age-structured population dynamics, with example application to the Peru anchoveta stock. 2020.

[83] Gerhard Wanner and Ernst Hairer. *Solving ordinary differential equations II*, volume 375. Springer Berlin Heidelberg, 1996.

[84] Henning Winker, Felipe Carvalho, and Maia Kapur. JABBA: just another Bayesian biomass assessment. *Fisheries Research*, 204:275–288, 2018. Publisher: Elsevier.

[85] Justin D. Yeakel and Marc Mangel. A generalized perturbation approach for exploring stock recruitment relationships. *Theoretical Ecology*, 8(1):1–13, February 2015.